Bronchial Artery Angiogenesis Drives Lung Tumor Growth

By
Lindsey Marie Eldridge

A dissertation submitted to Johns Hopkins University in conformity with the requirements for
the degree of Doctor of Philosophy

Baltimore, Maryland
July 2016

Abstract

Lung cancer is the leading cause of cancer related deaths and is responsible for over one million deaths worldwide each year. While it is widely acknowledged that angiogenesis plays an integral role in tumor growth, and therapeutic approaches have been taken to inhibit angiogenesis, clinical results have been unexceptional at best. Current research models discount the dual lung circulations that create a unique growth environment for tumors, by utilizing subcutaneous xenograft models that have little relevance to the lung, or orthotopic models in mice, which lack a bronchial circulation. In an effort to bridge the gap between animal models of questionable relevance, and clinical trials, we developed an orthotopic model of lung cancer in nude rats to examine the role of the bronchial artery in tumor growth. Using two methods of quantifying tumor perfusion *in vivo* we measured an increase in bronchial artery perfusion quantified by fluorescent microsphere injection (206%) and HRCT scan (276%), that paralleled the growth in tumor volume, while pulmonary perfusion remained unchanged. When ablating the bronchial artery after the initiation of tumor growth, we observed a 76% decrease in final tumor volumes at 4 weeks post ablation. In an effort to examine the innate differences in the pulmonary and bronchial circulations' response to tumor growth, primary endothelial cell lines were isolated from the bronchial artery, pulmonary artery, and pulmonary microvasculature of nude rats for the determination of their angiogenic potential. Bronchial artery endothelial cells uniquely showed increased proliferation, tube formation, and chemotaxis when exposed to angiogenic stimuli (VEGF, CINC-3, Adenocarcinoma Supernatant). We conclude that the pulmonary circulation initially sustains lung tumor establishment. As a tumor increases in size it is the bronchial

circulation that proliferates to sustain tumor growth beyond the point at which a tumor can be supported by the pulmonary circulation alone. The increased angiogenic potential of bronchial artery endothelial cells, suggests innate differences between lung circulations is due to its unique vascular niche.

Advisor: Dr. Elizabeth Wagner

Readers: Dr. Robert Brown
                Dr. Wayne Mitzner
                Dr. Fengyi Wan

Alternates: Dr. Wan-Yee Tang
                Dr. Mahendra Damarla

iv

Intentionally leave blank

Table of Contents

1. Introduction

Lung cancer is the leading cause of cancer related deaths and 220,000 new cases will be diagnosed in the United States this year alone, taking more lives than colon, breast, and pancreatic cancer combined (1). Lung cancer will have a significant impact on public health in the economic burden associated with lost productivity and the costs of illness and long-term therapy. Many successful public health interventions have been implemented with the education of the dangers of cigarette smoking, and assessing cancer risks from environmental exposures, however the economic burden will only continue to worsen as the population ages and the incidence of disease increases. Challenges in early detection of lung cancer, and the aggressive nature of the disease result in only 1 of 10 patients living beyond 3 years after diagnosis (1, 2). The high rate of disease prevalence and dismal prognosis highlight the need for continued research efforts, and in 2016, 362 million dollars from the NIH will go towards studying disease prevention, diagnosis, and treatment of lung cancer (3). Over the last century great strides have been made in understanding the pathology and mechanisms of lung cancer, coinciding with improved treatments and novel therapy approaches, however survival rates highlight the essential need for further research.

1.1 Histological Classifications of Lung Cancer

Increased specificity in the classification of lung tumor subtypes and their pathologies has resulted in more directed treatment options. Originally platinum-based chemotherapy was generally the first-line therapy until it was observed that patients

responded differently to treatment based on their specific tumor's molecular profile (4). Since then great efforts have been made to better align classification of lung cancer subpopulations, and in 2011 the International Association for the Study of Lung Cancer, the American Thoracic Society, and the European Respiratory Society collectively published international multi-disciplinary classifications specific to lung adenocarcinomas (5).

Lung cancer can be classified into three populations; Small Cell Lung Cancer, SCLC, (10-15% of cases), Non-Small Cell Lung Cancer, NSCLC, (85% of cases), and Lung Carcinoid Tumor (less than 5% of cases). NSCLC, the most prevalent diagnosis, is defined by any malignant epithelial lung tumor lacking a small cell component. NSCLC can be further sub-classified into three specific histological subtypes; adenocarcinomas, large cell carcinomas, and squamous cell carcinomas (5, 6). Classifications are based on tumor location and histological appearance and can be influenced by race, gender and environmental exposure (7).

Adenocarcinomas are the most common histological subtype of lung cancer making up more than half of lung cancer cases (7). They can be defined as a malignant epithelial neoplasm with gland formation and are typically found in the lung periphery. The degree of gland formation will also dictate if an adenocarcinoma is well, moderately, or poorly differentiated. In well-differentiated tumors, glandular structures are easily detected by column like epithelium and mucus production. Adenocarcinomas are further divided into bronchioalveolar carcinomas, mucinuous carcinomas, and papillary carcinomas. Bronchioalveolar carcinomas are characterized by their lepidic pattern where cells line the alveolar walls and appear to replace the normal epithelial lining of airspaces

2

without destruction to the basic lung architecture. Mucinuous carcinomas are usually detected by pooling of mucinous material accompanied by destruction of underlying lung architecture. Papillary carcinomas can be characterized by their complex papillary infoldings and necrotic regions of the alveolar lumen are frequently observed. Because adenocarcinomas are the most common diagnosis, and can be very well differentiated tumors, great lengths have been taken to standardize characterization of these tumors (8).

In contrast to adenocarcinomas, squamous cell carcinomas arise centrally within the main airways invading into the airway wall and lumen often times leading to airway obstruction. These cancer cells have a flattened and stratified appearance and are characterized by intracellular bridging and keratinization. When a poorly differentiated tumor lacks the defining features of an adenocarcinoma or squamous cell carcinoma, by exclusion it is usually categorized as a large cell carcinoma (5). Characterizing the lung tumor by these distinct histological patterns is the critical first step in designing a cancer therapy plan.

1.2 Original Treatments for Non-Small Cell Lung Cancer

In the 1980's, cisplatin and carboplatin were studied as treatment options for NSCLC. This work provided evidence that platinum-based chemotherapy increased survival in patients with response rates from 15-25% (9). When possible, surgery was the first option if the disease was localized and had only progressed to stage I or II, but survival rates after surgery were still less than 35% (10). In 2001, the "gold-standard" in treatment for patients with inoperable lung tumors was radiotherapy showing 5-year survival ranging anywhere from 0-45% (11). Studies examining chemotherapy coupled

with radiation therapy failed to show significant improvements with 5-year survival of patients less than 15% (12, 13). Because of severe toxicity of platinum-based drugs, and considerable low response and survival rates, treatment options for NSCLC stalled with all patients receiving the same therapy regardless of histological subtype. It was not until 2004 that it was recognized that tumor genotype was an important factor in a tumor's response to therapy (14).

Correctly identifying the histological subtype of NSCLC was advantageous for selecting the most direct treatment options. Green and colleagues highlighted the importance of subtype specific treatments by showing SCLC had the most favorable response to cyclophosphamide, and squamous cell carcinomas were more sensitive to nitrogen mustard than other histological subtypes (15). Molecular differences in tumor subtypes dictated the efficacy of the chemotherapy agent pemetrexed and the anti-angiogenic therapy bevacizumab to be effective in non-squamous histologies (16). Because subtypes of NSCLC responded differently to drug therapies it could be concluded that lung tumors not only differed in their origin and histology, but that molecular differences between pathological subtypes could also affect treatment responses. Traditionally, a distinction between SCLC and NSCLC dictated clinical treatment options. However, this limited observation was no longer considered sufficient and a more advanced classification of the NSCLC subtypes was necessary.

1.3 Molecular Pathology of Non-Small Cell Lung Cancer Subtypes and Customized Treatment

Incorporating molecular testing after histological identification provided a new approach to lung cancer therapy through the ability to target gene mutations that drove tumorigenesis specific to each patient. Molecular testing determined KRAS (Kristen Rat Sarcoma Viral Oncogene), EGFR (Epidermal Growth Factor Receptor) and ALK (Anaplastic Lymphoma Kinase) mutations make up 32%, 23%, and 3% of gene mutations observed in NSCLC (17, 18). Mutations to these genes result in increased tyrosine kinase activity, making drugs that inhibit tyrosine kinase activity ideal therapeutic options. Currently, after determining the histological subtype and the presence of an EGFR or ALK mutation, specific treatment protocols are followed. A NSCLC tumor will be further categorized as squamous or non-squamous. If a patient has a squamous cell carcinoma tumor, platinum-based chemotherapy is the first-line treatment option. If the tumor is a non-squamous cell carcinoma, such as an adenocarcinoma or a large cell carcinoma, detection of an EGFR or ALK mutation will dictate which first-line treatment is selected. Erlotinib or crizotinib would be selected for a first-line treatment in patients with EGFR and ALK mutations respectively (14).

Tyrosine kinase inhibitors target the intracellular kinase domain of EGFR and have been shown to be effective for the treatment of advanced-stage NSCLC with increased benefits compared to traditional platinum-based chemotherapy. Despite the initial favorable response rates and overall disease-control rates with use of Tyrosine kinase inhibitors specific for EGFR and ALK mutations, overall improvement in survival has not been reported (14). Classifying histological subtypes of lung cancer, coupled with genotyping each subtype has only modestly improved therapy options. However,

the lack of significantly improved outcomes highlights the need for novel therapeutic approaches.

1.4 Targeting Angiogenesis in Non-Small Cell Lung Cancer

Angiogenesis is defined as the growth of new vessels from existing vessels and is an attractive target for therapies for cancers. . Vascular Endothelial Growth Factor, VEGF, is considered the most potent growth factor for angiogenesis (19), is expressed in NSCLC, and its levels are correlated with increased tumor microvasculature and poor prognosis (20). VEGF is responsible for initiating signaling cascades that enhance endothelial cell proliferation, migration and invasion, mobilization of endothelial progenitor cells, and increase the permeability of the existing vasculature (21). Through VEGF activation of the phosphoinositide 3-kinase (PI3K) and AKT signaling pathway, endothelial cell survival, permeability, and migration is achieved. These changes coincide with Phospholipase C (PLCγ) signaling and result in endothelial cell proliferation (18). It is generally accepted that inhibiting a tumor's blood supply would block tumor growth, making components of the VEGF signaling pathway an attractive area of research for NSCLC. Extensive work that has been done in this field leading to the development of anti-angiogenic agents including monoclonal antibodies against secreted VEGF and tyrosine kinase inhibitors of the VEGF receptor.

The use of monoclonal antibodies against the secreted growth factor, or small molecules to inhibit the kinase domain of the VEGF receptor, is an extremely popular therapeutic option (22). Avastatin (Bevacizumab) was approved by the FDA in 2004 for the treatment of NSCLC. It is a recombinant, humanized, monoclonal antibody that binds with all free VEGF-A isoforms, inhibiting the ability of VEGF-A to bind to its

receptor, VEGFR 1 and 2. Bevacizumab was the first anti-angiogenic drug to show a favorable outcome with prolonged time to diseases progression (10.6 months vs. 6.2 months) and increased overall survival (20.3 months vs. 15.6 months) (23). Unfortunately, there were several common adverse side affects to bevacizumab including; arterial hypertension (one-third of patients), gastro-intestinal perforations, wound healing impairment, proteinuria, hemoptysis, arterial and venous thromboembolisms, and congestive heart failure (22). Several small-molecule anti-angiogenic tyrosine kinase inhibitors were developed; Sorafenib, Sunitinib, Pasopanib and Vandetanib, all inhibiting activation of the VEGF receptors 1-3. However, overall these drugs showed only modest increases in progress free survival and no increase in overall survival (24-26).

While classification of histological subtypes of lung cancer and molecular testing for pathological differences in subtypes advanced therapy protocols and facilitated the development of targeted therapies, there is still need for improvement. Targeting the kinase domains of EGFR and VEGFR were great advances from non-specific general radiation and chemotherapy combinations, and addressed both the growing tumor and its blood supply. However, the overall effectiveness of the treatments was modest at best, and the numerous side effects speak to the need for continued specificity in novel therapy development. Understanding the complexity of blood vessel formation in the lung in response to a growing tumor is essential for the development of better treatment options.

1.5 Methods of Tumor Vascularization

The development of a growing tumor requires oxygen, nutrition (glucose), and growth factors. Initially, tumor cells are maintained by passive diffusion, however growth in tumor volume beyond 2-3mm^3 requires the establishment of a vasculature to meet the metabolic needs of the tumor (21). Without access to a capillary bed, a tumor will remain dormant but viable as shown originally by Folkman's observations of xenografts implanted in non-vascular regions of the eye. In these cases, tumors did not exceed 2-3mm^3, but when removed and implanted in the muscle of rabbits, tumors underwent rapid neovascularization followed by rapid growth suggesting the essential need for angiogenesis in tumor growth (27, 28).

There are several methods in which a growing lung tumor can access a blood supply: endothelial sprouting, intussusceptive microvascular growth, vessel co-option, and vasculogenic mimicry. Endothelial sprouting is a process in which proteolytic degradation to the extracellular matrix of the parent vessel occurs. This is followed by chemotactic migration and proliferation of endothelial cells resulting in the formation of a lumen and mature endothelium, generation of new basement membrane and recruitment of pericytes (29). Intussusceptive microvascular growth, was first described by *Patan et al.* in 1995 as a state in which the capillary network expands by new formation of small intervascular tissue inside existing blood vessels that divides the lumen into two segments during tumor vascular remodeling (30). Vessel co-option, the use of pre-existing vessels, was first observed in one of the most densely vascularized organs, the brain. In these cases, tumors may develop without the need for angiogenesis, and therefore would not be affected by angiogenesis inhibition (31). In 1999 *Maniotis et al.* first described

vasculogenic mimicry as patterned vascular channels lined by human melanoma cells in primary metastatic tumors which subsequently generated a functional endothelial network in vitro (32). With several methods for a growing tumor to access a blood supply, and each method relying heavily on the type of tumor, location, and tumor microenvironment, it is reasonable to suggest tumor vascularization is highly heterogeneous. Therefore, research focusing on specific methods of vascularization in NSCLC is essential.

Folkman proposed the hypothesis that tumor growth was angiogenesis dependent. However, lung tumors uniquely challenge this assumption because of their oxygen rich and extremely well vascularized environment. With the discovery of alternative vascular acquisition methods of growing tumors, a more refined assumption in NSCLC is that angiogenesis may be involved, but is most likely not the only way a lung tumor is vascularized. Further examining the truly unique tumor growth environment of the lung could help us to better understand methods by which lung tumors acquire a blood supply and what dictates each method.

1.6 Methods of Tumor Vascularization specific to Non-Small Cell Lung Cancer

A tumor will acquire a blood supply, whether by co-option of neighboring vessels, or endothelial sprouting from existing vessels, that often leads to the development of a new vasculature that is structurally unsound. Angiogenic vessels are abnormal and highly permeable due to excessive angiogenic growth factor secretion (33), resulting in an inefficient vasculature and tumor hypoxia. The response to an hypoxic state is the activation of Hypoxia Inducible Factor (HIF) protein signaling, leading to the

secretion of VEGF, Platelet Derived Growth Factor (PDGF) and Transforming Growth Factor (TGF-α), all of which trigger angiogenesis and tumor microvessel formation from the surrounding vasculature (34). Studies of NSCLC have utilized microvessel density counting and endothelial staining as a determination of angiogenesis in hundreds of patients with NSCLC. Increased microvessel density in histological tumor cross sections was shown to predict a poor outcome and shorter survival (35, 36).

In a well-vascularized organ, angiogenesis does not always occur to support a growing tumor. Wesseling *et al* reported non-angiogenic growth of glioblastoma multiforme (37), and Hyjeck *et al* described indolent lymphomas with little formation of immature vessels, suggesting a non-angiogenic phenotype (38). In the lung, Pezzella *et al* characterized non-angiogenic carcinomas by lack of destruction to the parenchyma and absence of new vessels, coinciding with an alveolar filling pattern with the only vessels present throughout the tumor belonging to alveolar septa (39). Later this group was able to distinguish angiogenic and non-angiogenic tumors by the presence or absence of integrin alpha V and integrin beta 3(αVβ3), in blood vessels to describe mature and immature vasculature (40). Highly angiogenic renal cell carcinomas have been reported to have numerous non-angiogenic metastases in the lung. This may imply that the lung provides a unique environment for tumor growth without need the need for additional neovascularization (41). Further confirming this theory, Yuneva *et al* showed that tumors of the same lineage develop different metabolic needs depending on the host tissue (42).

There is plenty of evidence to support the idea of both angiogenic and non-angiogenic tumors arising from the same cell lineage (41). There is also evidence to suggest that the tumor host environment could dictate whether a tumor is angiogenic or

not (42). Hence, the poor track record of current anti-angiogenic therapies on non-angiogenic tumors may not be surprising. Overall a deeper understanding of the lung as a host environment is essential for the development of novel therapy options for NSCLC.

1.7 The Lung is A Unique Environment for Tumor Growth

The lung provides a unique growth environment for tumors because of its oxygen-rich environment, unique extracellular matrix and most importantly, its dual circulations (43). The dual circulations consist of the pulmonary circulation and the bronchial circulation. Each circulation differs in structure, function, and potential for angiogenesis, suggesting their roles in tumor perfusion could be drastically different as well. Understanding how each circulation would adapt to support tumor growth is essential for understanding the unique host environment of the lung.

1.8 Pulmonary Vasculature Remodeling and Angiogenesis

The pulmonary circulation, a high flow low-pressure circuit, is responsible for efficient gas exchange. It tightly regulates fluid movement and prevents fluid leakage from the pulmonary vessels into the interstitial space. This low-pressure system is extremely sensitive to any mechanical and chemical changes in the lung that threatens to disrupt endothelial function such as acute or chronic hypoxia and increased pulmonary flow or resistance.   These types of disruptive changes are often seen in pulmonary arterial hypertension, the progressive sustained increase in pulmonary load or vascular resistance, where vasoconstriction and remodeling of the pulmonary vasculature leads to endothelial cell barrier dysfunction, further exacerbating the increase in pulmonary pressure (44).

11

Pulmonary vascular remodeling can be characterized by pulmonary vascular cell proliferation, structural wall changes in larger pulmonary arteries, concentric medial thickening in small arterioles and muscularization of previously non-muscular capillaries, (45, 46). Drivers of pulmonary hypertension are comprised of several mechanical and chemical mediators. Increased vascular pressure, sheer stress and hypoxia result in increased pulmonary vascular resistance and reduced vessel compliance (47). Angiotensin II was shown to cause hypertrophy and proliferation of pulmonary arterial cells (48), while 5-hydroxytraptimine drives vascular remodeling through its vasoconstrictor/vasodilator properties and role in vascular smooth muscle cell hyperplasia (49). Inflammation and inflammatory cytokines have also been reported to play a role in pulmonary vascular remodeling (50). While pulmonary vascular remodeling has been described extensively, angiogenesis from the pulmonary vasculature has not been conclusively reported.

There have been few reports of pulmonary angiogenesis. In a model of pulmonary arterial hypoplasia in fetal lambs, Lambert *et al* showed transbronchial gene transfer of VEGF through an adenoviral vector resulted in pulmonary angiogenesis, proximal pulmonary artery growth, and lung parenchyma recovery (51). Pulmonary angiogenesis has also been reported in cases of hepatopulmonary syndrome; a disease in which patients with liver disease, due to excessive release of vasodilators, will experience vasodilation in the lungs and hypoxemia. In 2009 Zhang *et al.* showed in a chronic bile duct ligation model of hepatopulmonary syndrome, increased microvessels, PCNA, VE-cadherin, and Von Willibrand Factor (52). In 2012, they showed VEGF secreting monocytes adhere in the lung vasculature leading to increased angiogenesis (53). In

studies of pulmonary hypertension, angiogenesis was quantified by endothelial cell staining of CD34 or CD31, which was inconclusive of the process of vascular remodeling or true angiogenesis was occurring (54, 55). McLoughlin and colleagues showed increased pulmonary vessel length, volume, and increased endothelial cell count in a model of chronic hypoxia in Sprague Dawley rats. This model also did not show clear evidence that either angiogenesis or arteriogenesis was occurring (56). Beyond fetal development, post-pneumonectomy (57), and lung transplant, it is uncertain whether true pulmonary angiogenesis occurs.

1.9 The Bronchial Artery and Angiogenesis

The bronchial artery originates from the superior portion of the thoracic aorta, but in some cases can be found originating from the subclavian artery, descending aorta, or the brachiocephalic trunk (58). Typically, two left bronchial arteries and one right bronchial artery can be found on the dorsal surface of the main stem bronchi adjacent to the ventral surface of the esophagus. Each artery is approximately 1.5mm in diameter, decreasing to 0.5mm when entering the bronchopulmonary segment. The small diameter creates a high resistance, low capacitance vessel receiving only about 1% of the cardiac output. The bronchial artery is responsible for perfusing the esophagus, bronchial walls down to the level of the respiratory bronchioles, bronchovascular bundles, regional lymph nodes, visceral pleura, and eventually drains into the pulmonary arteries and veins (59-61).

Although it is unclear to what extent pulmonary angiogenesis occurs, bronchial artery angiogenesis has been described extensively in many different states of lung disease. In 1963 Turner-Warwick observed an extensive bronchial vascular network with

13

bronchial-pulmonary anastomoses, and an unchanged pulmonary vasculature in 12 of 16

lungs with diffuse pulmonary fibrosis (62). In two different models of pulmonary artery

obstruction, and functional measurements of blood flow in the bronchial circulation in

both the lamb and the rat, significant bronchial artery angiogenesis occurs after

pulmonary artery obstruction (63, 64). In a study of patients with asthma and COPD,

Calabrese *et al* described the presence of bronchial artery angiogenesis in histological

samples (44). Further animal studies of asthma confirmed the appearance of increased

blood vessels in the airway walls accompanied by increased responsiveness to

methacholine (65). While bronchial artery angiogenesis has been observed in several

lung diseases states, the role of the bronchial artery in tumor perfusion remains

controversial.

Whether tumors in the lung are angiogenic, non-angiogenic, or a combination of

both, it also remains to be determined which circulation is proliferating under angiogenic

conditions. Several studies utilizing contrast enhanced computed tomography (CT)

scanning have implicated major roles of both the pulmonary and bronchial circulations in

tumor perfusion. Since these studies were performed in patients, perfusion data was

limited to a single time point, without subsequent experiments examining how each

vascular bed changed with tumor size (66, 67). Further examining the angiogenic

potential of the pulmonary and bronchial circulation independently could provide

valuable information for novel NSCLC therapies and increased drug specificity by

targeting one circulation directly.

1.10   Aim of the current study

By understanding the physiology and intricate balance of the two circulations responsible for lung perfusion, it is possible to better understand how a growing lung tumor manipulates these circulations. Lung tumors can be heterogeneous in their methods of recruiting a vasculature, whether they are simply co-opting the existing pulmonary circulation, initiating neovascularization of the bronchial circulation, or a combination of both. In this study, we developed an orthotopic model of lung cancer in nude rats to examine the pulmonary and bronchial circulations in response to a growing tumor. We assessed tumor growth over time and each circulation's contribution to perfusion depending on tumor size. We ablated the bronchial circulation after tumor establishment and tracked tumor volumes weekly to determine the role of bronchial artery perfusion in tumor growth. We also closely examined endothelial cells from the pulmonary artery, pulmonary microvasculature, and bronchial artery to quantify the angiogenic potential of both the pulmonary and bronchial circulations. We hypothesize that a lung tumor will grow utilizing the pulmonary circulation until it reaches a critical size at which time this circulation can no longer support tumor growth. We predicted at this point the bronchial circulation undergoes angiogenesis and continues to proliferate driving lung tumor growth.

2.0 Development of orthotopic model of Non- Small Cell Lung Cancer.

2.1 Introduction

The dual circulations of the lung are not well described in context with lung tumor development. In part, this is due to the lack of physiologically relevant animal models in which to study the disease and the limited capacity for which bronchial perfusion can be studied in patients (67). Essential to examining both the pulmonary and bronchial circulatory contributions to tumor perfusion is the development of an animal model that allows longitudinal tracking of changes in tumor volumes and perfusion.

In the 1960's-1970 the first *in vivo* models of lung cancer were developed through the induction of pulmonary tumors by exposure to chemical carcinogens (68). Oral administration of dibenz (a, h) anthracene, isonicotinic acid hydrazide, urethane, nitrosamines, and chronic inhalation of bis (chloromethyl) ether, as well as two components of tobacco smoke; benzo (a) pyrene (B [a] P) and 4-(methylnitrosamino)-1-(3-pyridyl)-1-butanone (NNK, a nitrosamine), lead to the development of lung adenomas (69-75). These benign nodules were the first attempt at modeling carcinomas, and while they were novel and instrumental for proof of concept, the emphasis of each study was to block chemical-specific tumor induction. In further development of *in vivo* models, lung adenocarcinomas were induced by carcinogen inhalation paired with oncogene mutations in transgenic mice. Several lines of transgenic mice with P53, KRAS, ARF (ADP ribosylation factor 1), ALK and several other oncogene mutations were frequently used, with almost 100% of transgenic strains containing a KRAS mutation (76-78). Spontaneous formation of lung adenocarcinomas would typically arise without carcinogen exposure, however the latency period was long, incidence of nodule

formation was low and they were usually accompanied by other malignancies, making conclusive mechanistic studies more difficult (79). These original models of lung cancer were sufficient for studying specific carcinogenic mechanisms of lung adenocarcinoma development through precise oncogene mutations. Prevalence and size of nodule formation was an easy way to assess the efficacy of drug treatments aimed to block tumorigenesis. Since nodules were small and frequent, studying tumor perfusion was not feasible nor the priority of these studies.

While several current studies use p53/KRAS mutant mice to drive adenocarcinoma formation (80-82) the resulting small diffuse nodules throughout the lung are imperfect for studying angiogenesis. A single large tumor would be a better option. Efficacy of angiogenesis inhibiting drugs has been studied in large consolidated xenografts that are injected subcutaneously into the flank of nude mice (83-86). The use of nude mice is standard in xenograft models because their absence of T-cells makes it unlikely the animal will reject the xenograft. The ease of physically measuring the change in tumor size directly beneath the skin is appealing for large pre-clinical studies. However methods by which angiogenesis inhibiting drugs block angiogenesis in the flank seem unlikely to be translated to the lung. This is because the microenvironment of a tumor growing subcutaneously in the flank is hypoxic and nearly avascular, contrasting from the oxygen rich and extremely well vascularized environment of the lung. Additionally, inadequacies of the subcutaneous flank model are evident by the lack of effective anti-angiogenic therapies for NSCLC to date (87-90).

Given the shortcomings of the subcutaneous flank model of NSCLC, and that the more physiologically relevant transgenic mouse models result in small diffuse nodules,

additional xenograft models were developed to address this issue. Several orthotopic

studies modeling adenocarcinomas utilized A549, H1975, HCC4006 and HCC827 cells

derived from patients (91-93), and were injected along with a matrigel vehicle into the

lung of nude mice (91, 94, 95). The resulting lung tumor was ideal for studying

extracellular matrix, tumor microenvironment, and novel chemotherapy approaches.

With orthotopic mouse models being the most ideal, physiologically relevant model thus

far, only the issue of the lung's dual circulations remained.

To truly be able to study the dual circulations of the lung and their ability to

support tumor growth, it was essential to select a small animal that has an established

bronchial circulation. The mouse lacks a sub-carinal bronchial circulation (96, 97).

Studying lung tumor angiogenesis in the mouse would not be an accurate portrayal of

angiogenesis in patients with NSCLC because the growing lung tumor would rely

entirely on the pulmonary circulation for perfusion, which has been shown to have

diminished angiogenic capacity (98). The rat not only has an established bronchial

circulation, but one that has been studied in other lung disease states including asthma

(65), pulmonary fibrosis (99), and chronic pulmonary thromboembolism (63, 64). Thus,

the rat provides a more physiologically relevant way to study the bronchial circulation

than the mouse.

Additionally, the need for a single, rapidly growing tumor in the lung, made an

orthotopic xenograft model the best option. We chose to use RNU nude rats for the

xenograft because of their established bronchial circulation and anatomical relevance to

humans, with the experimental convenience and ease of having a small animal model. In

this study we developed an orthotopic model of NSCLC that is pathologically and

physiologically similar to patients with NSCLC that allowed us to study both the

bronchial and pulmonary circulations' involvement in lung tumor perfusion.

2.2 Methods:

Adenocarcinoma Cell Injection: The experimental protocol was approved by the Johns Hopkins Animal Care and Use Committee (Protocol #RA12M283). Human lung adenocarcinoma cells (Calu-3, ATCC, Manassas, VA) were grown in culture, DMEM+10% FBS, until confluent in T75 flasks. Cells were trypsinized, and 5million cells were resuspended in 50μl of sterile saline. Rats were anesthetized with isoflurane (2% with room air), intubated, placed on a rodent ventilator model 683, Harvard Apparatus, Holliston, Massachusetts (90 breaths/min; 8ml/kg tidal volume). A transverse incision (1.5inches) was made with a scalpel into the skin covering the thorax on the left side. The tissue was dissected until the rib cage was exposed. With a 31G Insulin Syringe (BD Biosciences, San Jose, CA), cells were injected through the thorax (between the 3rd and 4th rib) directly into the left lung. The incision was closed with methyl acrylamide adhesive and the rats were allowed to recover (5-10minutes) while being ventilated with room air before being extubated and returned to their cages. Animals were maintained in the lab and observed daily for weight loss and signs of distress for 2-12 weeks after adenocarcinoma cell injection.

Lung fixation for histological visualization of lung adenocarcinoma: Animals were sacrificed by lethal dose of pentobarbital sodium salt solution (Sigma, St Louis, MO; 50mg/ml) at a time course from 1-10 weeks after cancer cell injection. The trachea was exposed and a 14G, 1.5" blunt needle (SAI Infusion Technologies, Lake Villa, IL) was secured in the trachea. Z-FIX (Anatech LTD, Battle Creek, MI) was infused into the lung through the tracheal cannula and held at $10cmH_2O$ for 24hours. Lungs and heart were dissected en bloc from rat and placed in Z-FIX for an additional 48 hours and 70% ethanol for a minimum of 24hours. Samples were embedded in paraffin blocks and slides were made from 10μm thick tissue slices from the left lung cut transversely through the center of the lung tumor, which was visible by inspection. Haematoxylin &Eosin staining was performed on slides and pictures were taken at 40X original magnification using SPOT imaging software 5.1 (Diagnostic Instruments Inc, Sterling Heights, MI).

Immunohistochemistry for visualization of tumor vasculature: Slides were de-paraffinized by rinsing with 100% xylenes (Electron Microscopy Sciences, Hatfield PA), 100%, 95%, 70% and 50% ETOH. Antigen retrieval was performed by boiling 1mM EDTA (Thermo Fisher Scientific,) then adding to slides and microwaving on lowest power for 10minutes. Slides were then cooled with room temperature water. Blocking was performed with 10%FBS, 1%BSA, and 0.5%Tween20 in PBS for 60 minutes. Antibodies for Tomato Lectin (Endothelial cell marker; Sigma) and ERBb2 (Epithelial cell marker over expressed in lung adenocarcinomas; Thermo Scientific) were incubated at room temperature for 2 hours. Slides were dehydrated through ethanol series (50%, 70%, 80%, and 95%) and 100% xylenes for 1minute. 20ul of Prolong Gold anti-fade

reagent with DAPI (Nuclear stain; Life technologies) was added to each slide sealed with a coverslip. Images were taken at 100X original magnification using an Olympus IX51 microscope (Olympus, Center Valley, PA) and High Performance SensiCam (Cooke, Auburn Hills, MI).

Tumor volume determination by High Resolution Computed Tomography (HRCT) scans:

Rats were anesthetized with a ketamine/xylazine (75/25 mg/kg) solution. HRCT scans were performed in the Department of Radiology, CT at the Johns Hopkins Outpatient Center on a Siemens Definition Flash 256 slice dual source scanner. Scanner settings are listed below.

Representative images of a lung tumor six weeks after adenocarcinoma cell injection in one rat are depicted in Methods Figure 2. Scrolling through the stack of images, the apex and the base of the tumor were identified. Using Image J, a region of interest (ROI; yellow outline) was drawn around the border of the tumor in each image where the tumor was identified. Image J software was calibrated based on pixel size (0.10 x 0.10 mm). The sum of the areas from the ROI for each image was multiplied by the slice thickness (0.4 mm) and then summed over all the ROIs to calculate tumor volume. (Note: only five representative images are shown from approximately 50 total images per rat that was used to illustrate how the tumor volume was calculated).

Methods Fig 1: Tumor Volume Calculation
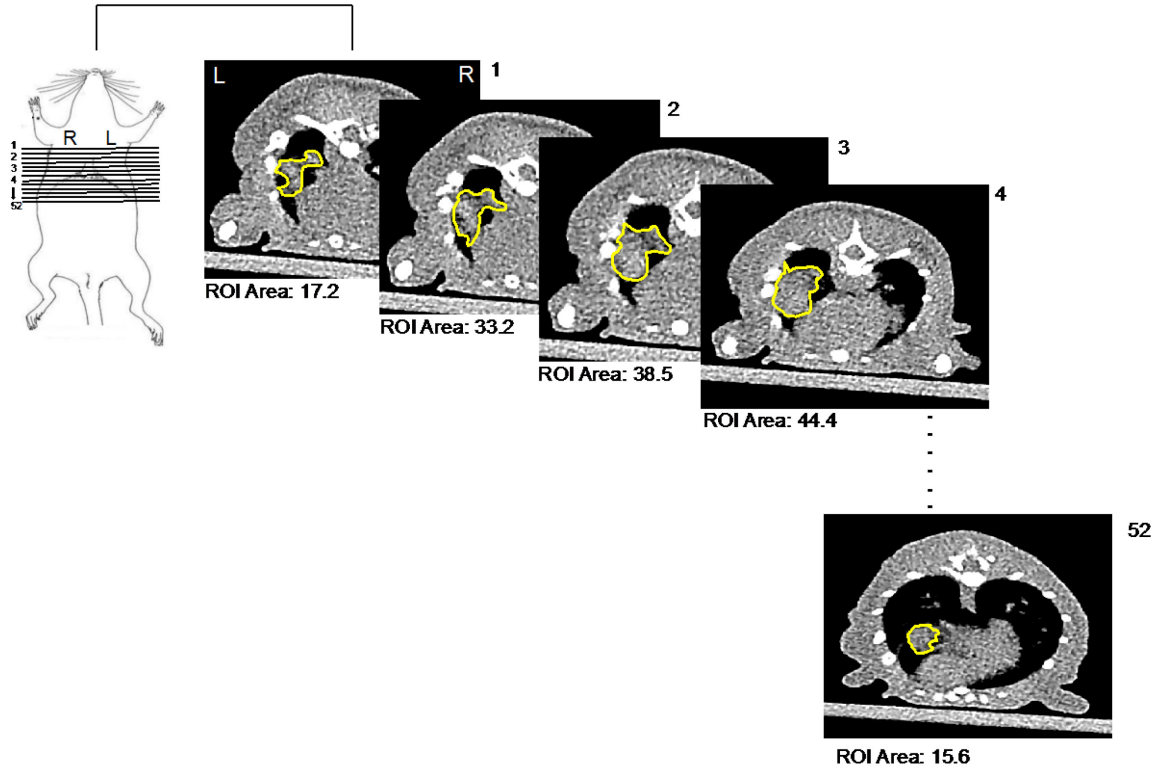
Table 1: Sample calculation of tumor volume by HRCT scanning

Image #	ROI Area
1	17.195
2	33.207
3	38.538
4	44.497
Σ (1-4)	=133.43
Σ (1-4) X Slice Thickness	=(133.43) X 0.4= 53.37mm^3
Tumor Volume	**53.37mm^3**

HRCT scanner settings:

     Collimator: Ultra High Resolution (16 x 0.3mm)
     Kernel: V80μ Very Sharp
     Effective mAs: 450
     Pitch value: 0.85
     kV: 120
     Direction: Craniocaudal
     Slice: 0.4 x 0.2 mm
     Rotation time: 1 second
     Lung window: Width-1600 Level-500
     Field of View: 50 mm
     Reconstructions: Iterative

Table 1: Sample calculation of tumor volume by HRCT scanning

Regions of interest were drawn around the tumor, on every image that a tumor was visible, in all of the images making up the thorax. All areas of regions of interest were summed and multiplied by 0.4 (slice thickness) to obtain tumor volume.

Left Pulmonary Artery Ligation:

Because the pulmonary circulation was presumed to be involved in tumor perfusion, in a separate series of rats the left pulmonary artery was ligated prior to adenocarcinoma cell injection to determine if the bronchial circulation was sufficient to support tumor establishment and growth.

The experimental protocol was approved by the Johns Hopkins Animal Care and Use Committee (RA13M461). Seven-week-old RNU nude rats (Charles River, Boston

Massachusetts) were anesthetized (2% Isoflurane in room air) intubated with 14G intracath and ventilated (90 breaths/min; 8ml/kg tidal volume) (Rodent ventilator Model 683, Harvard Apparatus, Holliston, Massachusetts). With rats lying on their right side, a transverse incision was made into skin directly over the left side of the thorax and tissue was dissected until ribs were exposed. A blunt incision was made between the 3rd and 4th rib on the left side of the thorax, and rib separators were inserted into the space creating an opening to visualize the left lung. The Left pulmonary artery was isolated from the left bronchus and ligated using 6-0 polypropylene suture (Myco Medical, Cary NC). The lung was hyper-inflated to reestablish thoracic pressure as thorax was closed with 4-0 suture (Myco Medical, Cary NC). Sensorcaine (Bupivaciane 2mg/kg) was injected at the site of the incision for analgesia and the incision was closed with methyl acrylamide adhesive. The rats were allowed to recover on ventilator breathing room air (5-10minutes), then were extubated and returned to their cages (69).

Statistics:

Linear regression and goodness of fit in Prism Graph Pad software was used to calculate the correlation of tumor weight with tumor volume.

2.3 Results:

Fig 1:Adenocarcinoma cell injection results in single tumor development

After the injection of 5 million adenocarcinoma cells, a single, solid tumor develops in the left lung. Depicted is a tumor that developed 6 weeks after adenocarcinoma cell injection.
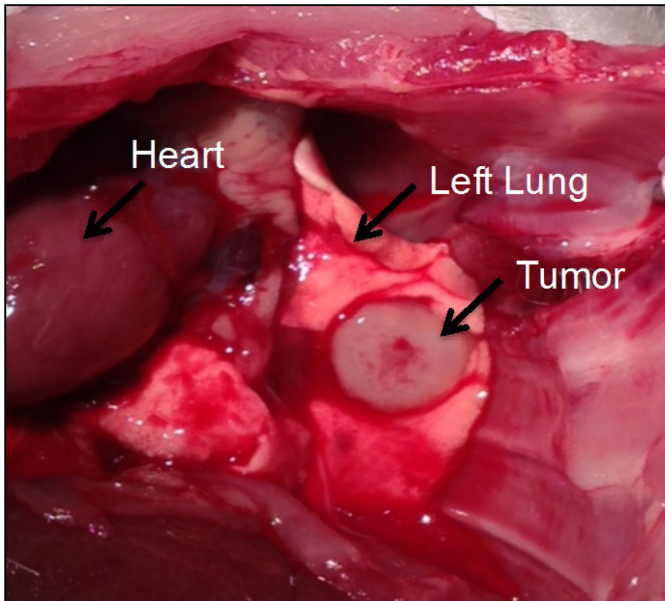
Histological confirmation of lung adenocarcinomas

After adenocarcinoma cell injection, histology was used to monitor tumor growth

and confirm the growing tumors displayed the same pathology that would typically be

found in a patient with NSCLC. Examination of tumor cross sections from 7 different

animals over a time course from 2-8 weeks after adenocarcinoma cell injection showed

the formation of one consolidated tumor. A progressive increase in tumor diameter over

time was observed (Fig 2A). Upon further examination through serial sections of the

right and left lung, only one tumor was detected indicating there were no metastatic

lesions to the rest of the lungs. H&E staining depicted well-differentiated epithelial cell

patterns, surrounding and filling airways and alveolar structures. Tumor histological

patterns were heterogeneous in nature, illustrating lepidic (alveolar lining), acinar (gland

forming), and papillary (fibrovascular core) patterns indicative of lung adenocarcinomas.

Each tumor had defined borders that both appeared to fill existing alveolar structure in

some areas, while pushing out and condensing the surrounding alveoli in others (Fig2B).

Lung tissue surrounding the tumor appeared to be normal and healthy based on

maintained alveolar structure, lack of inflammatory cell infiltrate and no apparent

vascular edema. Unfortunately from H&E staining, only the presence of red cells, and the

lack of necrotic regions could suggest that the tumors were vascularized.

Fig 2: Histological confirmation of tumor formation over eight weeks

Fig.2 A, C, E, F: H&E Staining of histological sections confirms presence of a single tumor, with a progressive increase in tumor diameter over time. No metastatic lesions were observed in the lung. The presence of red blood cells and absence of necrotic regions suggest a well-vascularized tumor. (40X original magnification)

B, D) Condensed alveoli surrounding tumor borders suggest tumor growth is achieved by pushing through nearby tissue (black arrows), while maintained alveolar structures suggest alveolar filling is occurring (red arrow).

A. 2 weeks- Diameter: 1.09mm
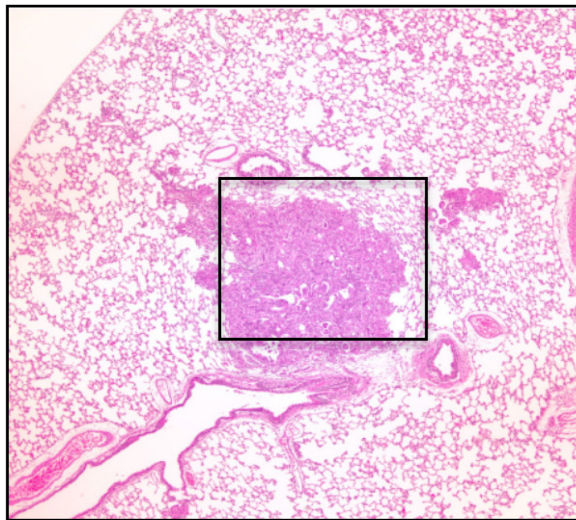
B.
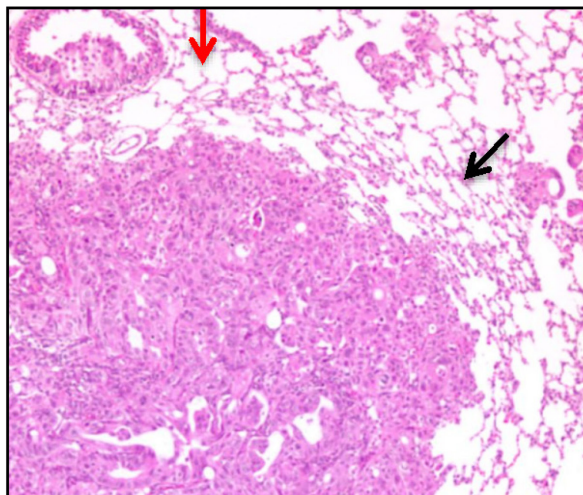
Fig 2: Continued

C. 3 weeks– Diameter: 2.47mm
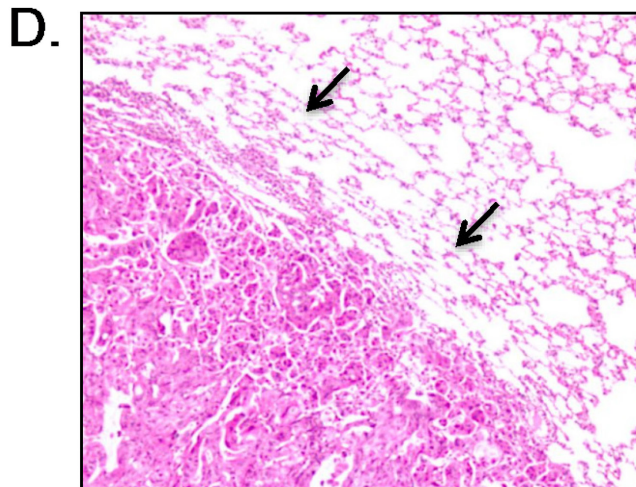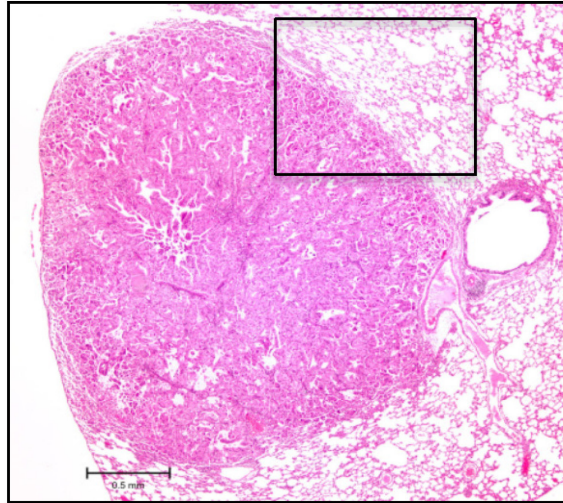
D.

E. 4 weeks- Diameter 4.72mm
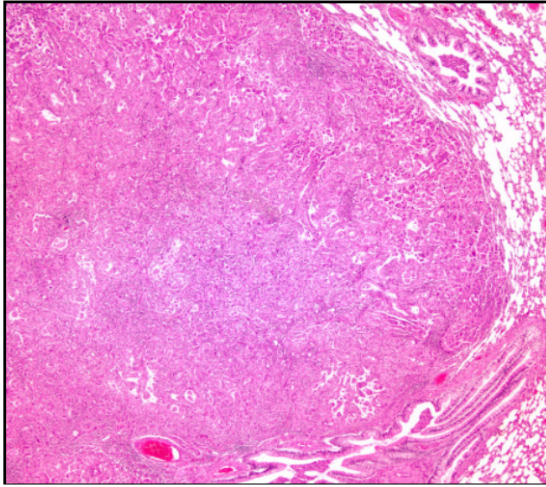
F. 8 weeks- Diameter 6.38mm
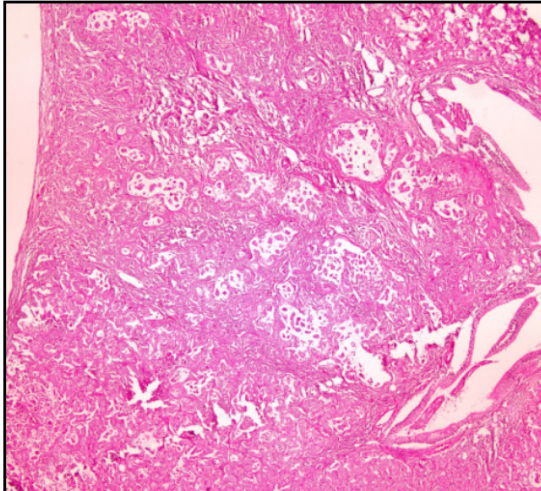
To better visualize the tumor vasculature, immunohistochemistry was used to distinguish the tumor vasculature from adenocarcinoma cells. Tomato lectin (red) was used to label endothelial cells, ERBb2 (green) was used to label adenocarcinoma cells, and DAPI (blue) was used as a nuclear stain. By utilizing fluorescently labeled antibodies, and multi-channel fluorescent microscopy, it was possible to visualize vascular patterns, and tumor growth patterns of adenocarcinoma (Fig 3). In patients, lung adenocarcinomas have been defined by well-differentiated tumors that display alveolar filling patterns with little destruction to lung parenchyma. Pathological reports have described the presence of a vasculature belonging to the existing alveolar septum with tumors growing around these structures. Distinct alveolar filling patterns were observed in the orthotopic xenograft after adenocarcinoma cell injection. The incidences of blood vessels also appear to be from the existing microvasculature (Fig 3A,B). Acinar and papillary patterns were confirmed in xenograft sections (Fig 3C). After histological examination of the orthotopic xenograft it appeared that the tumor pathology was similar to that observed in lung adenocarcinomas in patients.

Fig 3: Immunohistochemistry used to confirm adenocarcinoma pathology

Immunohistochemistry was used to confirm lung adenocarcinoma pathology (6 weeks after adenocarcinoma cell injection; images are 100X original magnification). Tomato Lectin (red) was used as endothelial cell marker, ERBb2 (green) was used as adenocarcinoma cell marker, and DAPI (blue) was used as a nuclear stain. A-B) Tumors display typical adenocarcinoma pattern; growing along alveolar septa, displaying alveolar filling, minimal structural damage to parenchyma (red arrows). C) Pathological heterogeneity is displayed in separate region of tumor. Acinar structures, with gland formation arranged around a central lumen (red arrow), are indicative of lung adenocarcinomas.
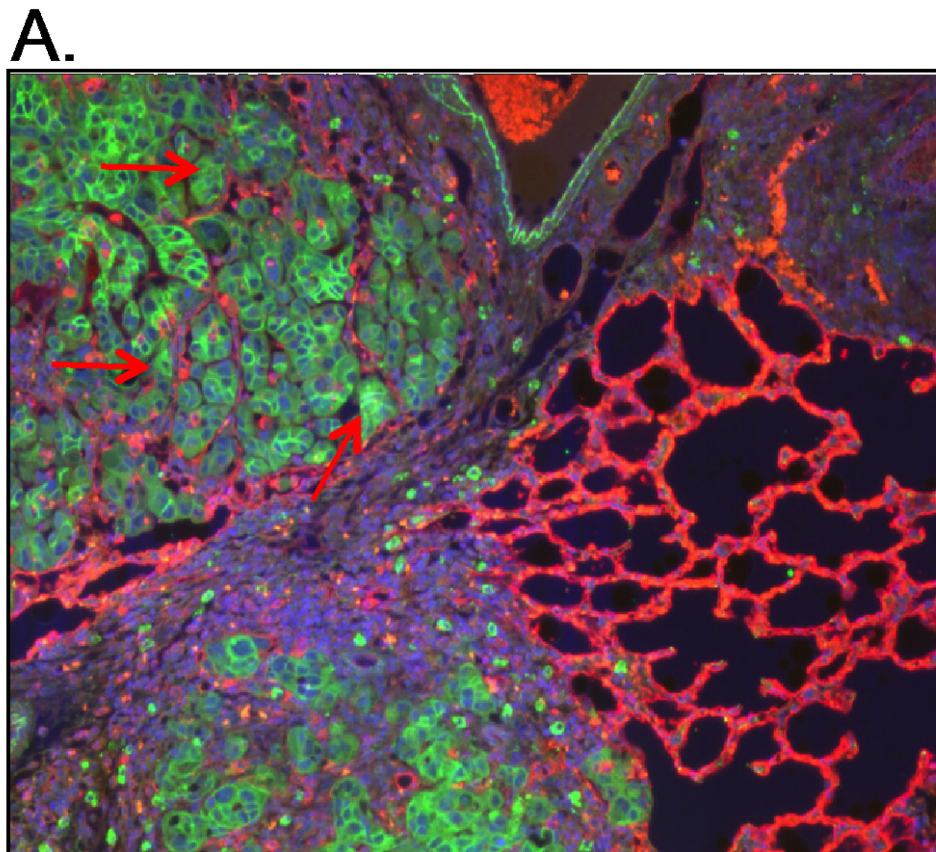
Fig 3: Continued

B.
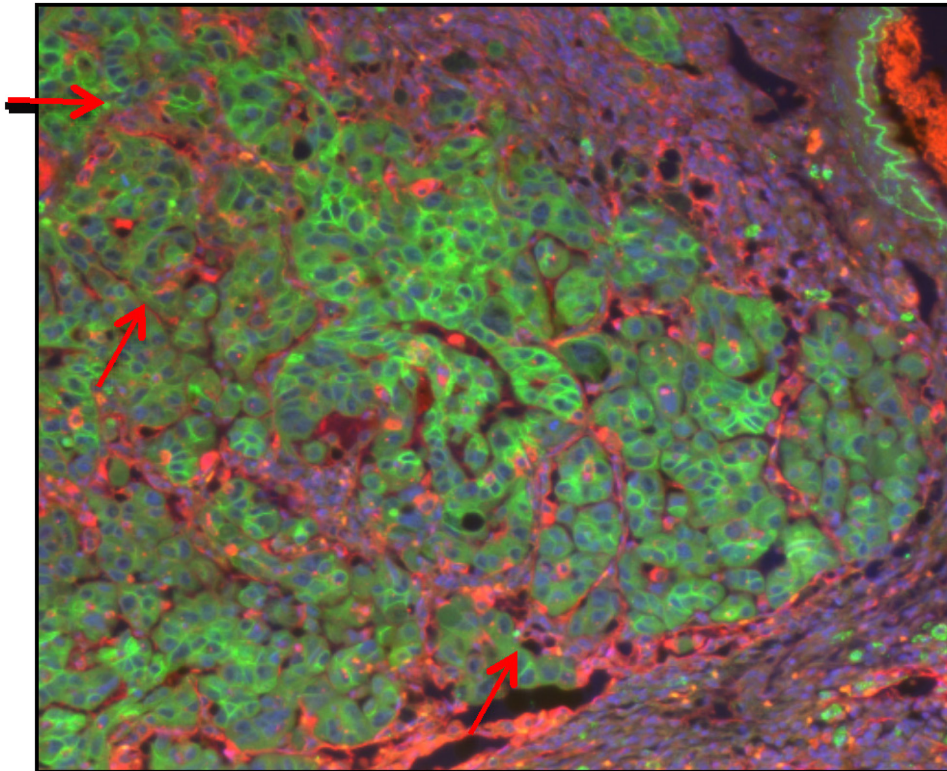
Fig 3: Continued

C.
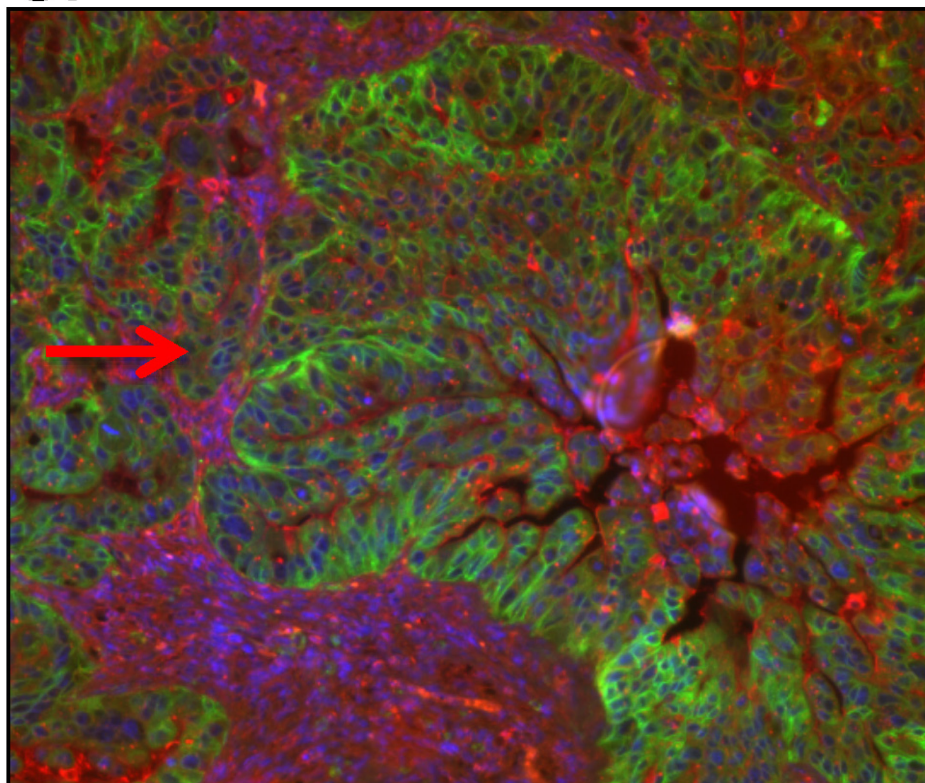
Tracking tumor growth by HRCT scanning

To quantify tumor growth over time, we utilized HRCT scanning to quantify tumor volume weekly in a series of 6 animals (see methods; Fig 1). A single tumor could first be visualized in the left lung between 2 and 3 weeks after adenocarcinoma cell injection. We then observed a progressive increase in tumor volume over the course of 8 weeks, with no sign of secondary lesions to other regions of the lung (Fig 4A). When tracking tumor volumes it was evident that growth patterns varied greatly in rate of tumor growth between animals, with some animals showing drastic increases in tumor volume from week to week while others' showed slower growth patterns while other even plateaued. Exact tumor location and final tumor volumes at the end of 8 weeks were also variable (Fig 4B).

Fig. 4: Tumor Volume Quantification by HRCT scanning

A) Thoracic HRCT images from a single rat at four time points after injection of adenocarcinoma cells. At week 3, a single solid adenocarcinoma can be seen in the left lung (Tumor is outlined in yellow). The HRCT scans at weeks 4 and 8 demonstrate the progressive increase in tumor size over time. Tumor volume was calculated from the summation of the serial regions of interest (yellow outline) on the image slices containing the tumor (see calculations in methods). B) Demonstrates the progressive increase in tumor volume (cm^3) in each rat as determined by HRCT scans over the course of eight weeks. Each line represents a single tumor in different individual rats (n=6; rat B depicted in CT scan).

A. 2 weeks   3 weeks

Volume: 19.14mm³   134mm³

4 weeks

8 weeks

233.6 mm³

800.58mm³

B.
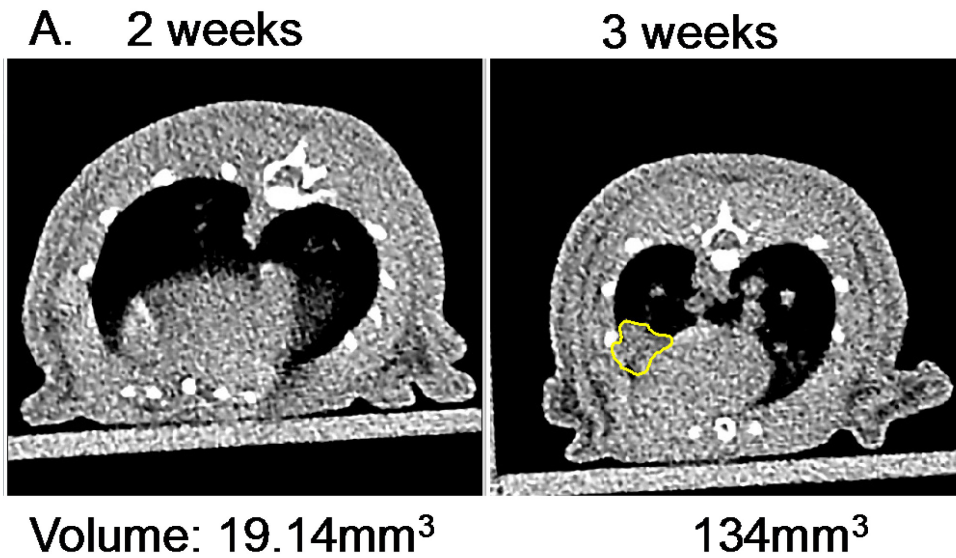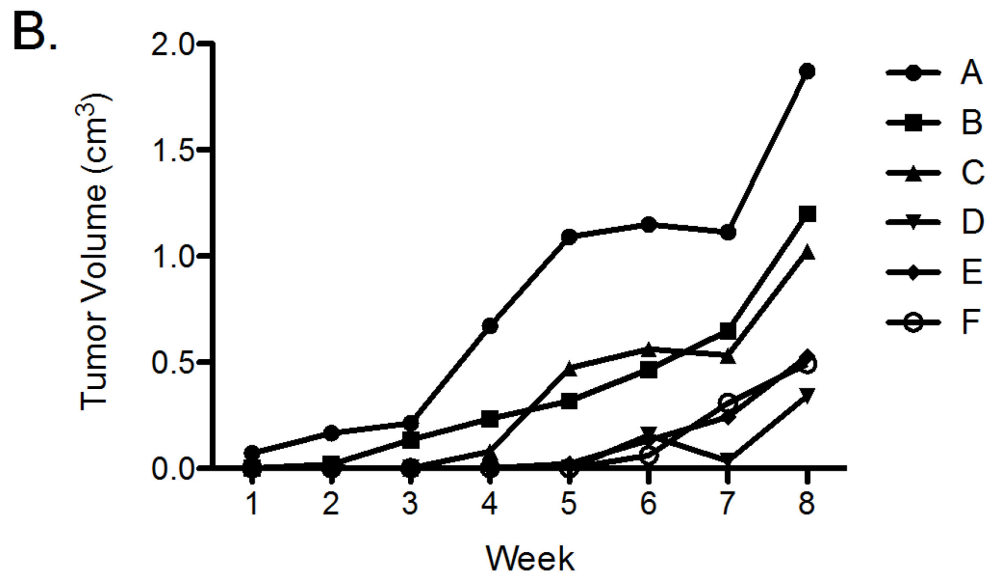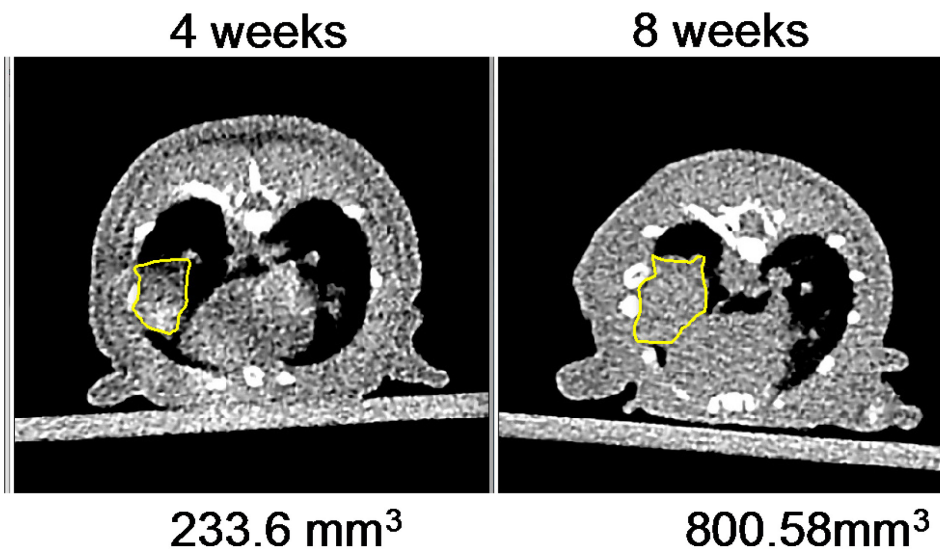
In a separate series of 7 animals, tumor volumes were quantified by HRCT scanning then dissected and their weight was measured. Tumor volume was significantly correlated with tumor weight (r^2=0.98, p<0.0001) demonstrating the accuracy and consistency of the HRCT scanning measurement to quantify tumor size. This correlation also demonstrates the consistency in density of tumor composition between animals (Fig 5).

Fig 5: Confirmation of HRCT volume measurements

In a separate series of rats (n=7), tumor volume as measured by HRCT was significantly correlated with tumor weight by pathology (r^2=0.98, p<0.0001). These results demonstrate the accuracy of the HRCT scanning method to measure tumor size. Correlation also indicates consistency in tumor density between animals.
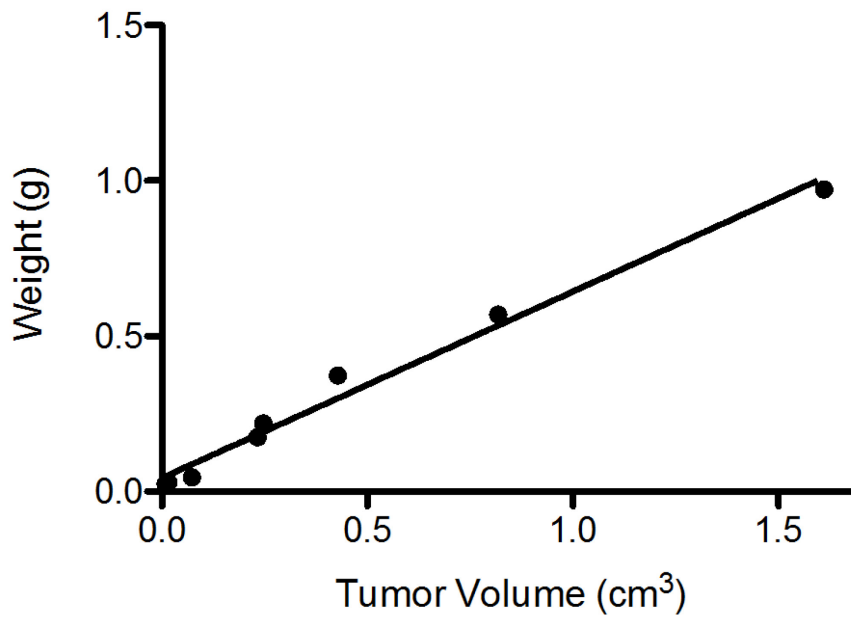
Determining the importance of the pulmonary circulation for lung tumor

establishment

Because the pulmonary circulation is presumed to be essential for tumor establishment, especially in the case of pulmonary metastases, we examined whether the bronchial circulation alone would be adequate for tumor establishment and growth. The left pulmonary artery was ligated immediately prior to adenocarcinoma cell injection (n=5). Animals were sacrificed and tumor weight was measured 4 weeks after adenocarcinoma cell injection. Tumor weights were significantly decreased in animals receiving the pulmonary artery ligation than animals with an intact pulmonary artery (*p=0.018) indicating the importance of the pulmonary circulation for tumor establishment and growth (Fig 6).

Fig 6: Tumor weight after pulmonary artery obstruction

 The pulmonary artery was ligated prior to adenocarcinoma cell injection. Tumor volume was significantly decreased in animals receiving pulmonary artery ligation (p=0.018, n=5).
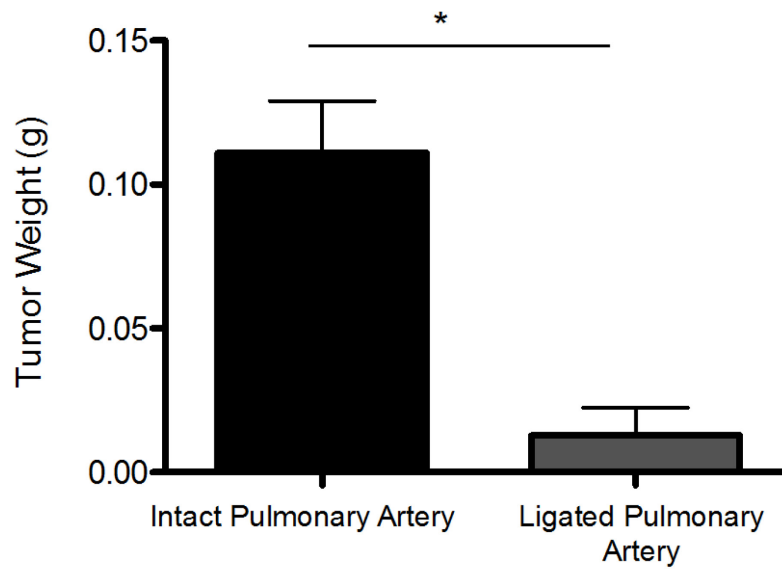
2.4 Discussion:

Models of NSCLC have evolved for decades to keep up with the discovery of new therapeutic targets or mechanism being examined, however the lack of a physiologically relevant lung cancer models has limited mechanistic studies of the vascular sources. Common xenograft models in rodents using the flank lack the circulatory complexity of the lung, and mouse lung models are inadequate due to the fact that mice lack a sub-carinal bronchial vasculature (100). In this study we developed a model that would allow us to quantify changes to the two vascular beds in response to tumor growth.

With the development of this model came measures to confirm that the adenocarcinoma cell injection would result in the formation of a single tumor. Xenografts typically use matrigel vehicles with cancer cell injections to maximize the incidence of tumor formation. We chose to use sterile saline as a vehicle in attempts to create the most native microenvironment for tumor growth. While the exact location of the injection would change slightly between animals, all developed tumors in the lung periphery. Because we were successful with saline, there was no need to include the additional extracellular matrix components with the injection.

In effort to make more refined quantifications of tumor growth than simply measuring tumor diameter in histological sections, we quantified tumor volume by HRCT scan and then measured the weight of each tumor. Not only did the correlation between weight and volume confirm the reproducibility of HRCT volume calculations, it gave us additional insight to the consistency of tumor density between animals. Because of the significant correlation between tumor volume and tumor weight, we concluded that the

42

density of the tumor remained constant between animals as it increased in volume (Fig 4).

By HRCT imaging and histological examination we confirmed that after adenocarcinoma cell injection a small, consistently solid tumors would begin to grow varying slightly in the location of origin depending on injection location. There were no observed necrotic regions in the tumors, or irregular growth patterns depicting a pathologically different subtype of NSCLC when assessed by histology. A progressive increase in tumor volume, as assessed by HRCT scans, and tumor diameter, as assessed by H&E staining, were observed over the course of eight weeks (Fig 2 and 4A). Growth rates varied between animals with differences in final tumor volumes at 8 weeks, with apparent peaks and plateaus in tumor growth from week to week. While the magnitude of growth differs, interestingly all animals seemed to have a plateau in tumor growth between 5 and 7 weeks, followed by an increase in tumor growth between 7 and 8 weeks (Fig 4B). Perhaps these growth patterns could be indicative of neovascularization facilitating further tumor growth.

Morales-Oyarvide and Mino-Kenudson extensively define the pathology of lung adenocarcinomas. They described tumor islands, a method by which lung tumors invade through and fill airways that is unique to the lung, as an atypical means of invasion characterized by the absence of parenchymal destruction (101). In observation of tumor pathology, airway filling and the presence of tumor islands was present in histological sections (Fig2; 4 week image, two airways depict tumor islands). Pezzella and colleagues discussed the alveolar filling pattern where tumors grow efficiently by exploiting the existing vascular network rather than destroying alveolar spaces (102). In

histological sections alveolar filling patterns were extremely common, occurring in every section analyzed (Fig 3 A, B) as well as gland forming, acinar patterns, with micropapillay structures that are hallmarks of adenocarcinomas (Fig 3C). It was evident that the adenocarcinoma cells grown in culture maintained their pathological phenotype of after injection into the lung as assessed by histology.

Since the pulmonary artery has been shown to play a large part in lung tumor perfusion (134) we questioned the importance of the pulmonary circulation for tumor growth. Tumor weight was significantly decreased in animals receiving the pulmonary artery ligation compared to those with an intact pulmonary artery, with two animals that failed to establish a tumor at all. These data indicate the pulmonary circulation is necessary for tumor establishment and growth. While there was a small amount of oxygen in the venous blood in the pulmonary circulation (PO_2=40mm Hg), and since the lung was ventilated creating an oxygen rich environment, perhaps the nutrients and small amount of oxygen in the venous blood from the pulmonary artery were necessary to aid in initial tumor establishment and growth, before the bronchial circulation was large enough to make a substantial contribution to perfusion.

This study focused on one cell line, grown in culture and then injected as a xenograft into the left lung of nude rats. Certainly a bolus of adenocarcinoma cells injected into the lung would not be as precise mechanistically as transgenic models where tumor formation occurs naturally. However considering time constraints, and the desire for a single rapidly growing tumor, a xenograft was the best option. While IHC staining of histological sections was informative and essential for visualization of tumor vasculature, tomato lectin antibodies stained all endothelial cells and did not allow us to

distinguish specifically between the bronchial and pulmonary circulations. Because of

the great heterogeneity of the adenocarcinoma pathological subtype in patients (103),

perhaps an even more relevant model would be to obtain patient samples of lung

adenocarcinomas for xenograft injection.

2.5 Conclusion:

In efforts to design an ideal model for studying the bronchial versus the

pulmonary circulatory involvement in lung tumor perfusion, we developed a

reproducible, physiologically and pathologically relevant orthotopic xenograft model in

nude rats. We observed a progressive increase in tumor size over the course of 8 weeks,

with variation in tumor growth rates and final tumor volumes between animals.

3.0 Quantification of angiogenesis by fluorescent microsphere injection

3.1 Introduction:

In a 1991 publication Auerbach and colleagues wrote, "Perhaps the most consistent limitation to progress in angiogenesis research has been the availability of simple, reliable, reproducible, quantitative assays of the angiogenesis response "(104). Indeed this statement still holds truth 25 years later. One of the biggest challenges in studying lung tumor angiogenesis *in vivo* is finding a simple, reliable, reproducible quantitative model. Determining the best method for quantifying new blood vessel formation is challenging and only made more difficult in a well-vascularized organ like the lung where there is the additional need to distinguish between the original and new vasculature as well as between the pulmonary and bronchial circulations.

Several *in vivo* models have been used to study angiogenesis. Perhaps the most common *in vivo* method over the last 15 years is the chick embryo chorioallantoic membrane (CAM) assay (105, 106). This extra-embryonic membrane mediates gas and nutrient exchange for a chick embryo during the 21 days of development. Neovascularization occurs rapidly, which is ideal for studying angiogenesis and angiogenesis inhibiting drugs (107). Other common models for studying angiogenesis *in vivo* include 3D subcutaneous implantation of matrigel plugs or polymer sponges into the back or flank of mice and rats (108, 109), and more recently zebra fish embryos for studying angiogenesis in tumor xenografts (110) . While these methods have had success in studying general angiogenesis, the differing angiogenic mechanisms in the CAM assay, or in a subcutaneous matrigel plugs decrease their value in studying angiogenesis specific to the lung.

The most direct methods for studying angiogenesis in the lung, which allow for visualization of functional blood vessels, are vascular casting in animal models and vascular angiography in patients (111, 112). Vascular casting involves the injection of a liquid into the vasculature of an animal that will polymerize and harden. The tissues of interest can be dissected and digested or made translucent for visualization of the vascular cast providing an excellent depiction of neovascularization. Vascular angiography is similar but can be done in patients for blood vessel visualization. Typically a contrast medium is injected to highlight the vasculature and images are obtained by X-ray or CT scan. A grading system can be used to quantify the degree of neovascularization in patients with different disease states. Both of these methods are ideal for visualization of a vascular bed, however quantification is not entirely objective. When studying small changes in tumor perfusion from two vascular beds an accurate, quantitative measurement is essential.

Currently the most common way of quantifying angiogenesis in the lung is in an *ex vivo* setting. It is extremely popular in both animal and patient studies of fibrosis, pulmonary hypertension, lung tumors, and ischemia-induced angiogenesis to use microvessel density counting (113-119). In this method of angiogenic assessment, histological sections are created from lung or tumor cross-sections (in animal models) or tumor biopsies from patient samples. These sections are incubated with endothelial cell markers, usually CD31, for identification of endothelial cells. Once the tumor vasculature is outlined by CD31 staining, vessel length, diameter, and endothelial cell count are calculated for a given region of interest. While this method is convenient, and useful in patient samples where tissue is limited, it does not provide much valuable

information in the context of the lung. Since the endothelial cells of the native pulmonary microvasculature will stain positively for CD31 there is no way to distinguish neovascularization from the native vasculature. Proper lung inflation during fixation for histological sectioning is critical. A section of condensed, underinflated lung would have a greater microvessel count/unit area than a lung that was inflated and fixed properly. This method also does not provide any information on the functionality of the vessels.

Additional *ex vivo* measurements of angiogenesis include quantifying circulating growth factors and endothelial cells. Circulating endothelial cells should be rare, but measurable in healthy individuals and have been shown to increase in patients with NSCLC (120). This population of cells can be defined by $CD105^+$, $CD146^+$, $Cd45^-$ markers (121). However, the correlation between circulating endothelial cells, disease prognosis, and progression free survival is still controversial (122-124). Circulating VEGF isoforms, VEGF receptors FLT1, and KDR, fibroblast growth factor (FGF), platelet derived growth factor (PDGF), and several other biomarkers have been used as indicators of angiogenesis in patients with NSCLC (113, 125-127). Vascular analysis by RT-PCR expression of these biomarkers has also been done in patient samples as well as xenograft models in the mouse (128). While all of these ex vivo models are informative and suggestive of an angiogenic response, they do not quantify or visualize neovascularization to the lung or the lung tumor.

Fluorescent microsphere injection has been used previously for quantification of systemic perfusion *in vivo* in models of pulmonary ischemia (69) as well as lung tumor xenograft models in (135). In this method, a predetermined number of labeled microspheres (10-15um) are injected into the systemic circulation where they flow to

peripheral organs and lodge in precapillary beds Use of fluorescent spheres has largely

replaced the use of radiolabelled microspheres used originally by Rudolph and Heymann

(129). Tissues of interest can easily be dissected, digested and fluorescence can be

quantified as total microspheres lodged in a specific tissue, or as a percentage of cardiac

output based on the total number of microspheres injected into the circulation. This

method provides a reproducible, quantitative measurement of functional perfusion (64).

In this study we sought to quantify lung tumor angiogenesis by fluorescent microsphere

injection. By adapting this method to include two different colored microspheres, and

two injection sites, we were able to quantify tumor perfusion from both the pulmonary

and bronchial circulations independently (130).

3.2 Methods:

Blood Flow Determination by Microsphere Injection:

By utilizing two injection sites, quantification of fluorescent microspheres was used to determine tumor perfusion from both the pulmonary and bronchial circulations. Microspheres injected into the aortic arch (via carotid artery catheter) represented the systemic perfusion to the lung and lung tumor, and microspheres injected into the pulmonary artery (via femoral vein catheter) represented the pulmonary perfusion to the lung and lung tumor.

Surgical Procedure:

Rats were anesthetized (2% isoflurane in room air), intubated and ventilated (90 breaths/min; 8ml/kg tidal volume) with a rodent ventilator (model 683, Harvard Apparatus, Holliston, MA). A midline incision was made directly over the trachea with a scalpel, the tissue was dissected to reveal the trachea, and the left carotid artery was isolated. A catheter filled with heparinized saline was placed with a cut down retrograde into the carotid artery, and secured (Methods Fig 2A). Another incision was made on the medial surface of the left hind limb and tissue was dissected to expose the femoral vein. The vein was isolated and a second catheter containing heparinized saline was inserted, and secured (Methods Fig 2B). One million, 10µl yellow polystyrene fluorescent microspheres (1×10^6 spheres/ml; Invitrogen, Eugene, OR) were infused into the femoral vein catheter using a syringe pump (rate: 500 µl/min; Genie Plus, Kent Scientific, Torrington, CT) (Methods Fig 2C). The catheter was flushed with 1ml heparinized saline by perfusion pump (500 µl/min). Subsequently, crimson polystyrene fluorescent

microspheres (1 x 10^6 spheres/ml; Invitrogen, Eugene, OR) were infused through the carotid artery catheter into the aortic arch and that catheter was flushed with a 1ml infusion of heparinized saline. Prior to this systemic microsphere infusion, the left pulmonary artery was transiently occluded (previously described in Chapter 2, methods for left pulmonary artery ligation) to prevent potential recirculation of systemic spheres to the left lung. After this infusion was complete, the rats were exsanguinated and the lungs were extracted. Lung tumors were easily visualized and carefully dissected from lung tissue (Methods Fig 2D).

Methods Fig 2: Surgical procedures for microsphere injection
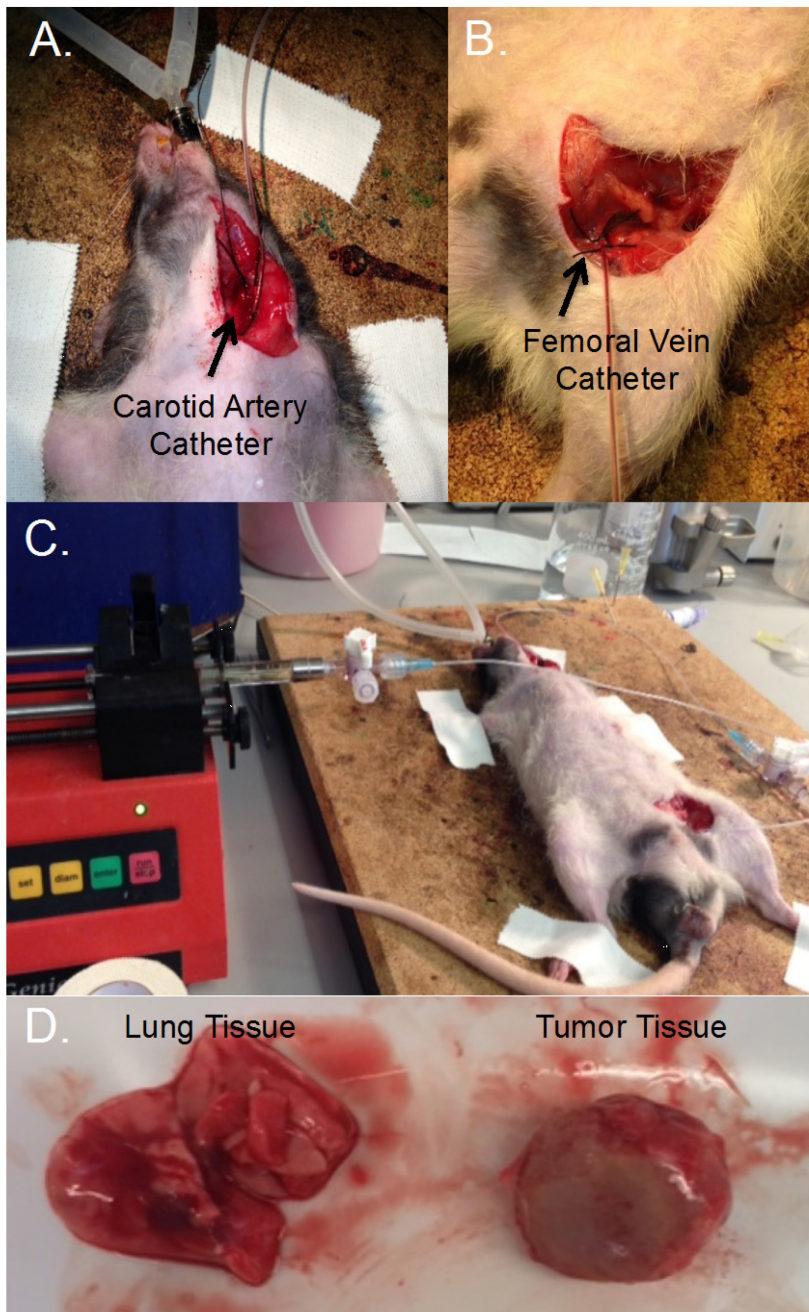
Tissue Digestion and Analysis:

The tumor, left lung, right lung, left kidney, and right kidney (kidneys were used as controls to ensure adequate and consistent systemic perfusion at the time of injection), were weighed and placed in 2M KOH (4-6ml) solution over night at 55°C. Tween 80 (0.25%) was added to wash microspheres and samples were centrifuged (2,000 rpm; 20°C for 10 min) according to methods established by manufacturer (Invitrogen, (64)). Supernatant was removed and 1ml of 2-ethoxyethyl acetate was added to each sample and incubated for 1 hour. Samples were centrifuged again and aqueous layer of 2-ethoxyethyl acetate containing fluorescence was collected and placed in a cuvette. Fluorescence of crimson microspheres (ex-625/em-645) and yellow microspheres (ex-505/em-515) was measured using a Hitachi F-2500 fluorescence spectrophotometer (Digilab, Holliston, MA). Using the slope of the standard curve (microsphere # vs. fluorescence) that was calculated from each bottle of microspheres, we delineated the number of microspheres lodged in each tissue sample.

Table 2: Sample Calculations of one rat for Microsphere Number from Fluorescence

Measured

CRIMSON					
	Fluorescence	Fluorescence corrected (- background)	Weight	Fluorescence/ Weight	Microsphere # (Fluorescence) X (Slope)
LL#1	30	30	0.31	96.77	2614.33
RL#1	153	153	0.7	218.57	13333.10
Tumor #1	65	65	0.37	175.67	**5664.39**
LK#1	467	467	0.78	598.71	40696.48
RK#1	256	256	0.86	297.67	22308.99
YELLOW					
	Fluorescence	Fluorescence corrected (- background)	Weight	Fluorescence/ Weight	Microsphere # (Fluorescence) X (Slope)
LL#1	6760	6620	0.31	21354.83	25156
RL#1	100569	100429	0.7	143470	381630.2
Tumor #1	1207	1067	0.37	2883.78	**4054.6**
LK#1	488	348	0.78	446.15	1322.4
RK#1	260	120	0.86	139.53	456
Tumor Microspheres					
YELLOW	**CHRIMSON**	**Total**	**%pulmonary**	**%bronchial**	
4054.6	**5664.39**	**9718.99**	**41.718**	**58.28**	

Cryomicrotome Imaging of Fluorescent Microspheres

In collaboration with Dr. Robert Glenny at the University of Washington, cryomicrotome imaging was used to visualize fluorescent microspheres from the pulmonary and bronchial circulations lodged in the lung and tumor microvasculature (131). For this imaging protocol, 1 million yellow 15 μm microspheres were infused into the systemic circulation, and 40,000 red 15μm microspheres were infused into the pulmonary circulation by methods previously described (red was used instead of crimson in this case for image optimization). Since the purpose of this experiment was to visualize the bronchial circulation's involvement in tumor perfusion, 40,000 microspheres were sufficient for visualization of the pulmonary circulation without overwhelming the images and impairing the imaging of the bronchial circulation. After microsphere injection 5ml of clear OCT was injected into the trachea to fix the lungs. Heart and lungs were removed *en bloc*, embedded in OCT and sent to Dr. Glenny's laboratory at the University of Washington for lung sectioning and imaging (131).

Briefly, the Imaging Cryomicrotome (Barlow Scientific, Inc., Olympia, WA, USA) sectioned the frozen lung and photographed the tissue auto-fluorescence and FMS distribution at high resolution (131). The Imaging Cryomicrotome consists of a Redlake MegaPlus II ES 3200 digital camera (San Diego, CA, USA) with a resolution of 2184 × 1472 pixels, a metal halide lamp (PE300BF Cermax, Excelitas Technologies, Fremont, CA, USA), and filters limiting the excitation and emission wavelengths. Fluorescence images were acquired with a 180 mm Micro-Nikkon lens (Nikon, Corp., Tokyo, Japan). A custom-built LabVIEW (version 8.2, National Instruments Inc., Austin, TX, USA) application controls the motor, emission and excitation filter wheels, fine-focus, and

image capture and display. The slice thickness was 24μm, and the camera was set at a distance from the sample surface to give an isotropic in-plane resolution of 24μm.

Statistics:

Prism Graphpad software was used to perform the statistical analyses. Linear regression and goodness of fit was used to calculate the correlation total microsphere number (total tumor perfusion) with tumor weight. A paired T-Test (two-tailed) was use to determine significance between perfusion to small and large tumor groups quantified by microsphere injection and an un-paired T-Test and Mann Whitney posttest were used to determine significance between left lung tissue in small and large tumors. An unpaired T-Test (two-tailed) was used to determine significance between the tumor weights at 5 weeks after left pulmonary artery ligation. Significance is represented by *=0.05, **=0.001, ***=0.0001.

3.3 Results:

Tumor Perfusion by fluorescent microsphere injection

In efforts to quantify lung tumor angiogenesis it was essential to utilize a functional measurement of tumor perfusion. In naïve rats, less than 0.5% (~5,000 microspheres) of the cardiac output could be detected by systemic microspheres in the left lung. We observed a significant correlation between total tumor perfusion (total microsphere number; pulmonary+ bronchial microspheres) and tumor weight (p=0.017; Fig 7A). When pulmonary and bronchial circulations were examined individually, similar patterns were observed. Both microspheres from pulmonary circulation (p= 0.0170) and bronchial circulation (p<0.0001) were significantly correlated with tumor weight (Fig 7B).

Figure 7: Tumor perfusion measured by microsphere injection

A) The total number of microspheres counted in the tumor (bronchial + pulmonary perfusion) was significantly correlated with tumor weight (r^2= 0.365; p=0.017).

B) Total microspheres from both the pulmonary circulation (r^2=0.3652, p= 0.0170) and the bronchial circulation (r^2=0.7671, p< 0.0001) are significantly correlated with tumor weight.
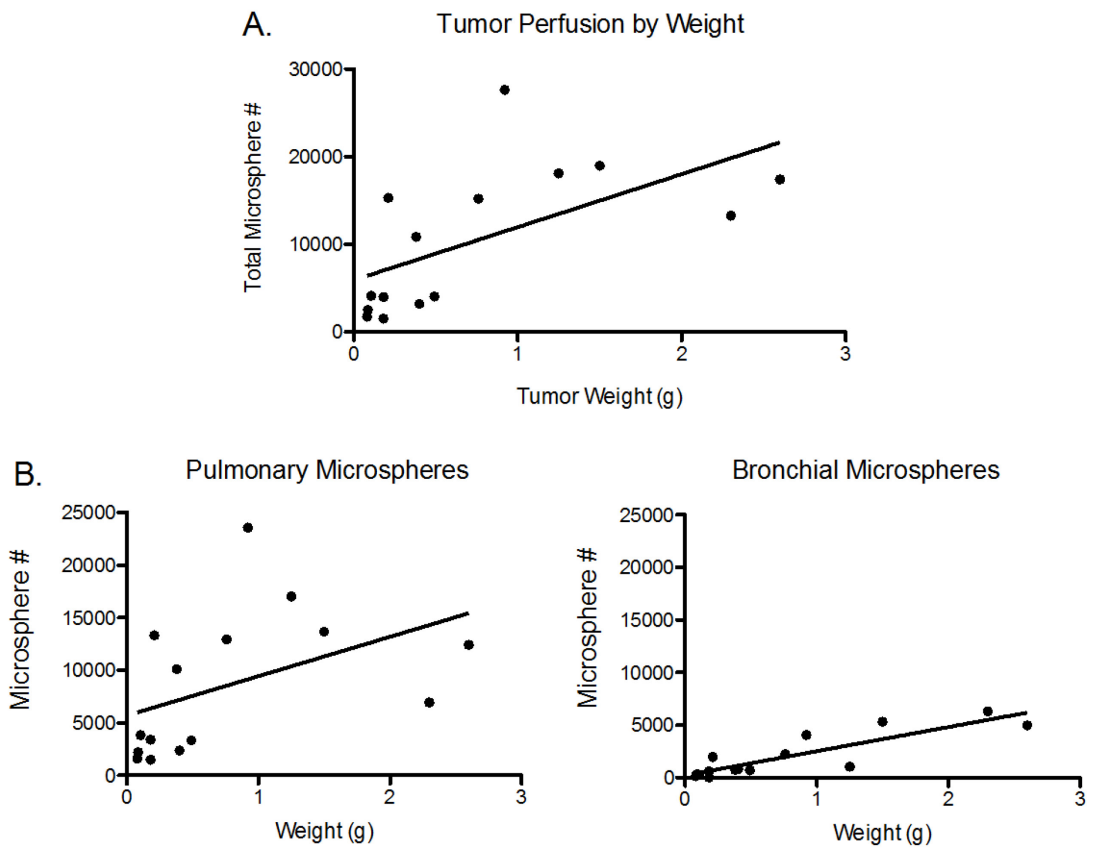
Originally, when quantifying tumor perfusion we examined each circulation's contribution from 4-12 weeks after adenocarcinoma cell injection. Because of variable tumor growth rates between animals, confirmed by HRCT scanning, tumor weight and perfusion were variable at any given time point. Since we observed a correlation between total tumor perfusion and tumor weight, all subsequent perfusion measurements were correlated with tumor size instead of a pre-selected time point after adenocarcinoma cell injection. We divided tumors into two groups by weight; large tumors (>0.5g) and small tumors (<0.5g) and quantified total tumor perfusion from each circulation. The percentage of total tumor perfusion from the pulmonary circulation is significantly decreased in large tumors, and the percentage of total tumor perfusion from the bronchial circulation is significantly increased in large tumors (p=0.003; Fig 8A, B).

Figure 8: Tumor perfusion in small and large tumors

When tumors were partitioned into two groups by weight (small;<0.5g vs. large; >0.5g),

A) The large tumors had a significant decrease compared to the small tumors in the percentage of

microspheres from the pulmonary circulation (**p=0.003). B) Coinciding with a significantly

higher percentage of microspheres from the bronchial circulation in large tumors than small

tumors (**p=0.003).
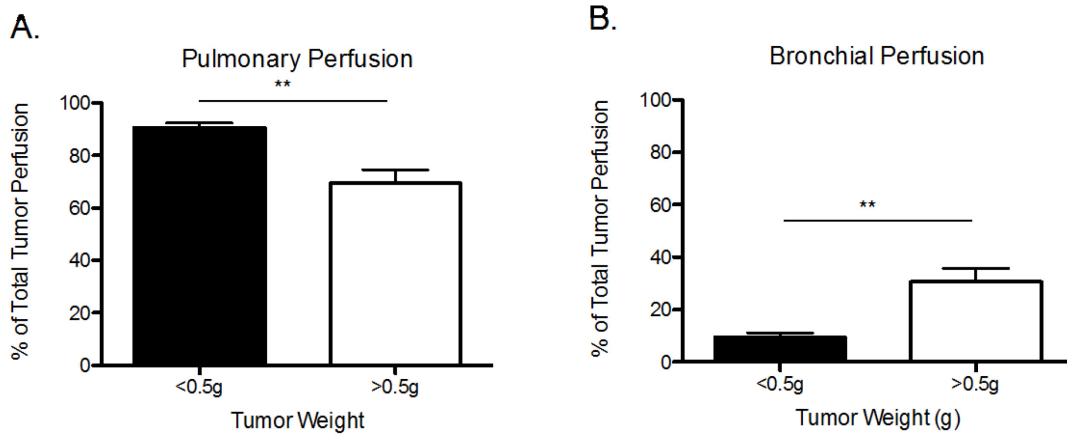
Left lung perfusion by microsphere injection

When quantifying tumor perfusion from each circulation it was also of interest to quantify perfusion to the remaining tissue from the left lung to determine if angiogenesis was isolated to only the tumor or if there were global changes to the entire left lung. There was no significant change in pulmonary circulation (p=0.73) or bronchial circulation (p=0.12) to the left lung between animals with small or large tumors indicating that neovascularization was localized to the tumor (Fig 9A,B).

Figure 9: Tumor perfusion from pulmonary and bronchial circulations does not increase in left lung tissue.

Microspheres from the pulmonary and bronchial circulations in the left lung tissue surrounding the tumor were quantified. There was no change to A) the pulmonary circulation in the left lung between small and large tumors (p=0.73) or B) the bronchial circulation in the left lung between small and large tumors (p=0.12).
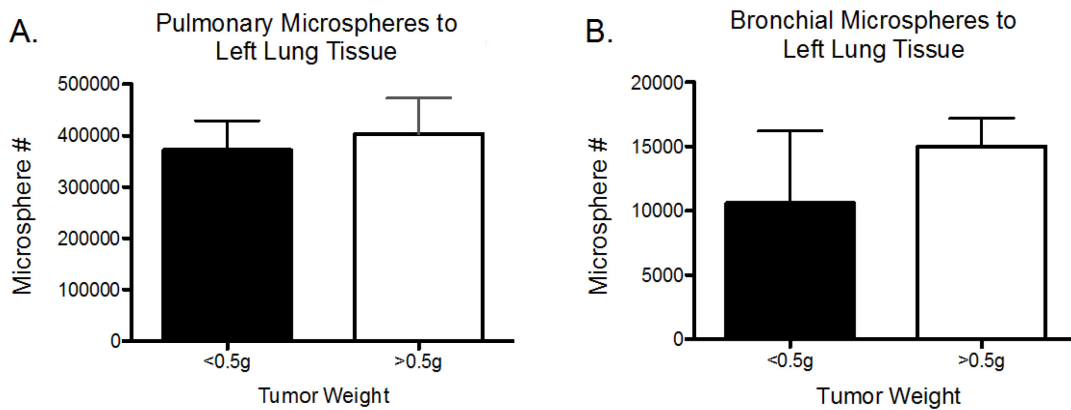
Microsphere Visualization by Cryomicrotome Imaging

After quantifying lung and tumor perfusion by fluorescent microsphere injection, we sought to visualize the fluorescent microspheres and their location in a tumor using cryomicrotome imaging. The bronchial circulation was well defined in lung cross-section images with clear lodging of microspheres in bronchial vessels (indicated by red arrows) in the mainstem bronchi. Other small systemic vessels, originating from the aorta and esophagus, could be visualized by fluorescent microspheres as well. (A and E in Fig 10C). Clusters of microspheres can be seen throughout the tumor as well as sporadically throughout the lungs depicting the bronchial vessels (Fig 10C). The pulmonary circulation was well defined by red fluorescent microspheres spread diffusely throughout the pulmonary capillaries and tumor (Fig 10D).

Figure 10: Cryomicrotome Imaging for visualization of fluorescent microspheres

Approximately 2,000 lung sections from base to apex of lung were imaged, each section 24μm thick. A) Caudal view of lungs and heart section embedded in black OCT block. B) Section in UV light exposure highlights collagen for depiction of heart; lung structures (RB-right Bronchus, LB- Left Bronchus, LV- Left Ventricle and tumor. C) Depiction of microspheres lodging in the bronchial circulation of the lung and tumor. Right mainstem bronchus (RB) and Left mainstem bronchus (LB) can be visualized with systemic microspheres lodging in bronchial arteries (indicated by red arrows). Systemic microspheres can also be seen lodged in the descending aorta (A) and esophagus (E). D) Depiction of microspheres lodging in the pulmonary capillaries of the lung and tumor. Pulmonary microspheres are diffuse throughout the lung and lung tumor.
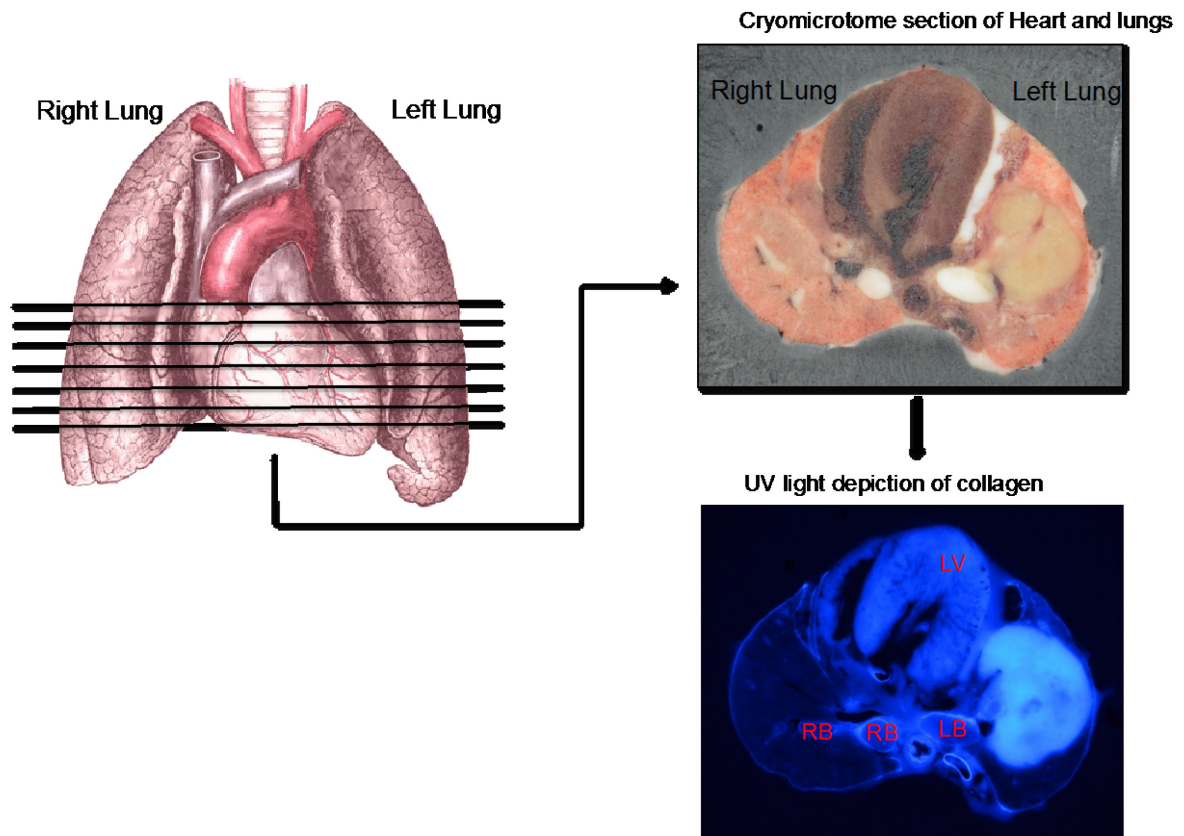
Figure 10: Continued

Systemic Microsphere Injection
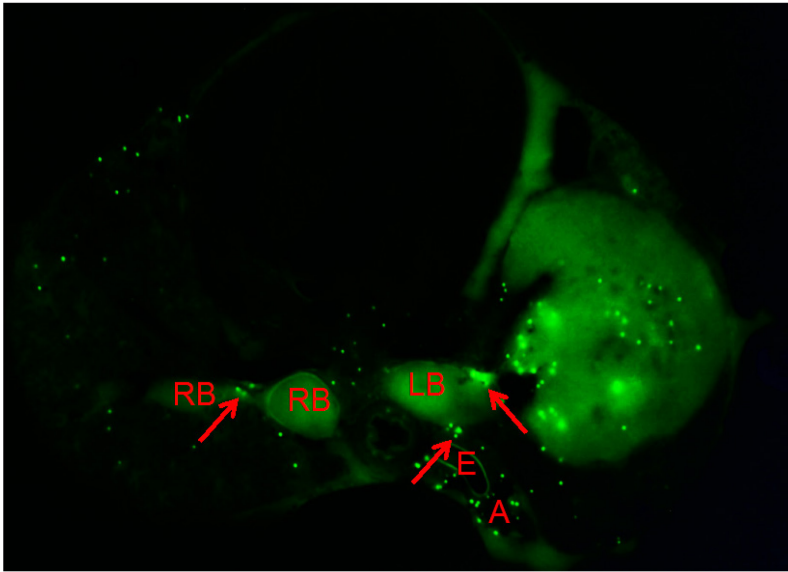
Pulmonary Microsphere Injection
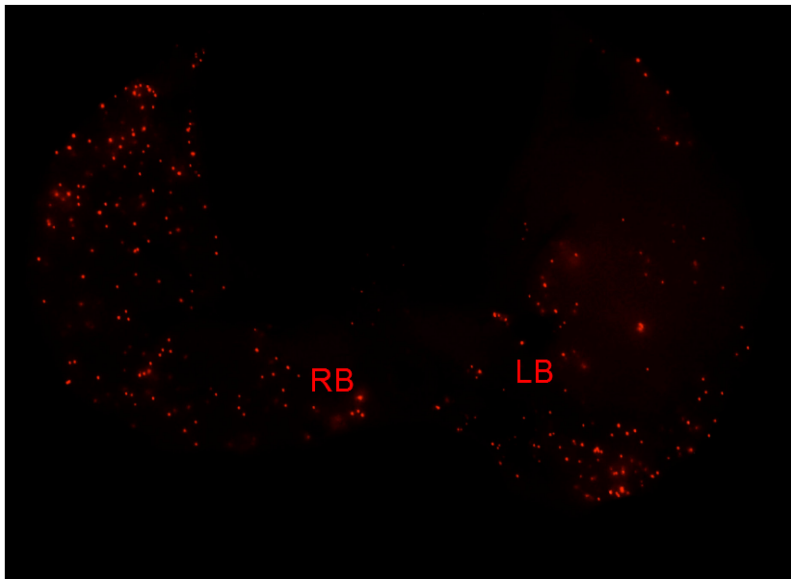
3.4 Discussion:

Previous studies describing the pro-angiogenic phenotype of the bronchial artery in lung disease begged the question of its role in lung tumor perfusion. While there are conflicting reports suggesting each circulations involvement in tumor growth (66, 67, 130), the goals of this study were to address this question using a functional measurement of quantifying tumor perfusion in the newly developed model of NSCLC. The use of fluorescent microsphere injection for quantification of angiogenesis was previously used in our lab in a model of pulmonary ischemia (64, 132, 133). Adapting the protocol to include two different colored microspheres and two injection sites in an already established method that allowed quantification of tumor perfusion from the bronchial and pulmonary circulations independently.

When examining tumor perfusion at a wide range of tumor sizes, the total number of microspheres lodged in each tumor was significantly correlated with tumor size. It is not surprising that tumor perfusion would increase with tumor size, and since there were no cases in which a tumor grew without an increase in perfusion, this correlation suggested that tumor growth was reliant on an increase in tumor perfusion. Although we see the increase in total perfusion, it is unclear from this observation if angiogenesis is occurring or these tumors were growing around the existing vasculature.

When the bronchial and pulmonary circulations were examined separately, each showed an increase in perfusion with tumor size. The correlation of the bronchial circulation with tumor weight was highly significant ($p < 0.0001$) indicating that while perfusion from both circulations increased with tumor size, the bronchial circulation had more significant change. Because tumor growth and increased perfusion could occur

without angiogenesis if the tumor was simply growing around the existing pulmonary and bronchial circulations, this initial examination of correlations alone was not sufficient to determine if angiogenesis was occurring.

In order to better address angiogenesis of each bed, microspheres from the pulmonary and bronchial circulations were totaled and each circulation was assessed as a percentage of total tumor perfusion. In small tumors (<0.5g) the pulmonary circulation accounted for approximately 90% of the total tumor perfusion and significantly decreasing to 69% of total tumor perfusion in large tumors (>0.5g). Subsequently, the bronchial circulation increased from 10% of total tumor perfusion in small tumors to 31% in large tumors resulting in a 227% increase in bronchial perfusion between small and large tumors. While the pulmonary tumor perfusion was not changing, the percent of total tumor perfusion from the pulmonary circulation was decreasing coinciding with the increase in the percent of total tumor perfusion from the bronchial circulation. If angiogenesis was occurring in the pulmonary circulation equaling that of the bronchial circulation, the percentage of total tumor perfusion from each circulation should not change. Therefore, we infer that the pulmonary circulation remained unchanged and the bronchial circulation increased as tumor size increased.

Visualization of fluorescent microspheres was possible by cryomicrotome imaging. For the purpose of these images alone, 96% less microspheres were injected into the pulmonary circulation than the bronchial circulation. The resulting images depict a pulmonary circulation, which appears to look the same in the lung tumor as in the surrounding lung tissue. It is hard to distinguish in the images of the pulmonary circulation where the lung tissue ends and the tumor tissue begins. The bronchial

circulation was also well defined in these images. Because of OCT filling the airways it was easy to find the major airways and corresponding bronchial vessels where fluorescent microspheres were lodged. Microspheres infused through the aorta defined the entire systemic vasculature, which can be depicted in small vessels branching from the aorta and esophagus where microspheres had lodged. Additional bronchial vessels were observed sparsely throughout the lung depicted by microspheres in the lung parenchyma, however the majority of microspheres were lodged in the tumor vasculature. Though perfusion measurements were not possible from these images, the tumor tissue did appear to have more bronchial microspheres (42 spheres visible) in this specific cross-section than the right lung (27 spheres visible). Some auto fluorescence was observed in the tumor throughout lung sections, however this did not interfere with visualization of microspheres from the bronchial circulation. These images, while not quantitative, confirm the data from our perfusion measurements that the bronchial circulation is increasing in response to tumor growth.

In models of pulmonary ischemia and asthma (69,70) bronchial angiogenesis occurs throughout the airway tree. Because of these observations, we questioned if bronchial artery angiogenesis was localized to only the lung tumor or the rest of the left lung tissue as well. There was no change in the pulmonary or bronchial circulation to the left lung between animals that had small or large tumors. These data suggest that bronchial artery angiogenesis was occurring within the tumor. It could be hypothesized that pro-angiogenic growth factors secreted by a growing lung tumor were acting locally on adjacent bronchial vessels versus circulating growth factors acting on the entire bronchial circulation.

While fluorescent microsphere quantification of angiogenesis has many advantages there were some shortcomings to this method. With this method we assumed the 10μm microspheres were lodging in the capillaries of the tumor, however there was no way to visualize the microspheres in each animal before perfusion quantification. Great lengths were taken to visualize the fluorescent microspheres in a few animals that could not be used for quantification. This method also required some flexibility with tumor size since tumor growth rates varied between animals and a tumor could not be visualized before the experiment.

3.5 Conclusion:

Tumor perfusion from the pulmonary and bronchial circulations was determined using two different colored fluorescent microspheres and two injection sites. This method provided a functional and reproducible way of quantifying angiogenesis *in vivo*. We observed a significant correlation between total tumor perfusion and tumor size, as well as pulmonary and bronchial perfusion with tumor size. The percentage of total tumor perfusion from the bronchial circulation significantly increased in large tumors and bronchial angiogenesis was specific to tumor tissue Further *in vivo* quantification of angiogenesis from the bronchial and pulmonary circulations need to be done to confirm the results observed from this study.

4.0 Quantification of tumor perfusion by contrast enhanced HRCT scanning

4.1 Introduction:

Bronchial artery angiogenesis has been implicated in several lung disease states, though lung tumor angiogenesis specifically from the bronchial artery is still controversial (63, 64, 134-137). As early as 1967, a postmortem study revealed a dual vascular supply in lung tumors (138). However, quantification of these vascular beds was not possible until more recently leading to the controversial topic of which circulation was primarily responsible for sustaining lung tumor growth.

Vascular imaging studies have increased in popularity because of their value in diagnosis and determining the effectiveness of angiogenesis inhibiting drugs in both primary and metastatic lung cancer (139-141). Nambu and colleagues conducted a small study (9 patients) of hemodynamics by bronchial arteriography after thoracic irradiation therapy with different subtypes of lung cancer. Bronchial angiogenesis was observed in patients who developed radiation pneumonitis. The bronchial arteries in these patients were unaffected by the thoracic irradiation therapy, and subsequently bronchial artery infusion of anti-cancer agents was performed with excellent outcomes (142). Yuan et al. recently outlined a detailed method for contrast enhanced CT scanning to quantify tumor perfusion. They concluded that the bronchial circulation was dominant and tumor circulation was moderately dependent on tumor size (66). Complimenting this finding, Nguyen-Kim and colleagues also described tumor perfusion to be reliant on tumor size as well as histological subtype utilizing similar methods of blood flow quantification by CT scanning (67). While these studies advanced imaging protocols for bronchial perfusion

70

and provided information on potential vascular relationships with tumor size, the fact that they were performed in patients limited the ability for multiple scanning and surgical interventions that could be possible in an animal model.

Adapting HRCT scanning protocols from patient studies to animal models is essential for acquiring more detailed information regarded tumor vasculature/size relationships. Quantification of the bronchial perfusion in Sprague Dawley rats by contrast enhanced micro-CT was performed to image the dual circulations of the lung with and without pulmonary occlusion surgery (143). In a model of hepatocellular carcinoma, perfusion CT scans were used to quantify hepatic perfusion index, transit time, liver distribution volume, and arterial and portal blood flow independently (144). Rat models of angiogenesis, gliomas, prostate cancer, and liver cirrhosis have all utilized perfusion CT imaging for hemodynamic studies (145-148).

In this study, we sought to confirm the increase in bronchial circulation that was observed by fluorescent microsphere injection by using a more refined technique of perfusion quantification, contrast enhanced HRCT scanning. Given the common bronchial artery manipulations in patients with NSCLC, we ablated the bronchial circulation to confirm its essential role in lung tumor growth.

4.2 Methods:

Quantification of tumor perfusion by contrast enhanced CT imaging.

Contrast enhanced CT imaging was used to quantify tumor perfusion from the bronchial and pulmonary circulations independently.

Rats were anesthetized with a ketamine/xylazine/DiH$_2$O (1:1:2) solution. An incision was made on the medial surface of the left hind limb and tissue was dissected to expose the femoral vein. The vein was isolated and a catheter containing heparinized saline was inserted and secure in the vein. Contrast medium (Visipaque 320, GE Healthcare, Little Chalfont, Buckinghamshire, United Kingdom) was infused through the femoral catheter during HRCT scan.

Methods Fig 3: Tumor perfusion quantified by contrast enhanced HRCT scan
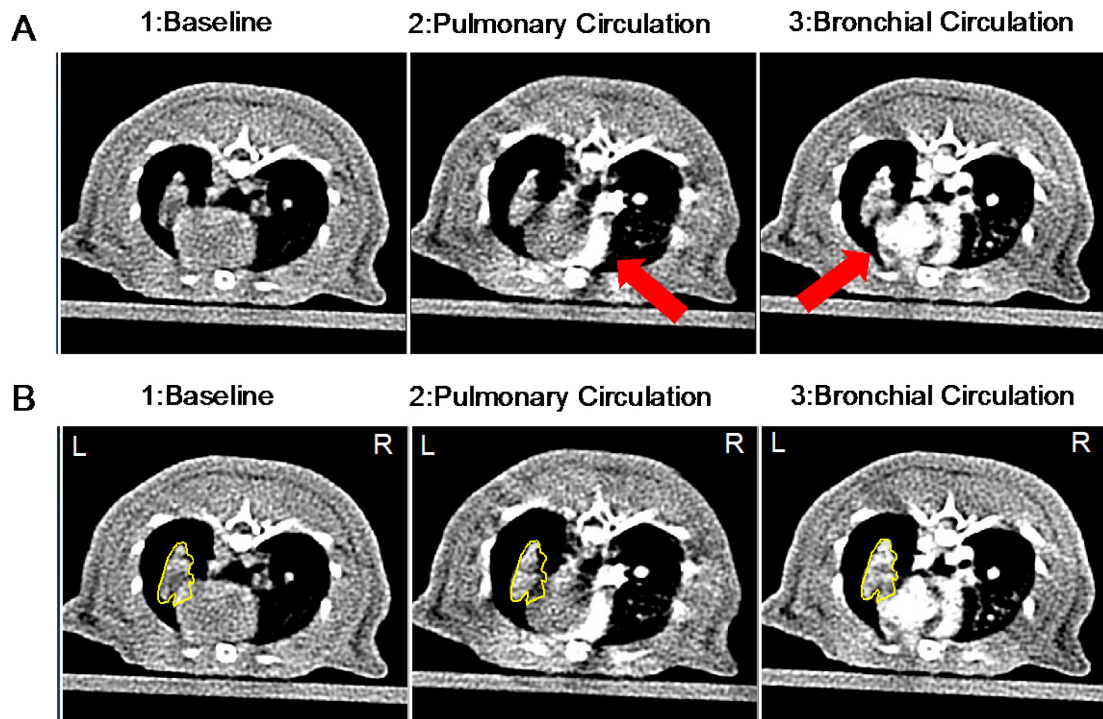
After the baseline scans were acquired (far left images top and bottom), repeated total thoracic scans were acquired while intravenous (IV) contrast medium (0.25% Visipaque) was injected through a femoral venous catheter. Approximately 50 images covering the thorax from apex to base were repeatedly acquired every 0.1 seconds during the contrast infusion over a total 9-second time interval. From the repeatedly acquired thoracic scans, we selected 3 sets of HRCT chest scans: 1) at baseline (prior to IV contrast, far left top and bottom), 2) on the first pass of the IV contrast through the right heart and into the pulmonary circulation (middle top and bottom), and 3) after the IV contrast passed through the right heart, the pulmonary circulation, the left heart, and into the systemic circulation (far right top and bottom).

On the three HRCT thoracic image sets, a Region of Interest (ROI) was drawn around the lung tumor perimeter on every scan where the tumor could be identified (methods fig 4, bottom left, middle and right). To determine perfusion to the tumor, the mean intensity (HU) of the tumor was measured during IV contrast infusion. On each of the three thoracic images sets, the mean intensity of the tumor ROI was calculated on each slice. The overall mean HU intensity for the tumor for each rat at each time point was then averaged over all the scans in that HRCT image set.

Any increase in tumor contrast intensity during the first pass of the IV contrast through the right heart and the pulmonary circulation, but not yet in the left heart was considered due to the pulmonary circulation alone (methods fig 4, middle top). Any increase in tumor intensity after the IV contrast passed through the right heart, the pulmonary circulation, and the left heart, was considered due to the pulmonary and the systemic

(bronchial) circulations (methods fig 4, right top). In order to determine the contribution

of the bronchial circulation alone, we subtracted the tumor contrast intensity after

contrast passed through the right heart, the pulmonary circulation, and the left heart

(methods fig 4, right top) from the tumor intensity after the IV contrast passed through

the right heart and the pulmonary circulation (methods fig 4, middle top).

Table 3: Sample calculation of ROI intensity

ROI	Baseline Intensity	Pulmonary Intensity	Bronchial Intensity
1	-88.355	-74.216	77.271
2	-43.497	63.995	31.238
3	-56.405	-25.96	20.234
4	-24.054	7.66	22.664
5	0.918	29.209	4.983
6	4.611	18.191	2.84
7	19.74	41.363	2.379
8	12.846	37.379	6.267
9	23.756	-6.616	14.646
10	34.356	32.595	30.358
11	13.555	33.354	35.377
12	31.265	28.511	45.721
13	40.983	37.861	40.359
14	21.057	19.648	46.283
15	8.018	16.363	32.562
16	6.342	24.749	36.042
17	12.956	31.18	48.027
18	25.731	29.485	44.729
19	18.921	32.211	39.851
20	32.166	29.303	43.514
21	38.974	26.328	44.962
22	33.48	36.111	46.105
23	44.721	28.078	53.42
24	35.78	30.636	63.351
25	42.045	41.161	70.462
26	39.732	25.549	56.639
27	25.346	22.73	66.451
28	21.725	8.029	67.234
29	14.834	-0.469	67.904
30	26.141	31.933	51.905
31	1.495	-78.698	53.362
32	-15.997	-48.158	37.921

B.

	Column 1: Mean Intensity of ROI	Column 2: (-) Baseline	Column 3: (-) Pulmonary	Intensity/ max intensity (784 HU)
Baseline	12.59			
Pulmonary	16.54	3.95		**0.005**
Bronchial	40.78	28.19	24.24	**0.031**

Note: Intensity values range from -1000 to 1000 Hounsfield units (HU). (-1000: Blood, 0: Air, 1000: Bone)

Table 3: Sample calculation of ROI intensity

A) After the perfusion scan, images were divided into three time points: baseline, pulmonary circulation and bronchial circulation. A region of interested was draw around the tumor in each image and mean intensity for each region of interest was measured. This was repeated for every image that the tumor was visible (in this case 32 images).

B) The average intensity for all 32 images was calculated for each time point (column 1). The intensity of the baseline perfusion was subtracted from both the pulmonary and bronchial perfusion time points (column 2). The intensity of the pulmonary perfusion was then subtracted from the bronchial perfusion time point to calculate only the intensity from the bronchial circulation (column 3). To normalize the values and account for any differences in the rate or

quantity of IV contrast delivered between animals or in the same animal on different days, the

measured pixel intensities in the tumor were divided by the maximum intensity detected in the

initial bolus of IV contrast in the IVC of the rat.

HRCT scanner settings:
    Collimator: 128 x 0.6mm
    Kernel: H70h Very Sharp
    Effective mAs: 350
    kV: 120
    Scan time: 6 sec + 2 sec delay
    Slice: 0.6 x 0.4mm
    Time increment: 0.05 sec
    Lung window: Width-1600 Level-500
    Field of View: 50 mm
    Reconstructions: Standard filtered back projection

Bronchial Artery Ablation:

To confirm the role of the bronchial artery in lung tumor growth we eliminated the left

branch of the bronchial artery and measured tumor volume 4 weeks after ablation

surgery.

After an initial measurement of tumor volume by HRCT 4 weeks after adenocarcinoma

cell injection, rats were anesthetized in 2% isoflurane with room air. The anesthetized rat

was intubated, placed on a ventilator, and a transverse incision was made into the skin

covering the thorax on the left side. A thoracotomy was performed between the 4th and 5th

rib. The left lung was repositioned with forceps and the airway was exposed to visualize

bronchial arteries on the dorsal surface of the left main stem bronchus. Bronchial arteries were cauterized using a Gemini Cautery System (Braintree Scientific, Braintree, MA). In sham animals, the same surgical procedure was followed, but an intercostal artery was cauterized instead of the bronchial artery. The lungs were hyper-inflated to reestablish thoracic pressure as the thorax was closed with 4-0 suture (Myco Medical, Cary NC). Sensorcaine (Bupivacaine 2mg/kg) was injected at the site of the incision for analgesia and the incision was closed with methyl acrylamide adhesive. The rats were allowed to recover on the ventilator breathing room air (5-10 breaths/minutes), then were extubated and returned to their cages.

Validation of contrast enhanced CT imaging in established model of bronchial angiogenesis:

Quantifying the bronchial circulation by contrast enhanced HRCT scan was performed in an established model of bronchial angiogenesis to validate scanning measurements. All protocols were approved by the Johns Hopkins and Washington University Animal Care and Use Committees. Male Brown Norway rats (BN, Charles River, 100 g) were anesthetized with 2% isoflurane and room air. Rats were then given house dust mite allergen (HDM, Der p 1; 50 l g/challenge, Greer Laboratories) by intranasal aspiration twice/week for 1, 2, or 3 weeks duration. Contrast enhanced HRCT scanning was performed 2 days after the last intranasal challenge of HDM.

Validation of perfusion quantification by contrast enhanced HRCT scanning

Representative images of lungs from Naïve vs. HDM treated rats showed increased bronchial circulation, made visible by the infusion of contrast medium into the vasculature (indicated by red arrows) after HDM treatment. Intensity (Hounsfield Units; HU) was measured for regions of interest including the left and right lungs then totaled for each image slice comprising the entire lung from apex to base. This initial study of 7 animals showed an increase in bronchial circulation after 1, 2 and 3 weeks of HDM treatments. Most important, these studies confirmed that the HRCT protocol could separate and quantify the pulmonary and bronchial circulations by contrast enhanced HRCT scanning.

Increased bronchial circulation observed in HDM treated rats

Contrast Enhanced HRCT scanning was used to quantify the bronchial circulation in HDM treated rats. A) In a model that has previously shown an increase in bronchial vessels after HDM treatment, we confirmed that the increased bronchial vessels could be detected by contrast enhanced HRCT scan. Increased bronchial perfusion can be seen in representative scan from an animal treated with HDM for 3 weeks (indicated by red arrows). B) An increase in intensity from the bronchial circulation was observed by contrast enhanced HRCT scan 1,2 and 3 weeks after HDM treatment in a pilot study of 7 animals.
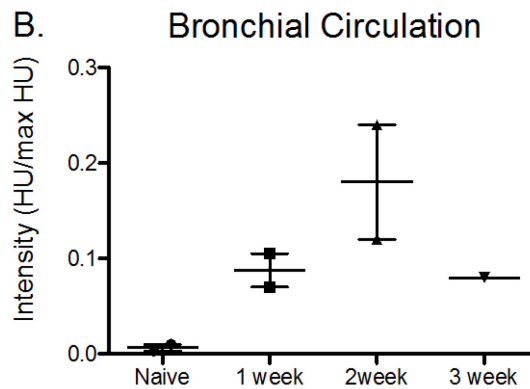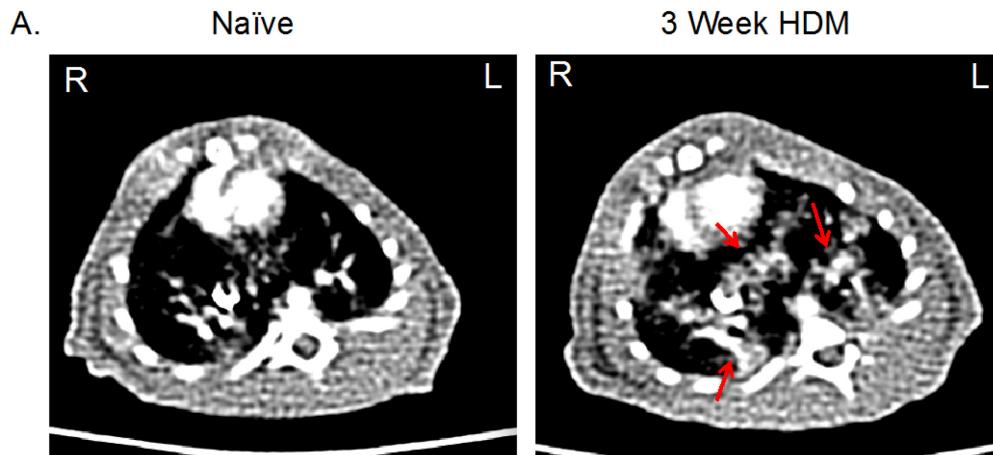
Statistics:

Prism Graphpad software was used to perform the statistical analyses. Linear regression and goodness of fit was used to calculate the correlation of tumor intensity (HU) with tumor weight. A paired T-Test (two-tailed) was use to determine significance between perfusion to small and large tumor groups quantified by intensity. An unpaired T-Test (two-tailed) was used to determine significance between the change in tumor volume and the final tumor volumes at 8 weeks with an intact BA or ablated BA. Significance was considered to be $p \leq 0.05$.

4.3 Results:

Tumor perfusion quantification by HRCT scanning

We quantified tumor volume and tumor perfusion from the pulmonary and bronchial circulations in 11 different animals. Tumor volumes ranged from 0.01 to 1.5 cm^3. Tumor perfusion from the bronchial circulation was significantly correlated with tumor volume (r^2=0.56; p=0.005) (Fig 11A). When tumors were partitioned by volume into groups of small tumors (<0.3cm^3) versus large tumors (>0.3cm^3) significantly greater bronchial perfusion was observed in large tumors (p<0.0001; Fig 11B). Unlike the bronchial circulation, there was no difference in pulmonary perfusion with tumor size (Fig 12A), and no change in pulmonary perfusion between small and large tumors (Fig 12B).

Fig11: Bronchial tumor perfusion increases with tumor volume

Bronchial tumor perfusion was determined by contrast enhanced HRCT scanning.

A) Tumor perfusion (intensity of contrast medium Hounsfield units (HU) as a fraction of maximum HU [also see methods]) from the bronchial circulation was significantly correlated with tumor volume (r^2=0.56; p=0.005; n=11). B) When tumors were partitioned by volume (<0.3cm^3 vs. >0.3cm^3) there was a significantly greater bronchial perfusion to the larger tumors (***p<0.0001).
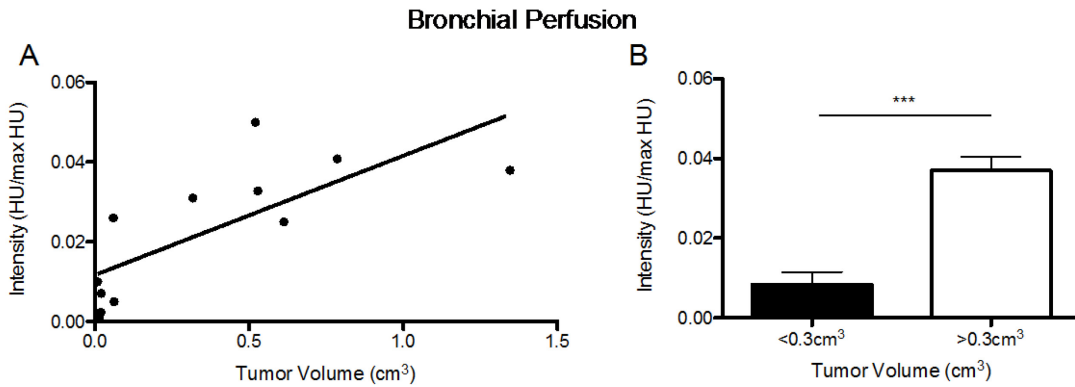
Fig 12. Pulmonary tumor perfusion does not change with tumor volume

Pulmonary tumor perfusion was determined by contrast enhanced HRCT scanning.

(A) In contrast to the bronchial circulation there was no difference in pulmonary perfusion as measured by contrast enhanced HRCT by tumor volume, and B) When tumors were partitioned by volume ($<0.3cm^3$ vs. $>0.3cm^3$) there was no significant difference in pulmonary perfusion between small and large tumors.
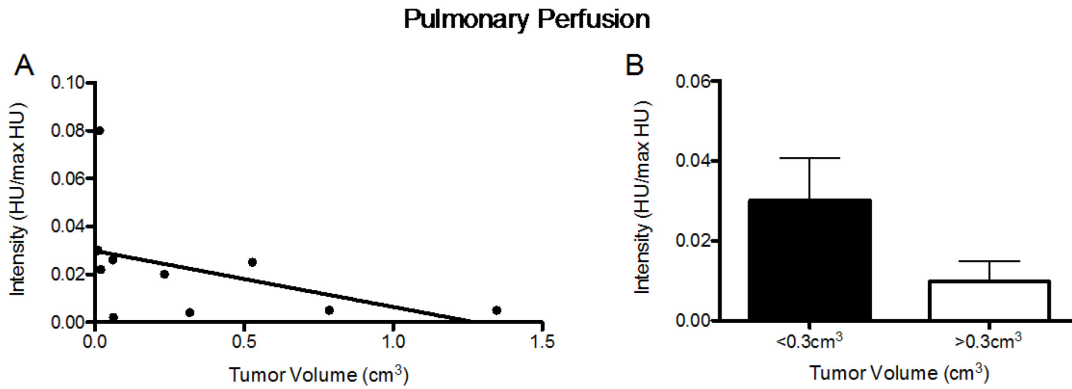
Tumor volume assessment after bronchial artery ablation

Because we observed an increase in bronchial perfusion with tumor size, we examined tumor growth after the bronchial artery was ablated. Animals in which the bronchial artery was ablated little to no change in tumor volume occurred over 4 weeks. In several cases, tumor volumes decreased after ablation surgery and in a single case a tumor was no longer detectible by CT scan. One animal in which the bronchial artery was ablated (indicated by blue point) had recruited blood vessels visible by gross dissection from the chest wall and subsequently had an increase in tumor volume over 4 weeks (Fig 13A). The two animals receiving a sham surgery (indicated by red points in Fig 13) had the largest final tumor volumes compared to animals receiving the bronchial artery ablation surgery. Initial and final tumor volumes between 4 and 8 weeks after adenocarcinoma cell injection were calculated in animals with an intact bronchial artery or sham (indicated by triangles) compared to animals in which the bronchial artery was ablated. Animals with intact bronchial arteries had increasing tumor volumes between 4 and 8 weeks in contrast to the animals receiving bronchial ablation surgery that had no tumor growth (Fig 13B). In the bronchial artery ablation group, there were significantly less changes in tumor volumes between 4 and 8 weeks (P=0.0009; Fig 14A) and significantly smaller final tumor volumes at 8 weeks (p=0.0076; Fig 14B) compared to the sham group.

Fig 13: Tumor volume assessed by HRCT scan after bronchial artery ablation

Tumor volume was calculated weekly after bronchial artery ablation.

A) Initial tumor volume measurements were taken by HRCT scan immediately prior to bronchial artery ablation surgery. Subsequent volume measurements were taken to track tumor volume for 4 weeks after BA ablation. Sham animals (see methods; indicated by red points, n=2) had the largest tumor volumes 4 weeks after surgery. Animals receiving BA ablation surgery had a decrease, or no change in tumor volume over 4 weeks, and one animal (indicated by blue point) had recruited blood vessels from the chest wall and showed an increase in tumor volume over 4 weeks. B) Initial and final tumor volumes between 4 and 8 weeks after adenocarcinoma cell injection were calculated from animals with an intact BA or sham (indicated by triangles; n=8), compared to animals receiving bronchial artery ablation surgery (n=6). Animals with intact BAs have an increase in tumor volume between 4 and 8 weeks that was not observed in animals receiving bronchial ablation surgery.
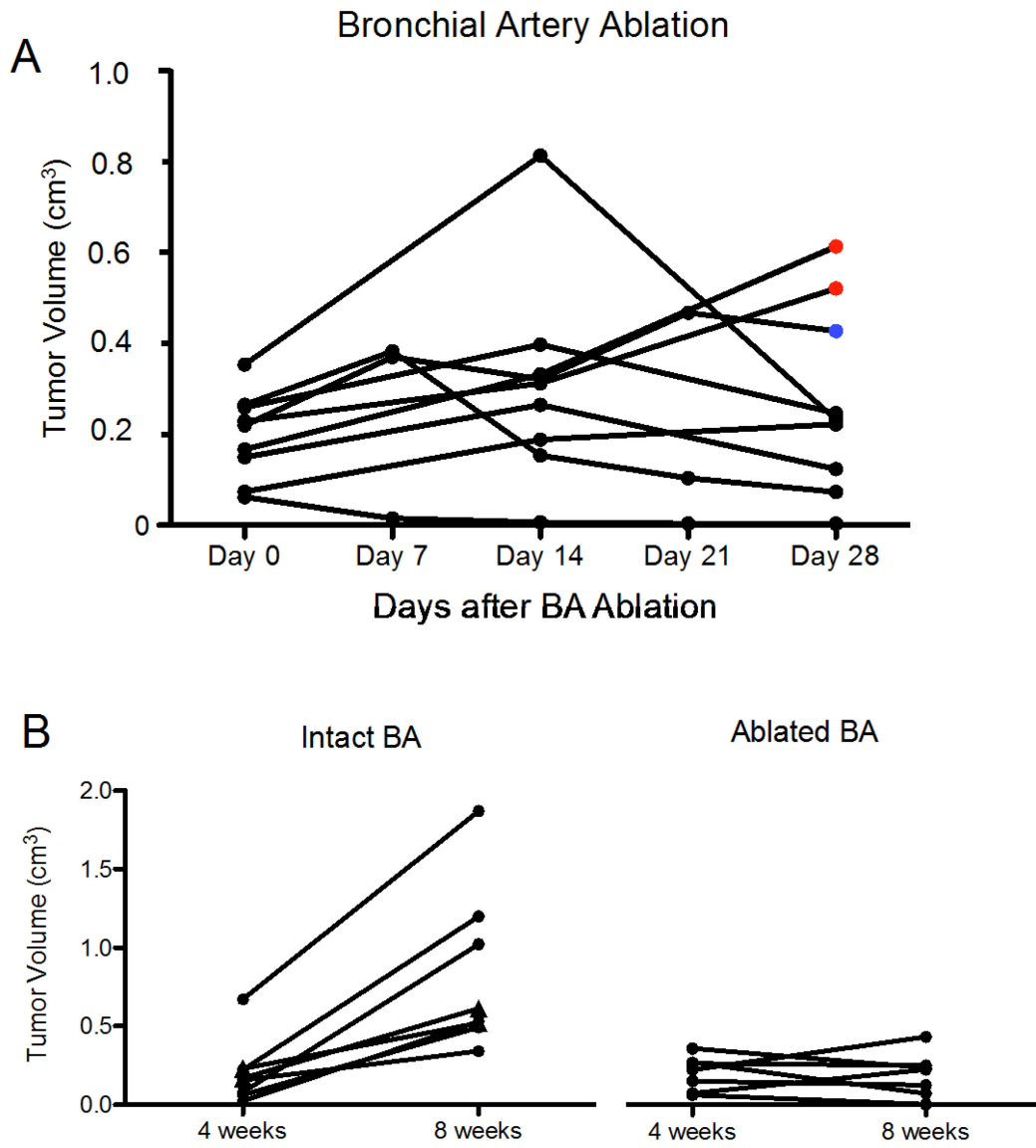
Fig 14. Change in tumor volume and final tumor volumes with Intact vs. Ablated BA.

Tumor volumes were assessed by HRCT scans four weeks after bronchial artery ablation. A) There was significantly less change in tumor volume between 4 and 8 weeks in animals with bronchial artery ablation (**p=0.0009). B) At 8 weeks, tumor volume were significantly decreased in rats after BA ablation (**p=0.0076).
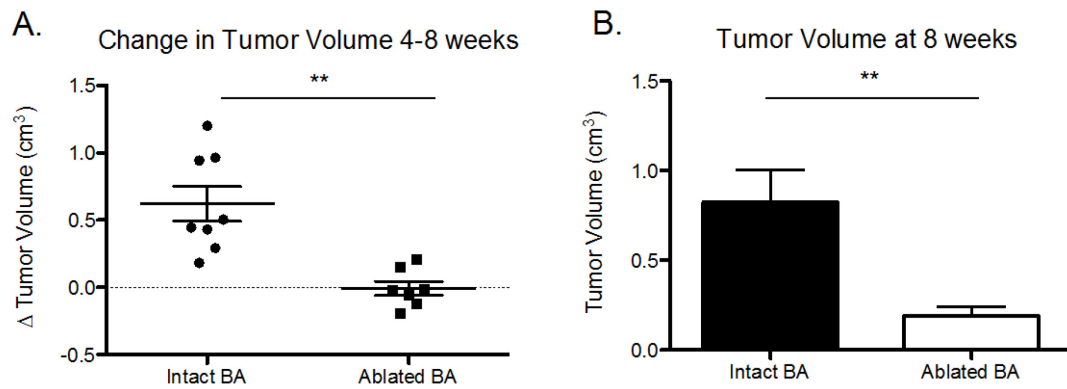
To confirm that the bronchial artery ablation surgery did attenuate the bronchial circulation from lung tumors, we use contrast enhanced HRCT scanning to quantify tumor perfusion. In the 6 animals that received the bronchial artery ablation, bronchial tumor perfusion was decreased compared to animals with intact bronchial arteries. There was no correlation between bronchial perfusion and tumor volume in animals after bronchial artery ablation, indicating that ablation was effective in diminishing bronchial tumor perfusion (Fig 15).

Fig 15: Attenuation of bronchial perfusion confirmed by perfusion CT scan.

The systemic perfusion four weeks after bronchial artery cauterization was measured by perfusion CT scan (represented in red). Bronchial tumor perfusion was less than normal perfusion patterns observed with intact bronchial artery. The slope is not significantly different from zero (p= 0.33).
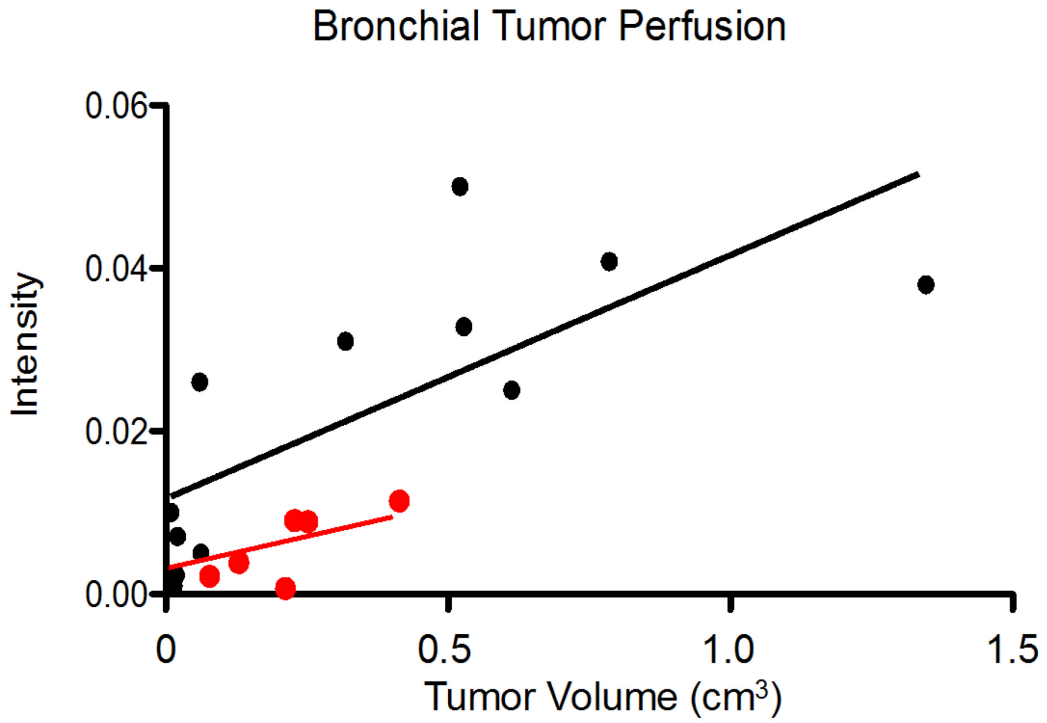
4.4 Discussion:

While previous studies using HRCT scanning to quantify the lung's circulations in tumor perfusion were successful in patients, we were uncertain if this method of perfusion quantification could be translated to a small animal model. Wieholt and colleagues successfully quantified bronchial perfusion by HRCT scanning in the rat after pulmonary artery obstruction where there was increased bronchial circulation (143). When developing a protocol for quantification of tumor perfusion by contrast enhanced HRCT scanning, we validated our technique in an already established model of bronchial angiogenesis.

We previously quantified tumor perfusion by fluorescent microsphere injection, and while the data obtained was valuable, and showed a correlation between tumor size and bronchial perfusion, there was only an estimate of tumor size before the experiment took place. The use of HRCT made it possible to monitor tumor growth longitudinally and quantify tumor perfusion at predetermined tumor volumes. This refined method provided the ability to acquire perfusion data from a complete range of tumor volumes instead of estimating tumor volume based on time after adenocarcinoma cell injection, which was shown to vary between animals.

With perfusion HRCT the overall change in perfusion confirmed the results quantified by fluorescent microsphere injection. In small tumors, systemic bronchial perfusion contributed approximately 21% of total perfusion. In large tumors, greater than $0.3cm^3$ median volume, bronchial perfusion contributed approximately 79% of total tumor perfusion resulting in an increased average bronchial tumor perfusion of 276% between small and large tumors. Despite the increase in bronchial circulation, there was

no change in pulmonary circulation to tumor perfusion. While it appears that the pulmonary circulation decreases from small to large tumors, the results were not significant, suggesting that pulmonary circulation is not correlated with tumor size and does not increase as tumor size increases.

While the percentages of tumor perfusion contributed between small and large tumors from the bronchial circulation were much lower when measured by fluorescent microsphere injection (~10% in small vs. 30% of total tumor perfusion in large tumors) the magnitude of average increase in bronchial perfusion between small and large tumors (206% vs. 276%) was quite similar. Differences in magnitude of the initial perfusion with the two methods can likely be attributed to the different tumor sizing methods (weight vs. calculated volume) and different median tumor sizes for the analysis. Importantly, both perfusion measurements demonstrated that the bronchial circulation increased with tumor size and the pulmonary circulation remained relatively constant and did not increase with tumor size. These functional results demonstrate that the bronchial circulation undergoes angiogenesis to support the needs of the growing lung tumor over the course of 8 weeks, while the pulmonary vasculature remains unchanged.

Beginning in 1969, bronchial artery infusion therapy was used as a route for more direct delivery of chemotherapy to lung tumors in patients with lung cancer (149). Such approaches to treat NSCLC and hepatocellular carcinoma lung metastases are still being used (150, 151). It is also common for patients with NSCLC to experience life-threatening hemoptysis, and for decades it has been routine practice to embolize small branches of the bronchial artery as an effective treatment (152, 153). In cases where bronchial artery embolization has been performed, there have been no reports on how this

procedure specifically alters tumor growth. Since only small branches of the bronchial artery are typically embolized and patients generally are also undergoing chemotherapy, results of embolization on lung tumor growth have not been established.

To further confirm the critical role of bronchial angiogenesis in tumor growth, we surgically intervened and studied subsequent tumor growth after the elimination of the bronchial circulation. After 4 weeks of tumor growth, the left bronchial artery was cauterized. After this ablation, we observed small changes in tumor volume in weekly, or biweekly measurements of tumor growth. While growth rates between animals varied slightly there was no overall change in tumor volume for at least 4 weeks after the surgical intervention. Final tumor volumes at 8 weeks were significantly smaller than the 8 week tumor volumes in animals with an intact bronchial artery. Perfusion measurements made at the corresponding 8 week tumor volume determination confirmed the continued absence of any new systemic blood flow, as determined by the significant decrease in the both the baseline and slope of the relationship between bronchial perfusion and tumor size.

In this study, we integrated imaging protocols for quantifying lung tumor perfusion typically found in patient studies and adapted them for a model of NSCLC in the rat. Our data compliments patient findings that tumor perfusion from the bronchial circulation is dependent on tumor size, but given the use of an animal model we had the ability to track tumor volume before perfusion measurements to depict a more complete tumor volume/perfusion relationship than was observed in patient studies. The animal model also afforded us the ability to surgically ablate the bronchial circulation and continually track tumor growth after surgery. A decrease in tumor growth and final

tumor volumes suggested the essential role of bronchial artery angiogenesis in lung tumor growth.

4.5 Conclusion:

From contrast enhanced HRCT scanning we observed an increase in tumor perfusion from the bronchial circulation that correlated with tumor size. There was no change in tumor perfusion from the pulmonary circulation. Because of the inhibition of tumor growth after bronchial artery ablation, we concluded that angiogenesis of the bronchial circulation was critical for tumor growth. Without new blood vessels supplied by the systemic bronchial vasculature, lung tumors could not grow beyond a minimal size that could be supported by the pulmonary circulation alone.

5.0 Potential mechanisms of angiogenesis and endothelial cell heterogeneity

5.1 Introduction:

Angiogenesis promoting tumor growth in the lung is unique because of the dual circulations responsible for tumor perfusion. Studying the ability of each circulation to undergo angiogenesis individually, in the context of tumor growth, provides new potential for the discovery of new drug therapies that can specifically target a single vasculature therefore eliminating global side effects typically seen from current anti-angiogenic drugs. A better understanding of the mechanisms of angiogenesis, and how endothelial cells from the pulmonary and bronchial circulations differ in their angiogenic phenotype, is the first step to understanding lung tumor angiogenesis.

Angiogenesis can occur through both sprouting and non-sprouting processes (29). Sprouting angiogenesis involve the formation of new capillaries from pre-existing vessels beginning with angiogenic stimuli, the most common being vascular endothelial growth factor (VEGF). The responsiveness of an endothelial cell is dictated by levels of VEGF receptor activation and NOTCH signaling in response to a VEGF gradient (154). In addition to cellular activation, VEGF is responsible for cell migration, vessel dilation, and permeability (155). After a VEGF gradient is established to guide endothelial sprouting, the local extracellular matrix is degraded to allow for endothelial cell migration. Proliferation of endothelial cells, at the branching end of the migration column, begin to elongate and organize into three dimensional tubes eventually forming a new capillary lumen (29). VEGF, Interleukin-8 (IL-8), basic fibroblast growth factor (bFGF), angiopoietins, and matrix metalloproteinases (MMPs) tightly regulate the

process of endothelial sprouting through matrix degradation and endothelial cell stimulation (156). Non-sprouting angiogenesis involves the enlargement, splitting and fusion of pre-existing vessels relying on endothelial proliferation within the vessel walls. Both sprouting and non-sprouting angiogenesis have been shown to be involved in tumor angiogenesis (157).

In addition to the complex role of VEGF in vessel sprouting, Interleukin-8 (IL-8) has been shown to play a large role in regulating angiogenesis. IL-8 is a CXC chemokine, which are ELR+ (glutamic acid, leucine, arginine) that can be stored in endothelial cells or secreted by macrophages and mediates immune responses through its powerful chemoattractant properties. IL-8 is responsible for endothelial cell proliferation, capillary tube formation, and MMP production (158). The silencing of IL-8 and the blocking of its receptor (CXCR2) has led to the inhibition of angiogenesis (132, 159).

Because lung tumors have been shown to use several methods of vascularization outside of vessel sprouting, including vasculogenesis, vessel co-option, and vasculogenic mimicry, it is reasonable to suggest that tumor vascularization could be dictated by the innate properties of each circulation. The innate properties of each circulation's ability to undergo angiogenesis are a direct representation of the endothelial cells in each vascular bed. Examining heterogeneity between endothelial cells of the pulmonary and bronchial circulation could explain the differences between each circulation's responses to lung tumor growth.

Endothelial cells have shown great heterogeneity between organ systems, vascular beds within an organ system, and even cells within the same region of a single vascular

bed (160). Endothelial cells are responsible for vessel permeability, leukocyte trafficking, vasomotor tone and angiogenesis. The structure of endothelium lining capillaries can be continuous, fenestrated, or discontinuous depending on the function of that specific vascular bed (160). A continuous endothelium, as in the lung, is responsible for tightly regulating permeability and transport of fluids and solutes across cell barriers, while a fenestrated endothelium can be found in the kidneys where filtration and secretion occur (161, 162).

Several studies have investigated differences in the endothelium of the pulmonary circulation (170). The endothelium of the pulmonary circulation contrasts greatly between the large pulmonary artery, smaller arterioles, and the microvasculature (171). Differences between the endothelium's role in barrier function between sections of the pulmonary circulation have been of great interest given the vital role of barrier function in maintain efficient gas exchange. Microarray analysis revealed differential gene expression of cellular adhesion molecules in microvascular endothelial cells compared to pulmonary artery endothelial cells contributing to highly regulated tight junctions and decreased permeability (172, 173). Differences in leukocyte trafficking, expression of calcium channels and cell surface markers have been observed between endothelial cells of the pulmonary artery and microvasculature (174, 175). While heterogeneity of the endothelium in the pulmonary circulation has been examined, little is known about the bronchial endothelium responses relative to the pulmonary endothelium.

In this study we examined endothelial cell heterogeneity specifically as it relates to angiogenesis. Through assays of proliferation, chemotaxis and tube formation we quantified the angiogenic potential of endothelial cells from the bronchial artery,

pulmonary artery and pulmonary microvasculature in their response to angiogenic stimuli. By examining the innate differences in the angiogenic phenotype of each endothelial cell type we obtained a better understanding of the differences between the pulmonary and bronchial circulations' contrasting angiogenic phenotype.

5.2 Methods:

PCR Array: Left lung, right lung, and lung tumors were collected and rapidly frozen in liquid nitrogen from naïve rats, and 1, 4 and 9 weeks after adenocarcinoma cell injection. RNA was isolated from tissue according to the RNeasy mini kit protocol (Qiagen, Hilden Germany). All samples were run in Angiogenesis RT^2 Profiler PCR Arrays (Qiagen; http://www.sabiosciences.com/rt_pcr_product/HTML/PAHS-024A.html) for both rat and human. Array included:

Angiogenic Factors:

Growth Factors and Receptors: Angpt1 (Agpt), Bai1, Col18a1, Ctgf, Ereg, Fgf1, Fgf2, Fgf6, Fgf16, Fgfr3, Figf (Vegf-d), Flt1, Fzd5, Itgav, Jag1, Kdr, Nrp1, Pgf, Tek, Vegfa, Vegfb, Vegfc.

Adhesion Molecules: Col18a1, Ctgf, Eng, Itga5, Itgav, Nrp1, Tek.

Proteases, Inhibitors and Other Matrix Proteins: Anpep, Col4a3, Fn1, Mmp19, Serpinb5, Serpinf1.

Transcription Factors and Others: Angpt2 (Agpt2), Epas1, Mapk14, Tbx4.

Other Factors Involved in Angiogenesis:

Cytokines and Chemokines: Ccl2, Cxcl1 (GRO), Cxcl2 (GRO2), Cxcl9, Ifna1, Ifnb1, Ifng, Il1b, Il6, Tnf.

Other Growth Factors and Receptors: S1pr1, Efna5, Egf, Hgf, Igf1, Itgb3, Lep, Mdk, Npr1, Nrp2, Pdgfa, Pdgfb, Tgfa, Tgfb1, Tgfb2, Tgfb3, Tgfbr1.

Adhesion Molecules: Cdh5, Itgb3, Lama5, Nrp2, Pecam1, Thbs4.

Proteases, Inhibitors and Other Matrix Proteins: Tymp, F2 (CF-2), Mmp2, Mmp3, Mmp9, Plau, Plg, Timp1, Timp2, Timp3.

Transcription Factors and Others: Akt1, Efna1 (Ephrin A1), Efna2, Hif1a, Id1, Id3, Lect1, Ptgs1, Sphk1

Endothelial Cell Isolation:

Bronchial artery, pulmonary artery, femoral artery and aorta were dissected from RNU nude rats. Arteries were washed in DMEM and antibiotics, cut in 0.5mm pieces and placed in growth factor reduced matrigel (Corning Life Sciences, Tewksbury, MA) coated 24 well dishes, lumen side down. Tissue sections were incubated for 20minutes before media (20%FBS and Endothelial Cell Growth Supplement, EMD Millipore, Darmstadt, Germany) was added to wells. Tissue was removed after 5 days of culture and cells were allowed to grow until confluent in well. Cells were trypsinized and cultured in T25 flasks until confluent at which point they were purified by using a Biotin Selection Kit (Stemcell Technologies, Vancouver, BC). Biotinylated tomato Lectin (Vector Laboratories, Burlingame, CA) was used for positive endothelial cell selection (176, 177) and cells were purified using magnetic nanoparticles (Stemcell Technologies) according to the manufacturer's protocol. Pure populations of endothelial cells were cultured on T25 flasks and angiogenic potential was measured between passages 3 and 6. In all

subsequent experiments, samples were run in triplicates for cells from each animal. Cell lines were isolated from 6 different animals, and samples from each animal were run in triplicate for each in vitro determination of angiogenesis (n=6).

Pulmonary microvasculature endothelial cell isolation: Lungs were dissected from RNU nude rats and sections from peripheral lung parenchyma, devoid of large vessels, were cut from remaining lung tissue. Tissue was minced and incubated with 1% collagenase (Worthington, Lakewood, NJ) and incubated at $37^{o}C$ for 15minutes. Red blood cells were removed using 3ml ACK lysing buffer (Quality Biological, Gaithersburg, MD) for 5 min on ice. Cells were collected and washed thoroughly with cold DMEM and cultured on T25 flasks coated in 0.2% gelatin. Endothelial cells were purified as previously described.

Stimuli used for *in vitro* angiogenic assays:

To determine the angiogenic potential of each endothelial cell type, *in vitro* cultures were treated with three different angiogenic stimuli. Recombinant human VEGF (R&D systems, Minneapolis, MN) was used in 10 and 100ng/ml concentrations. Rat CINC3/CXCL2, Cytokine-Induced Neutrophil Chemoattractant-3 (R&D systems, Minneapolis, MN) was also used in 10 and 100ng/ml concentrations as stimulus. A confluent T75 flask of adenocarcinoma cells were incubated for 24 hours with 10% FBS to yield the adenocarcinoma supernatant used as the third angiogenic stimuli for *in vitro* assays of angiogenesis.

Fluorescence-activated Cell Sorting (FACS) analysis of cultured cells for proliferation:

To determine differences in proliferation between endothelial cell types we used Ki67 intracellular staining, an antigen found exclusively in the nucleus during interphase, as an indication of cell proliferation.

Endothelial cells grown in culture ($5x10^3$) isolated from the bronchial artery, pulmonary artery, and pulmonary microvasculature were seeded in triplicate on 12 well dishes coated in 0.2% gelatin. Cells were incubated with angiogenic stimuli: rhVEGF, CINC3 and adenocarcinoma culture supernatant. Cells were trypsinized, washed in cold DMEM, and stained for FACS analysis of proliferation. Cells were incubated with endothelial cell marker, FITC conjugated Tomato Lectin (*Lycopersicon esculentum*, Sigma-Aldrich) for 30minutes on ice, washed and stained for live cell selection using VIVID (Invitrogen, Grand Island, NY). For cell proliferation marker, cells were incubated with Fixation/Permeabilization buffer (Ebiosciences, San Diego CA) for 30minutes on ice, then washed and incubated with Ki67 (PE, BD Pharmingen, San Jose, CA). Cell counts were acquired on a BD FACSaria (BD, San Jose, CA). Data was analyzed with FlowJo Software (Tree Star, Ashland, OR).

Chemotaxis Assay:

To determine the potential for each endothelial cell type to move toward an angiogenic stimulus we used a transwell migration assay.

Chemotaxis to angiogenic stimuli: rhVEGF, CINC3 and adenocarcinoma culture supernatant, was determined using transwell, 12 well plates (6.5mm diameter inserts, 5.0μm pore size polycarbonate transwell membrane, Corning Incorporated, Corning, NY). $5x10^3$ endothelial cells from in vitro cultures of the bronchial artery, pulmonary artery and pulmonary microvasculature were cultured in triplicate on upper chamber of transwell inserts in 2% FBS, while stimulus was added to lower chamber. Cultures were incubated for 24hours. Transwell inserts were removed and remaining cells in lower chamber were counted using a hemocytometer.

Tube Formation Assay:

To determine the differences between endothelial cell types in their ability to form tubes in response to angiogenic stimuli, we cultured cells in 3D matrigel conditions and quantified the total tube lengths of cells in culture.

Endothelial cells from the bronchial artery, pulmonary artery and pulmonary microvasculature were cultured in 12 well dishes coated with growth factor reduced matrigel. $5x10^4$ cells were added to 3 wells/ cell type in DMEM with 2% FBS. Tube formation in the presence of angiogenic was determined 24 hours after cells had been cultured. 3 representative images of each well were obtained (Olympus IX51 microscope, Olympus, Center Valley, PA and High Performance SensiCam, Cooke, Auburn Hills, MI) and tube lengths per image were measured (indicated by red arrows; methods Fig 6).

Total tube lengths of connecting cells were measured by use of Image Pro Plus 5.1

software (Media Cybernetics, Bethesda, MD).

Methods Fig 6: Quantification of Tube Formation
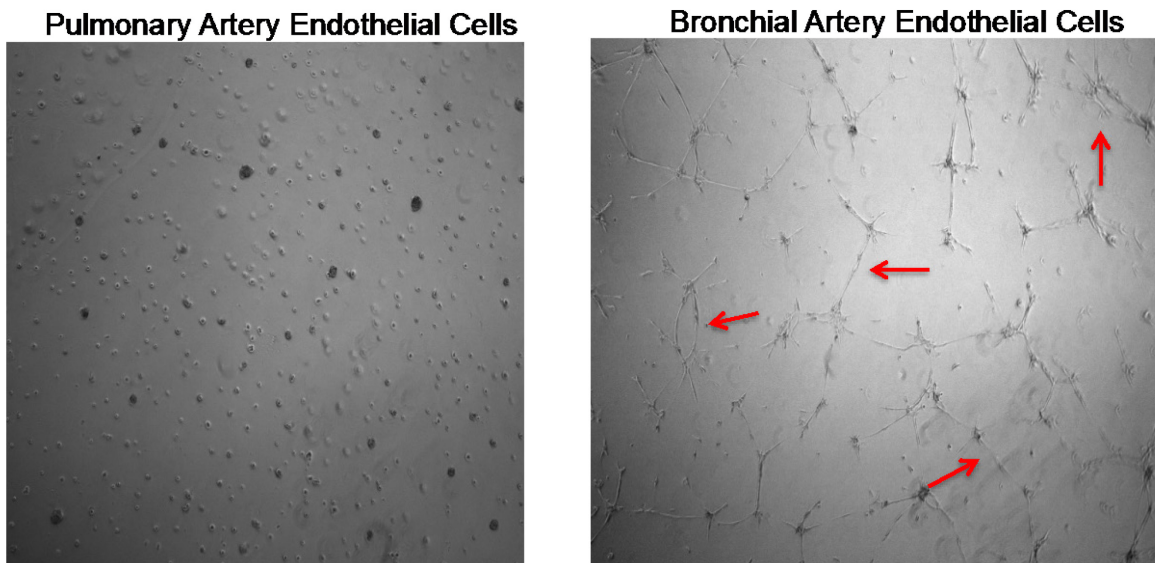
Statistics:

Prism Graphpad software was used to calculate statistics. A One-way ANOVA

with Bonferroni's adjustment for multiple comparisons was used to calculate the

significance between endothelial cell types for proliferation, chemotaxis, and tube

formation assays. Significance was considered $p \leq 0.05$.

5.3 Results:

Survey of angiogenic factors involved in lung tumor angiogenesis by PCR array

A PCR array was used to determine the gene expression of proteins related to angiogenesis in both the tumor and lung tissue 2, 4 and 9 weeks after adenocarcinoma cell injection. While this was a survey of proteins involved in angiogenesis in a limited sample size, in general there was an increase in gene expression of the left lung tissue 4 weeks after adenocarcinoma cell injection that was not observed at 9 weeks. This included proteins responsible for degrading the extracellular matrix during angiogenesis: (MMP 2, 9, 19, 14), PLAU (Urokinase-type plasminogen activator), and Alanyl Membrane Aminopeptidase (Anpep). Tumor associated membrane protein (TMP) responsible for endothelial membrane disruption, and Fibronectin1 (FN1) involved in the remodeling of extracellular matrix were also increased at only 4 weeks (Table 1). In addition to extracellular matrix related proteins, the vast majority of angiogenic growth factors were increased at only at 4 weeks including VEGF A, B and VEGF receptors, transforming growth factor (TGF) alpha and beta, and fibroblast growth factor (FGF) (Table 2).

Table 4: Survey of matrix degrading enzymes of rat left lung tissue

Gene expression of extracellular matrix proteins involved in angiogenesis showed an increase in matrix degrading proteins at 4 weeks after adenocarcinoma cell injection compared to naïve left lung tissue.

Matrix Components	2weeks	4weeks	9weeks
Anpep	1.56	13.64	2.45
Col4a3	1.75	7.21	1.45
Fn1	-1.01	4.56	1.62
Mmp14	1.97	19.56	1.49
Mmp19	-1.07	4.17	-33.59
Mmp2	1.45	6.82	2.97
Mmp9	2.55	5.62	18.13
Plau	2.17	19.29	3.81
Tymp	1.79	8.22	-1.34

Table 5:PCR array of angiogenic growth factors in the left lung

Gene expression of angiogenic growth factors from rat left lung tissue were increased at 4 weeks after adenocarcinoma cell injection compared to naïve left lung tissue.

Growth Factors

	2weeks	4weeks	9weeks
Ang	2.57	4.82	-5.1
Angpt2	-1.67	3.92	-2.36
Egf	2.17	11.24	2.16
Erbb2	1.65	8.75	6.77
Fgf1	3.2	12.47	6.77
Fgfr3	1.32	9.92	3.51
Figf	-1.42	6.28	1.33
Flt1	1.73	6.45	2.64
Hgf	1.23	4.59	1.18
Itga5	2.11	9.45	4.23
Itgav	1.31	5.39	1.66
Kdr	1.39	5.74	1.75
Nrp1	1.27	10.27	2.99
Nrp2	1.44	8.22	3.84
Pdgfa	1.66	6.96	2.77
Pdgfb	1.06	7.73	-1.52
S1pr1	-1.11	4.59	2.03
Tek	1.18	4.63	1.39
Tgfa	2.43	11.24	-2.71
Tgfb1	2.14	8.46	3.84
Tnf	4.86	10.41	9.92
Vegfa	-1.33	3.56	1.29
Vegfb	-1.17	7.94	1.93

Different patterns of gene expression were observed when examining the angiogenesis related proteins in tumor tissue. The four growth factors with the highest gene expression were Interleukin8 (IL-8), VEGFB, TGFB-1 and tumor-homing peptide F3. Matrix degrading proteins had decreased gene expression, small increases in gene expression of matrix remodeling proteins were observed (Table 6).

Table 6: Survey of angiogenic growth factors in human tumor tissue

Gene expression of angiogenic growth factors from tumor tissue was increased at 4 and 9 weeks after adenocarcinoma cell injection. The biggest increases were observed in IL-8, F3, and VEGFB.

	2weeks	4weeks	9weeks
COL18A1	5.24	1.96	2.06
COL4A3	5.24	2.38	2.81
FGF1	5.24	-2.55	-10.48
FGF2	-1.65	-2.07	-2.85
FGFR3	5.24	11.88	7.57
MMP14	-1.47	-1.46	-6.45
MMP2	-1.74	-27.47	-139.1
PLAU	5.24	68.59	45.57
TGFB1	5.24	29.65	23.59
IGF1	-3.61	-10.78	-71.51
IL8	5.24	93.05	58.89
ERBB2	1.16	31.78	20.11
ANPEP	-1.04	15.78	23.26
F3	5.24	184.82	58.89
VEGFA	-3.92	-63.12	-237.21
VEGFB	5.24	25.46	44.02

Determining angiogenic potential of endothelial cells

After determining which growth factors had the highest gene expression in tumor tissue, we examined the endothelial cells from each vascular bed individually. We isolated primary endothelial cells from the bronchial artery (BAEC), pulmonary artery (PAEC) and pulmonary microvasculature (MVEC) to determine the angiogenic potential of each endothelial cell type. We first examined common surface markers used to identify endothelial cells to see if they were expressed on all endothelial cell types. CD31, a typical marker of endothelial cells was not expressed on any cell type that had been cultured, however it was observed on endothelial cells from tissue samples. Lycopersicon Esculentum (Tomato Lectin) was expressed in nearly 100% of cells in all cell types and thus used as the primary marker of endothelial cells for histological imaging and proliferation experiments.

Because we had observed an increase in IL-8 and VEGF in tumor tissue, we used VEGF, CINC-3 (the rat homolog of IL-8) and adenocarcinoma supernatant, in *in vitro* assays of angiogenesis. We measured endothelial cell proliferation by FACS analysis. As a positive control 20% FBS was used to stimulate endothelial cells, showing no significant difference in proliferation between cell types. When stimulated by adenocarcinoma supernatant, there was a significant increase in proliferation in only BAECs ($p < 0.0001$; Fig 16B). After stimulation with CINC-3 at both 10 and 100ng/ml concentrations, there was a significant increase in proliferation of BAECs when compared to PAECs and MVECs (10ng/ml, $p < 0.05$, 100ng/ml, $p < 0.001$; Fig 16C). Similarly, stimulation with recombinant VEGF resulted in a significant increase in proliferation in BAECs (10ng/ml; BAEC vs. MVEC $p < 0.05$, 100ng/ml; $p < 0.001$; Fig

16D).   Proliferation response to basal conditions (2% FBS) was similar between all cell

types.

Figure 16: Cell proliferation of BAECs, PAECs, and MVECs was determined by FACS analysis in response to 20% fetal bovine serum, adenocarcinoma supernatant, CINC-3, and VEGF.

A) When 20% FBS was used as a positive control, there was no significant difference in proliferation between cell types (n=6). B) After stimulation with adenocarcinoma supernatant, there was a significant increase in proliferation of BAECs when compared to PAECs and MVECs (***$p < 0.0001$, n=6). C) Stimulation with CINC-3 at both 10ng/ml and 100ng/ml concentrations resulted in a significant increase in proliferation from BAECs when compared to PAECs and MVECs (10ng/ml; *$p < 0.05$. 100ng/ml; **$p < 0.001$, ***$p < 0.0001$, n=6). D) Stimulation with recombinant VEGF at 10ng/ml resulted in a significant increase in proliferation of BAECs compared to MVECs (*$p = .02$, n=6). At 100ng/ml there was a significant increase in proliferation of BAECs when compared to PAECs and MVECs (**$p < 0.001$, n=6).

Figure 16: Continued
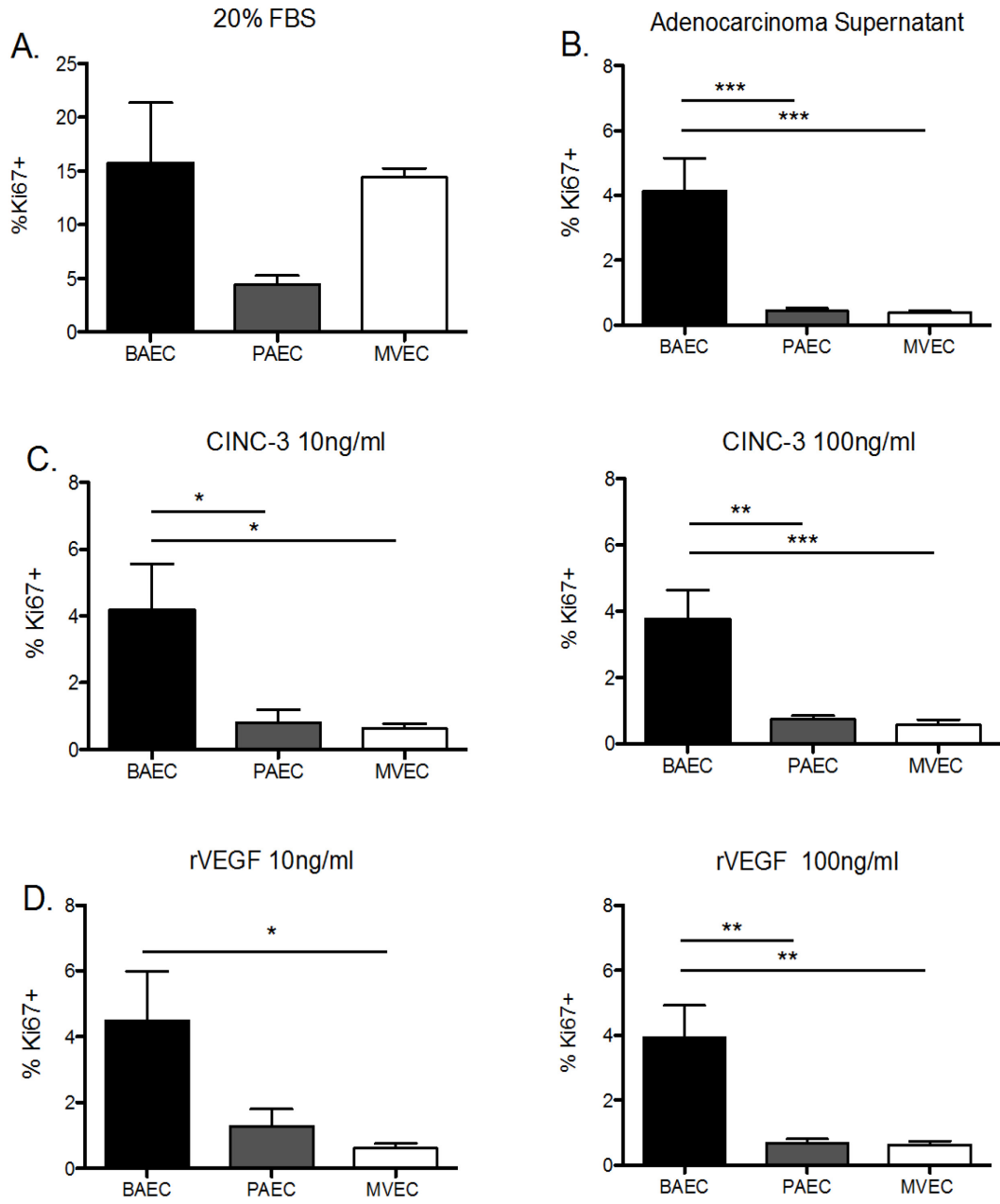
Next, the ability for each endothelial cell type to migrate towards an angiogenic stimulus was quantified. When stimulated with adenocarcinoma supernatant there was a significant increase in chemotaxis from BAECs compared to PAECs (p=0.03; Fig17A). After stimulation with CINC-3 we observed a significant increase in both BAECs and MVECs compared to PAECs and 10ng/ml (BAEC vs. PAEC p<0.001, MVEC vs. PAEC p<0.05) and 100ng/ml concentrations (BAEC vs. PAEC p<0.0001, MVEC vs. PAEC p<0.0001; Fig 17B). Upon stimulation with recombinant VEGF there was no significant difference in chemotaxis between any of the cells types at either 10ng/ml or 100ng/ml concentrations (Fig 17C).

Figure 17: Cell chemotaxis of BAECs, PAECs, and MVECs, determined by transwell migration assay, in response to adenocarcinoma supernatant, CINC-3, and VEGF.

A) There was a significant increase in chemotaxis from BAECs compared to PAECs when stimulated by adenocarcinoma supernatant (*p=0.03, n=6). B) When stimulated by CINC-3 there was a significant increase in chemotaxis of BAECs and MVECs when compared to PAECs at both 10ng/ml (**p<0.001, *p<. 05) and 100ng/ml (***p<0.0001, **p<0.001) concentrations (n=6).

C) There was no significant difference in chemotaxis between cell types when stimulated by recombinant VEGF at 10ng/ml or 100ng/ml concentrations.

A. Adenocarcinoma Supernatant

B. CINC-3 10ng/ml   CINC-3 100ng/ml

C. rVEGF (10ng/ml)   rVEGF (100ng/ml)
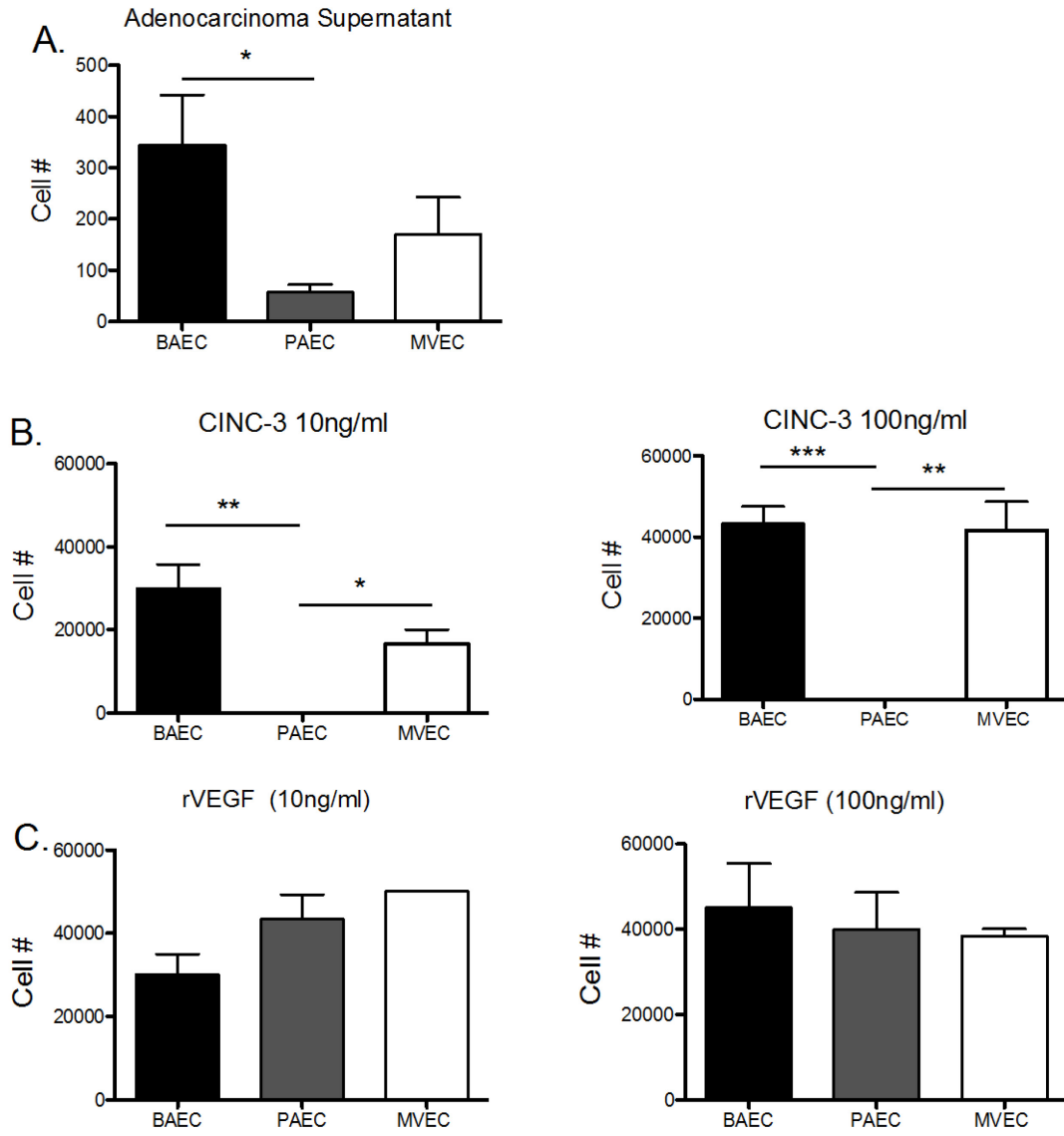
A tube formation assay was used to quantify the ability of endothelial cells from each vascular bed to elongate and connect to adjacent endothelial cells when stimulated with adenocarcinoma supernatant, CINC-3, and VEGF. When cells were stimulated with adenocarcinoma supernatant, BAECs had a significant increase in total tube lengths when compared to PAECs and MVECs (BAEC vs. PAEC $p<0.0001$, BAEC vs. MVEC $p<0.001$; Fig 18A). After CINC-3 stimulation MVECs had the greatest total tube lengths overall, with a significant increase from PAECs ($p<0.001$; Fig 18B). When stimulated with VEGF, BAECs had a significant increase in total tube lengths compared to PAECs and MVECs ($p<0.0001$; Fig 18C).

Figure 18: Tube formation of BAECs, PAECs, and MVECs, quantified by total tube lengths in tube formation assay, in response to adenocarcinoma supernatant, CINC-3, and VEGF.

A) When exposed to adenocarcinoma supernatant there was a significant increase in total tube lengths of BAECs when compared to PAECs and MVECs (***$p<0.0001$, **$p<0.001$,n=6)

B) After stimulation with CINC-3 there was a significant increase in total tube lengths of MVECs compared to PAECs (**$p<0.001$,n=6). C) In response to recombinant VEGF there was a significant increase in total tube lengths of BAECs compared to PAECS and MVECs (***$p<0.0001$,n=6).
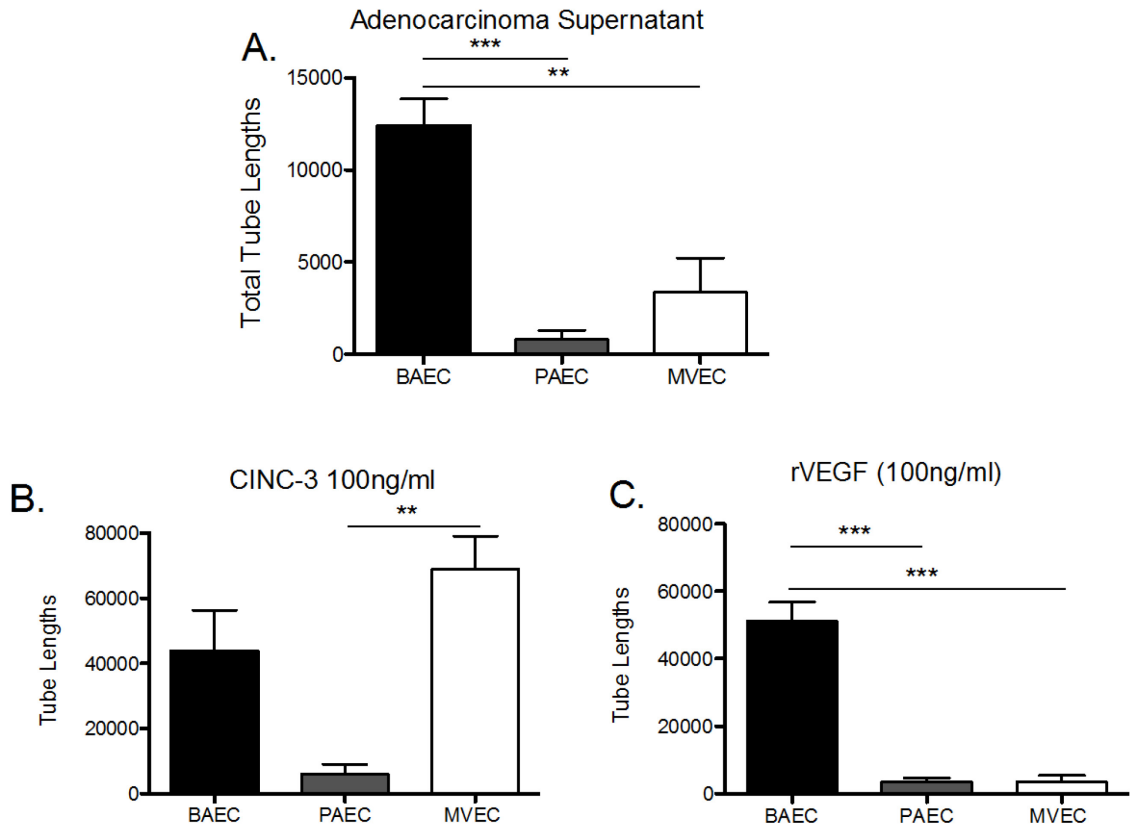
5.4 Discussion:

After observing an increase in bronchial circulation with tumor growth, we questioned which growth factors in both the lung tissue and tumor were involved in bronchial artery angiogenesis. Gene expression for the left lung was assessed by an angiogenesis RT^2 Profiler PCR Array designed for rat tissue and gene expression was calculated relative to naïve left lung tissue from a nude rat. While this experiment was just a survey of potential growth factors involved in angiogenesis, the most interesting observation was the time course at which the majority of pro-angiogenic growth factors were increasing in the left lung tissue. 23 of 39 growth factors and their receptors that were measured in this array were significantly up-regulated (greater than 2 fold increase in gene expression) at 4 weeks followed by drop in expression at 9 weeks. From the increase in angiogenic growth factor gene expression at 4 weeks coinciding with the up-regulation of matrix degrading enzymes in the surrounding tissue, it was possible that the tissue surrounding the tumor was primed by the tumor for neovascularization.

Gene expression of tumor tissue was assed by an angiogenesis RT^2 Profiler PCR Array designed for human tissue. When analyzing tumor tissue, relative gene expression from tumors 2,4 and 9 weeks after adenocarcinoma cell injection were compared to gene expression of adenocarcinoma cells in culture. The peak of growth factor expression observed at 4 weeks in lung tissue was not observed in tumor tissue. Overall only 16 genes out of the 39 measured had a significant increase in gene expression. Several proteins involved in matrix remodeling had increased gene expression (COL18A1, COL4A3, PLAU) with a large decrease in gene expression of matrix degrading proteins (MMP14, MMP12). The largest increases in gene expression were observed in IL-8,

VEGF B, and F3. F3 is a tumor-homing peptide that binds to endothelial cells and tumor cells through its receptor Nucleolin. It also binds to endothelial progenitor cells and is a useful marker for angiogenesis (178). Because we observed an increase in the bronchial circulation in large tumors, we can hypothesize that these growth factors are important for bronchial artery angiogenesis.

Along with F3, IL-8 (4wk: 93 fold increase, 9wk: 59 fold increase) and VEGF B (4wk: 25 fold increase, 9wk: 44 fold increase) had the highest gene expression relative to control adenocarcinoma cells. While VEGF A is thought to play a large role in the growth of new blood vessels, we did not observe an increase in gene expression in the tumor tissue. VEGF B however, which has shown to be critical in maintaining the new blood vessels (179) was significantly increased at 2, 4 and 9 weeks after adenocarcinoma cell injection. Because of these results, and the literature supporting their critical role in angiogenesis, we used recombinant human VEGF and the counterpart of IL-8 in the rat (CINC-3) for stimulation for *in vitro* determinations of angiogenesis.

Because the differences in each circulation's ability to undergo angiogenesis could in part be due to the innate differences in endothelial cells from each vasculature, we sought to determine the angiogenic potential of endothelial cells isolated from the bronchial artery (BAEC), pulmonary artery (PAEC) and pulmonary microvasculature (MVEC). Angiogenic potential was determined by quantifying the ability of each cell type to proliferate, move toward angiogenic stimuli, and elongate and connect to adjacent cells (form tubes) in response to adenocarcinoma supernatant, CINC-3, and VEGF.

Endothelial cell proliferation, elongation and connection to other endothelial cells, and movement toward angiogenic stimuli are necessary steps in the process of

angiogenesis (180). When examining endothelial cells these methods are frequently used as indications of angiogenesis (181-183). FACS analysis of proliferation in all endothelial cell types showed a significant increase in BAECs compared to PAECs and MVECs after stimulation with adenocarcinoma supernatant, CINC-3, and VEGF when normalized to basal levels of proliferation.

When chemotaxis was quantified, MVECs and BAECs both showed an increased response to adenocarcinoma supernatant and CINC-3 compared to PAECs. Quantification of tube lengths showed a unique increase in tube formation in BAECs in response to VEGF and adenocarcinoma supernatant. However, MVECs responded robustly to CINC-3 stimulation in their ability to form tubes. When assessing all of the *in vitro* data together, it is clear that BAECs have the greatest angiogenic potential to the three stimuli tested. MVECs seem to have a more specific affinity of CINC-3 made evident by the increase in chemotaxis and tube formation upon CINC-3 stimulation. Since there was no increase in MVEC proliferation in response to adenocarcinoma supernatant, VEGF, or CINC-3, perhaps MVECs are more likely to rearrange and remodel than to undergo angiogenesis.

When performing angiogenic assays it is common practice to purchase cell lines, most commonly human umbilical vascular endothelial cells (HUVEcs), and pulmonary artery endothelial cells as a model of angiogenesis in the lung. Unfortunately, as was shown above, each endothelial cell type has its own unique angiogenic potential, and using purchased HUVEC and PAECS for *in vitro* angiogenic assays could be misleading. Previous studies have extensively examined heterogeneity among endothelial cells from the pulmonary artery, pulmonary microvascular and aortic endothelial cells. However,

120

this study includes endothelial cells isolated from the bronchial artery providing a better representation of the lungs endothelium. The angiogenic phenotype of endothelial cells rely heavily on their extracellular matrix cues, therefore there is always some question if the cells maintain their phenotype when grown in culture. Because of this we sought to confirm our observations of a highly angiogenic bronchial circulation both *in vivo* and *in vitro*.

Further studies into the mechanisms by which the bronchial circulation responds uniquely to angiogenic stimuli could be valuable in the discovery of novel therapeutic targets. Differences in *in vivo* extracellular matrix among BAECs, PAECs and MVECs could contribute to innate differences in proliferation. BAECs could have increased receptors for VEGF (VEGFR1/2) and CINC-3 (CXCR1/2), and may be more metabolically active than the other cell types contributing to their increased proliferative response to those angiogenic stimuli. If surface markers differ on the bronchial artery endothelium versus the rest of the lung endothelium, vascular disrupting agents and anti-angiogenic therapies could be targeted specially to the bronchial circulation to avoid the unfavorable side effects seen when these therapy options are used globally. Differences in cellular metabolism should also be measured in these endothelial cell types. Targeting metabolic enzymes like glucose transporters, hexokinase or pyruvate kinase could affect BAECs uniquely if they had an increased metabolic rate.

5.5 Conclusion:

The results of the *in vitro* determinations of angiogenesis complement the *in vivo* observations depicting a pro-angiogenic bronchial circulation. Under all conditions the

BAECs had a robust response to angiogenic stimuli with significant increases in proliferation, chemotaxis and tube formation compared to MVECs and PAECs. Further research on targeting the endothelium of the bronchial circulation uniquely could lead to more specific treatment options and novel cancer therapies.

6.0 Summary:

Lung cancer is the leading cause of cancer related deaths in the United States. The lack of effective angiogenesis-inhibiting drugs creates challenges in increasing life expectancy. Understanding the nuances of lung tumor angiogenesis is essential for the development of more effective therapeutic options. In this study, we sought to develop a physiologically relevant *in vivo* model of NSCLC. We quantified lung tumor angiogenesis from the bronchial and pulmonary circulations independently and their contribution to lung tumor growth. Finally, we examined the angiogenic potential of endothelial cells isolated from the pulmonary and bronchial circulations.

The development of a physiologically relevant animal model was critical for the study of lung tumor angiogenesis. It was essential for the xenograft to be injected into the lung of an animal with an established bronchial circulation. Injecting adenocarcinoma cells directly into the left lung of a nude rat resulted in the formation of a single, well-vascularized tumor. After adenocarcinoma cell injection we observed a non-linear increase in tumor size over the course of 8 weeks. By histological examination we confirmed the pathological phenotype of adenocarcinomas typically seen in patients. Developing this model of NSCLC allowed us to independently examine the bronchial and pulmonary circulation's ability to support tumor growth.

In the first method for quantification of tumor perfusion, fluorescent microsphere injection was used with two different colored microspheres and two injection sites to quantify tumor perfusion from the bronchial and pulmonary circulations independently. We observed an increase in total tumor perfusion correlated with tumor size, and an increase in the percent of tumor perfusion from the bronchial circulation in large tumors.

123

The pulmonary circulation remained unchanged in response to tumor growth. Because this method of tumor perfusion quantification did not allow tumor visualization, a more sensitive approach where tumor size could be tracked longitudinally was ideal.

In the second method for quantification of tumor perfusion contrast enhanced HRCT scanning was used for independent measurements of tumor perfusion from the bronchial and pulmonary circulations. Bronchial perfusion was correlated with tumor size with an increased bronchial perfusion to large tumors compared to small tumors. Consistent with previous observations, the pulmonary circulation remained unchanged in response to tumor growth.

After confirming by two methods of tumor perfusion quantification that there was an increase in the bronchial circulation with tumor volume, we ablated the bronchial artery to confirm its significance in tumor growth. After bronchial artery ablation surgery, tumor growth was inhibited indicating the critical role of the bronchial circulation in lung tumor growth.

To further examine the innate differences in the pulmonary and bronchial circulations we isolated endothelial cells from each circulation to quantify their angiogenic potential. Endothelial cells from the bronchial circulation had increased proliferation, chemotaxis and tube formation in response to angiogenic stimuli when compared to endothelial cells from the pulmonary artery and pulmonary microvasculature.

In summary, as a lung tumor grows it is initially sustained primarily by the pulmonary circulation. However, given the limited capacity of the pulmonary circulation to undergo angiogenesis, it is the bronchial circulation that must proliferate to sustain

tumor growth beyond the point at which a tumor can be supported by the pulmonary circulation alone. Given the increased angiogenic phenotype of the bronchial artery endothelial cells, it is reasonable to conclude that innate differences in each circulations' ability to undergo angiogenesis is in part due to the angiogenic phenotype of each circulations' endothelial cells.
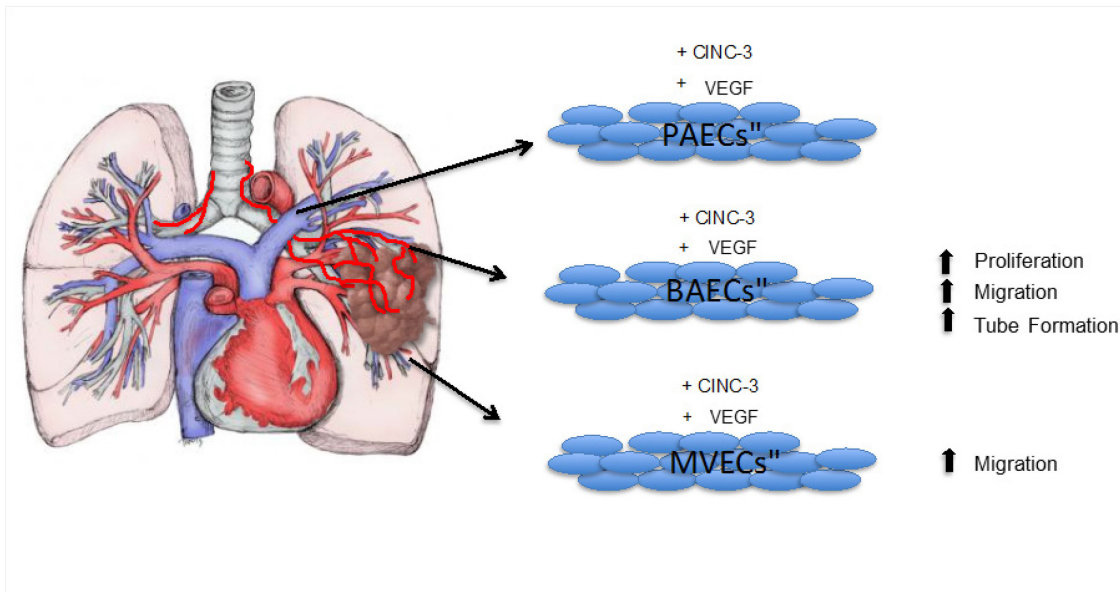
References

1.   Insititute NC. Seer stat fact sheet: Lung and bronchus. 2015 [cited 2015. Available from: http://seer.cancer.gov/statfacts/html/lungb.html.
2.   Travis WD, Brambilla E, Nicholson AG, Yatabe Y, Austin JH, Beasley MB, Chirieac LR, Dacic S, Duhig E, Flieder DB, Geisinger K, Hirsch FR, Ishikawa Y, Kerr KM, Noguchi M, Pelosi G, Powell CA, Tsao MS, Wistuba I. The 2015 world health organization classification of lung tumors: Impact of genetic, clinical and radiologic advances since the 2004 classification. *Journal of thoracic oncology : official publication of the International Association for the Study of Lung Cancer* 2015;10:1243-1260.
3.   Services USDoHaH. Estimates of funding for various research, condition, and disease categories (rcdc). 2016.
4.   Cosaert J, Quoix E. Platinum drugs in the treatment of non-small-cell lung cancer. *British journal of cancer* 2002;87:825-833.
5.   Travis WD, Brambilla E, Noguchi M, Nicholson AG, Geisinger K, Yatabe Y, Powell CA, Beer D, Riely G, Garg K, Austin JH, Rusch VW, Hirsch FR, Jett J, Yang PC, Gould M. International association for the study of lung cancer/american thoracic society/european respiratory society: International multidisciplinary classification of lung adenocarcinoma: Executive summary. *Proceedings of the American Thoracic Society* 2011;8:381-385.
6.   Beasley MB, Brambilla E, Travis WD. The 2004 world health organization classification of lung tumors. *Seminars in roentgenology* 2005;40:90-97.
7.   Saika K, Matsuda T. Comparison of time trends in lung cancer incidence (1973 97) in east asia, europe and USA, from cancer incidence in five continents vols iv viii. *Japanese journal of clinical oncology* 2007;37:474-476.
8.   Moran CA. Pulmonary adenocarcinoma: The expanding spectrum of histologic variants. *Archives of pathology & laboratory medicine* 2006;130:958-962.
9.   Grant SC, Kris MG. New antineoplastic agents in lung cancer 1988-1993. *Cancer treatment and research* 1995;72:323-347.
10.   Deslauriers J, Gregoire J. Surgical therapy of early non-small cell lung cancer. *Chest* 2000;117:104S-109S.
11.   Rowell NP, Williams CJ. Radical radiotherapy for stage i/ii non-small cell lung cancer in patients not sufficiently fit for or declining surgery (medically inoperable): A systematic review. *Thorax* 2001;56:628-638.
12.   Leong SS, Fong KW, Ong YK, Foo KF, Ang P, Wee J, Lee KM, Tan EH. Chemo-radiotherapy for stage iii unresectable non-small cell lung cancer long-term results of a prospective study. *Respiratory medicine* 2004;98:1080-1086.
13.   Su S, Hu Y, Ouyang W, Ma Z, Lu B, Li Q, Li H, Wang Z, Wang Y. The survival outcomes and prognosis of stage iv non-small-cell lung cancer treated with thoracic three-dimensional radiotherapy combined with chemotherapy. *Radiat Oncol* 2014;9:290.
14.   Thomas A, Liu SV, Subramaniam DS, Giaccone G. Refining the treatment of nsclc according to histological and molecular subtypes. *Nature reviews Clinical oncology* 2015;12:511-526.

15.   Green RA, Humphrey E, Close H, Patno ME. Alkylating agents in bronchogenic carcinoma. *The American journal of medicine* 1969;46:516-525.

16.   Ricciardi S, Tomao S, de Marinis F. Pemetrexed as first-line therapy for non-squamous non-small cell lung cancer. *Therapeutics and clinical risk management* 2009;5:781-787.

17.   Schrock AB, Frampton GM, Herndon D, Greenbowe JR, Wang K, Lipson D, Yelensky R, Chalmers ZR, Chmielecki J, Elvin JA, Wollner M, Dvir A, Soussan-Gutman L, Bordoni R, Peled N, Braiteh F, Raez L, Erlich R, Ou SI, Mohamed M, Ross JS, Stephens PJ, Ali SM, Miller VA. Comprehensive genomic profiling identifies frequent drug-sensitive egfr exon 19 deletions in nsclc not identified by prior molecular testing. *Clinical cancer research : an official journal of the American Association for Cancer Research* 2016.

18.   Amadio M, Osera C, Lupo G, Motta C, Drago F, Govoni S, Pascale A. Protein kinase c activation affects, via the mrna-binding hu-antigen r/elav protein, vascular endothelial growth factor expression in a pericytic/endothelial coculture model. *Molecular vision* 2012;18:2153-2164.

19.   Ferrara N, Gerber HP, LeCouter J. The biology of vegf and its receptors. *Nature medicine* 2003;9:669-676.

20.   Fontanini G, Boldrini L, Chine S, Pisaturo F, Basolo F, Calcinai A, Lucchi M, Mussi A, Angeletti CA, Bevilacqua G. Expression of vascular endothelial growth factor mrna in non-small-cell lung carcinomas. *British journal of cancer* 1999;79:363-369.

21.   Hicklin DJ, Ellis LM. Role of the vascular endothelial growth factor pathway in tumor growth and angiogenesis. *Journal of clinical oncology : official journal of the American Society of Clinical Oncology* 2005;23:1011-1027.

22.   Pallis AG, Serfass L, Dziadziusko R, van Meerbeeck JP, Fennell D, Lacombe D, Welch J, Gridelli C. Targeted therapies in the treatment of advanced/metastatic nsclc. *Eur J Cancer* 2009;45:2473-2487.

23.   Fontanini G, Vignati S, Boldrini L, Chine S, Silvestri V, Lucchi M, Mussi A, Angeletti CA, Bevilacqua G. Vascular endothelial growth factor is associated with neovascularization and influences progression of non-small cell lung carcinoma. *Clinical cancer research : an official journal of the American Association for Cancer Research* 1997;3:861-865.

24.   Heymach JV, Johnson BE, Prager D, Csada E, Roubec J, Pesek M, Spasova I, Belani CP, Bodrogi I, Gadgeel S, Kennedy SJ, Hou J, Herbst RS. Randomized, placebo-controlled phase ii study of vandetanib plus docetaxel in previously treated non small-cell lung cancer. *Journal of clinical oncology : official journal of the American Society of Clinical Oncology* 2007;25:4270-4277.

25.   Nikolinakos PG, Altorki N, Yankelevitz D, Tran HT, Yan S, Rajagopalan D, Bordogna W, Ottesen LH, Heymach JV. Plasma cytokine and angiogenic factor profiling identifies markers associated with tumor shrinkage in early-stage non-small cell lung cancer patients treated with pazopanib. *Cancer research* 2010;70:2171-2179.

26.   Scagliotti G, Novello S, von Pawel J, Reck M, Pereira JR, Thomas M, Abrao Miziara JE, Balint B, De Marinis F, Keller A, Aren O, Csollak M, Albert I, Barrios CH, Grossi F, Krzakowski M, Cupit L, Cihon F, Dimatteo S, Hanna N. Phase iii study of

carboplatin and paclitaxel alone or with sorafenib in advanced non-small-cell lung cancer. *Journal of clinical oncology : official journal of the American Society of Clinical Oncology* 2010;28:1835-1842.

27.   Folkman J. Tumor angiogenesis: Therapeutic implications. *The New England journal of medicine* 1971;285:1182-1186.

28.   Greene HS. Heterologous transplantation of mammalian tumors : I. The transfer of rabbit tumors to alien species. *The Journal of experimental medicine* 1941;73:461-474.

29.   Risau W. Mechanisms of angiogenesis. *Nature* 1997;386:671-674.

30.   Patan S, Munn LL, Jain RK. Intussusceptive microvascular growth in a human colon adenocarcinoma xenograft: A novel mechanism of tumor angiogenesis. *Microvascular research* 1996;51:260-272.

31.   Leenders WP, Kusters B, de Waal RM. Vessel co-option: How tumors obtain blood supply in the absence of sprouting angiogenesis. *Endothelium* 2002;9:83-87.

32.   Maniotis AJ, Folberg R, Hess A, Seftor EA, Gardner LM, Pe'er J, Trent JM, Meltzer PS, Hendrix MJ. Vascular channel formation by human melanoma cells in vivo and in vitro: Vasculogenic mimicry. *The American journal of pathology* 1999;155:739-752.

33.   Jain RK. Molecular regulation of vessel maturation. *Nature medicine* 2003;9:685-693.

34.   Chatterjee S, Heukamp LC, Siobal M, Schottle J, Wieczorek C, Peifer M, Frasca D, Koker M, Konig K, Meder L, Rauh D, Buettner R, Wolf J, Brekken RA, Neumaier B, Christofori G, Thomas RK, Ullrich RT. Tumor vegf:Vegfr2 autocrine feed-forward loop triggers angiogenesis in lung cancer. *The Journal of clinical investigation* 2013;123:1732-1740.

35.   Fontanini G, Lucchi M, Vignati S, Mussi A, Ciardiello F, De Laurentiis M, De Placido S, Basolo F, Angeletti CA, Bevilacqua G. Angiogenesis as a prognostic indicator of survival in non-small-cell lung carcinoma: A prospective study. *Journal of the National Cancer Institute* 1997;89:881-886.

36.   Tanaka F, Otake Y, Yanagihara K, Kawano Y, Miyahara R, Li M, Yamada T, Hanaoka N, Inui K, Wada H. Evaluation of angiogenesis in non-small cell lung cancer: Comparison between anti-cd34 antibody and anti-cd105 antibody. *Clinical cancer research : an official journal of the American Association for Cancer Research* 2001;7:3410-3415.

37.   Wesseling P, van der Laak JA, de Leeuw H, Ruiter DJ, Burger PC. Quantitative immunohistological analysis of the microvasculature in untreated human glioblastoma multiforme. Computer-assisted image analysis of whole-tumor sections. *Journal of neurosurgery* 1994;81:902-909.

38.   Hyjek E, Chadburn A, Dias S, Zhu Z, Witte L, Hicklin D, E C, Knowels D, S. R. Non-hodgkin's lymphomas and hodhkin's disease are associated with increase density of kdr+sma (-) immature microvessels. *Blood* 1999.

39.   Pezzella F, Gatter K. Non-angiogenic tumours unveil a new chapter in cancer biology. *J Pathol* 2015;235:381-383.

40.   Passalidou E, Trivella M, Singh N, Ferguson M, Hu J, Cesario A, Granone P, Nicholson AG, Goldstraw P, Ratcliffe C, Tetlow M, Leigh I, Harris AL, Gatter KC,

Pezzella F. Vascular phenotype in angiogenic and non-angiogenic lung non-small cell carcinomas. *British journal of cancer* 2002;86:244-249.

41.   Sardari Nia P, Hendriks J, Friedel G, Van Schil P, Van Marck E. Distinct angiogenic and non-angiogenic growth patterns of lung metastases from renal cell carcinoma. *Histopathology* 2007;51:354-361.

42.   Yuneva MO, Fan TW, Allen TD, Higashi RM, Ferraris DV, Tsukamoto T, Mates JM, Alonso FJ, Wang C, Seo Y, Chen X, Bishop JM. The metabolic profile of tumors depends on both the responsible genetic lesion and tissue type. *Cell metabolism* 2012;15:157-170.

43.   Quail DF, Joyce JA. Microenvironmental regulation of tumor progression and metastasis. *Nature medicine* 2013;19:1423-1437.

44.   Calabrese C, Bocchino V, Vatrella A, Marzo C, Guarino C, Mascitti S, Tranfa CM, Cazzola M, Micheli P, Caputi M, Marsico SA. Evidence of angiogenesis in bronchial biopsies of smokers with and without airway obstruction. *Respiratory medicine* 2006;100:1415-1422.

45.   Aggarwal S, Gross CM, Sharma S, Fineman JR, Black SM. Reactive oxygen species in pulmonary vascular remodeling. *Compr Physiol* 2013;3:1011-1034.

46.   Welsh DJ, Peacock AJ. Cellular responses to hypoxia in the pulmonary circulation. *High Alt Med Biol* 2013;14:111-116.

47.   Jeffery TK, Wanstall JC. Pulmonary vascular remodeling: A target for therapeutic intervention in pulmonary hypertension. *Pharmacology & therapeutics* 2001;92:1-20.

48.   Rothman A, Wolner B, Button D, Taylor P. Immediate-early gene expression in response to hypertrophic and proliferative stimuli in pulmonary arterial smooth muscle cells. *The Journal of biological chemistry* 1994;269:6399-6404.

49.   Fanburg BL, Lee SL. A new role for an old molecule: Serotonin as a mitogen. *The American journal of physiology* 1997;272:L795-806.

50.   Voelkel NF, Tuder RM. Cellular and molecular mechanisms in the pathogenesis of severe pulmonary hypertension. *The European respiratory journal* 1995;8:2129-2138.

51.   Lambert V, Michel R, Mazmanian GM, Dulmet EM, Capderou A, Herve P, Planche C, Serraf A. Induction of pulmonary angiogenesis by adenoviral-mediated gene transfer of vascular endothelial growth factor. *The Annals of thoracic surgery* 2004;77:458-463; discussion 463.

52.   Zhang J, Luo B, Tang L, Wang Y, Stockard CR, Kadish I, Van Groen T, Grizzle WE, Ponnazhagan S, Fallon MB. Pulmonary angiogenesis in a rat model of hepatopulmonary syndrome. *Gastroenterology* 2009;136:1070-1080.

53.   Zhang J, Yang W, Luo B, Hu B, Maheshwari A, Fallon MB. The role of cx(3)cl1/cx(3)cr1 in pulmonary angiogenesis and intravascular monocyte accumulation in rat experimental hepatopulmonary syndrome. *Journal of hepatology* 2012;57:752-758.

54.   Zetterberg E, Popat U, Hasselbalch H, Prchal J, Palmblad J. Angiogenesis in pulmonary hypertension with myelofibrosis. *Haematologica* 2008;93:945-946.

55.   Farkas L, Farkas D, Ask K, Moller A, Gauldie J, Margetts P, Inman M, Kolb M. Vegf ameliorates pulmonary hypertension through inhibition of endothelial

apoptosis in experimental lung fibrosis in rats. *The Journal of clinical investigation* 2009;119:1298-1311.

56. Howell K, Preston RJ, McLoughlin P. Chronic hypoxia causes angiogenesis in addition to remodelling in the adult rat pulmonary circulation. *The Journal of physiology* 2003;547:133-145.

57. Turner-Warwick M. Precapillary systemic-pulmonary anastomoses. *Thorax* 1963;18:225-237.

58. Hartmann IJ, Remy-Jardin M, Menchini L, Teisseire A, Khalil C, Remy J. Ectopic origin of bronchial arteries: Assessment with multidetector helical ct angiography. *European radiology* 2007;17:1943-1953.

59. Osiro S, Wear C, Hudson R, Ma XX, Zurada A, Michalak M, Loukas M. A friend to the airways: A review of the emerging clinical importance of the bronchial arterial circulation. *Surg Radiol Anat* 2012;34:791-798.

60. Laitinen A, Laitinen LA, Moss R, Widdicombe JG. Organisation and structure of the tracheal and bronchial blood vessels in the dog. *Journal of anatomy* 1989;165:133-140.

61. Wagner EM, Brown RH. Blood flow distribution within the airway wall. *J Appl Physiol (1985)* 2002;92:1964-1969.

62. Polet F, Feron O. Endothelial cell metabolism and tumour angiogenesis: Glucose and glutamine as essential fuels and lactate as the driving force. *J Intern Med* 2013;273:156-165.

63. Charan NB, Carvalho P. Angiogenesis in bronchial circulatory system after unilateral pulmonary artery obstruction. *J Appl Physiol (1985)* 1997;82:284-291.

64. Jenkins J, Wagner E. Angiogenesis in the ischemic rat lung. *Journal of visualized experiments : JoVE* 2013.

65. Wagner EM, Jenkins J, Schmieder A, Eldridge L, Zhang Q, Moldobaeva A, Zhang H, Allen JS, Yang X, Mitzner W, Keupp J, Caruthers SD, Wickline SA, Lanza GM. Angiogenesis and airway reactivity in asthmatic brown norway rats. *Angiogenesis* 2015;18:1-11.

66. Yuan X, Zhang J, Ao G, Quan C, Tian Y, Li H. Lung cancer perfusion: Can we measure pulmonary and bronchial circulation simultaneously? *European radiology* 2012;22:1665-1671.

67. Nguyen-Kim TD, Frauenfelder T, Strobel K, Veit-Haibach P, Huellner MW. Assessment of bronchial and pulmonary blood supply in non-small cell lung cancer subtypes using computed tomography perfusion. *Invest Radiol* 2015;50:179-186.

68. Mori K. Experimental induction of pulmonary tumors in mice. *Showa Igakkai zasshi = The Journal of the Showa Medical Association* 1962;22:51-52.

69. Snell KC, Stewart HL. Induction of pulmonary adenomatosis in dba/2 mice by the oral administration of dibenz(a,h)anthracene. *Acta - Unio Internationalis Contra Cancrum* 1963;19:692-694.

70. Toth B, Shubik P. Mammary tumor inhibition and lung adenoma induction by isonicotinic acid hydrazide. *Science* 1966;152:1376-1377.

71. Kaye AM, Trainin N. Urethan carcinogenesis and nucleic acid metabolism: Factors influencing lung adenoma induction. *Cancer research* 1966;26:2206-2212.

72.   Greenblatt M, Mirvish S, So BT. Nitrosamine studies: Induction of lung adenomas by concurrent administration of sodium nitrite and secondary amines in swiss mice. *Journal of the National Cancer Institute* 1971;46:1029-1034.

73.   Rigdon RH, Neal J. Gastric carcinomas and pulmonary adenomas in mice fed benzo (a) pyrene. *Texas reports on biology and medicine* 1966;24:195-207.

74.   Hecht SS, Morse MA, Amin S, Stoner GD, Jordan KG, Choi CI, Chung FL. Rapid single-dose model for lung tumor induction in a/j mice by 4-(methylnitrosamino)-1-(3-pyridyl)-1-butanone and the effect of diet. *Carcinogenesis* 1989;10:1901-1904.

75.   Lavigueur A, Maltby V, Mock D, Rossant J, Pawson T, Bernstein A. High incidence of lung, bone, and lymphoid tumors in transgenic mice overexpressing mutant alleles of the p53 oncogene. *Molecular and cellular biology* 1989;9:3982-3991.

76.   Mallakin A, Sugiyama T, Taneja P, Matise LA, Frazier DP, Choudhary M, Hawkins GA, D'Agostino RB, Jr., Willingham MC, Inoue K. Mutually exclusive inactivation of dmp1 and arf/p53 in lung cancer. *Cancer cell* 2007;12:381-394.

77.   Jackson EL, Willis N, Mercer K, Bronson RT, Crowley D, Montoya R, Jacks T, Tuveson DA. Analysis of lung tumor initiation and progression using conditional expression of oncogenic k-ras. *Genes & development* 2001;15:3243-3248.

78.   Fisher GH, Wellen SL, Klimstra D, Lenczowski JM, Tichelaar JW, Lizak MJ, Whitsett JA, Koretsky A, Varmus HE. Induction and apoptotic regression of lung adenocarcinomas by regulation of a k-ras transgene in the presence and absence of tumor suppressor genes. *Genes & development* 2001;15:3249-3262.

79.   Wang Y, Rouggly L, You M, Lubet R. Animal models of lung cancer characterization and use for chemoprevention research. *Progress in molecular biology and translational science* 2012;105:211-226.

80.   Tan X, Carretero J, Chen Z, Zhang J, Wang Y, Chen J, Li X, Ye H, Tang C, Cheng X, Hou N, Yang X, Wong KK. Loss of p53 attenuates the contribution of il-6 deletion on suppressed tumor progression and extended survival in kras-driven murine lung cancer. *PloS one* 2013;8:e80885.

81.   DuPage M, Dooley AL, Jacks T. Conditional mouse lung cancer models using adenoviral or lentiviral delivery of cre recombinase. *Nat Protoc* 2009;4:1064-1072.

82.   Kasinski AL, Slack FJ. Mirna-34 prevents cancer initiation and progression in a therapeutically resistant k-ras and p53-induced mouse model of lung adenocarcinoma. *Cancer research* 2012;72:5576-5587.

83.   Zundelevich A, Elad-Sfadia G, Haklai R, Kloog Y. Suppression of lung cancer tumor growth in a nude mouse model by the ras inhibitor salirasib (farnesylthiosalicylic acid). *Molecular cancer therapeutics* 2007;6:1765-1773.

84.   Tanaka T, Delong PA, Amin K, Henry A, Kruklitis R, Kapoor V, Kaiser LR, Albelda SM. Treatment of lung cancer using clinically relevant oral doses of the cyclooxygenase-2 inhibitor rofecoxib: Potential value as adjuvant therapy after surgery. *Ann Surg* 2005;241:168-178.

85.   Rolff J, Becker M, Merk J, Hoffmann J, Fichtner I. Preclinical study of a combination of erlotinib and bevacizumab in early stages of unselected non-small cell lung cancer patient-derived xenografts. *Targeted oncology* 2016.

86.   Gao H, Xue J, Zhou L, Lan J, He J, Na F, Yang L, Deng L, Lu Y. Bevacizumab radiosensitizes non-small cell lung cancer xenografts by inhibiting DNA double-strand break repair in endothelial cells. *Cancer letters* 2015;365:79-88.

87.   Hilbe W, Manegold C, Pircher A. Targeting angiogenesis in lung cancer - pitfalls in drug development. *Translational lung cancer research* 2012;1:122-128.

88.   Johnson DH, Fehrenbacher L, Novotny WF, Herbst RS, Nemunaitis JJ, Jablons DM, Langer CJ, DeVore RF, 3rd, Gaudreault J, Damico LA, Holmgren E, Kabbinavar F. Randomized phase ii trial comparing bevacizumab plus carboplatin and paclitaxel with carboplatin and paclitaxel alone in previously untreated locally advanced or metastatic non-small-cell lung cancer. *Journal of clinical oncology : official journal of the American Society of Clinical Oncology* 2004;22:2184-2191.

89.   Ebos JM, Kerbel RS. Antiangiogenic therapy: Impact on invasion, disease progression, and metastasis. *Nature reviews Clinical oncology* 2011;8:210-221.

90.   Jain RK, Duda DG, Willett CG, Sahani DV, Zhu AX, Loeffler JS, Batchelor TT, Sorensen AG. Biomarkers of response and resistance to antiangiogenic therapy. *Nature reviews Clinical oncology* 2009;6:327-338.

91.   Su H, Bodenstein C, Dumont RA, Seimbille Y, Dubinett S, Phelps ME, Herschman H, Czernin J, Weber W. Monitoring tumor glucose utilization by positron emission tomography for the prediction of treatment response to epidermal growth factor receptor kinase inhibitors. *Clinical cancer research : an official journal of the American Association for Cancer Research* 2006;12:5659-5667.

92.   Akhtar S, Meeran SM, Katiyar N, Katiyar SK. Grape seed proanthocyanidins inhibit the growth of human non-small cell lung cancer xenografts by targeting insulin-like growth factor binding protein-3, tumor cell proliferation, and angiogenic factors. *Clinical cancer research : an official journal of the American Association for Cancer Research* 2009;15:821-831.

93.   Nogawa M, Yuasa T, Kimura S, Kuroda J, Sato K, Segawa H, Yokota A, Maekawa T. Monitoring luciferase-labeled cancer cell growth and metastasis in different in vivo models. *Cancer letters* 2005;217:243-253.

94.   Steiner P, Joynes C, Bassi R, Wang S, Tonra JR, Hadari YR, Hicklin DJ. Tumor growth inhibition with cetuximab and chemotherapy in non-small cell lung cancer xenografts expressing wild-type and mutated epidermal growth factor receptor. *Clinical cancer research : an official journal of the American Association for Cancer Research* 2007;13:1540-1551.

95.   Sakuma Y, Matsukuma S, Nakamura Y, Yoshihara M, Koizume S, Sekiguchi H, Saito H, Nakayama H, Kameda Y, Yokose T, Oguni S, Niki T, Miyagi Y. Enhanced autophagy is required for survival in egfr-independent egfr-mutant lung adenocarcinoma cells. *Laboratory investigation; a journal of technical methods and pathology* 2013;93:1137-1146.

96.   Verloop MC. The arteriae bronchiales and their anastomoses with the arteria pulmonalis in the human lung; a micro-anatomical study. *Acta Anat (Basel)* 1948;5:171-205.

97.   Mitzner W, Lee W, Georgakopoulos D, Wagner E. Angiogenesis in the mouse lung. *The American journal of pathology* 2000;157:93-101.

98.   Wagner EM, Mitzner W, Brown RH. Site of functional bronchopulmonary anastomoses in sheep. *The Anatomical record* 1999;254:360-366.

99.   Peao MN, Aguas AP, de Sa CM, Grande NR. Neoformation of blood vessels in association with rat lung fibrosis induced by bleomycin. *The Anatomical record* 1994;238:57-67.

100.   Verloop MC. On the arteriae bronchiales and their anastomosing with the arteria pulmonalis in some rodents; a micro-anatomical study. *Acta Anat (Basel)* 1949;7:1-32.

101.   Morales-Oyarvide V, Mino-Kenudson M. Tumor islands and spread through air spaces: Distinct patterns of invasion in lung adenocarcinoma. *Pathology international* 2016;66:1-7.

102.   Pezzella F, Pastorino U, Tagliabue E, Andreola S, Sozzi G, Gasparini G, Menard S, Gatter KC, Harris AL, Fox S, Buyse M, Pilotti S, Pierotti M, Rilke F. Non-small-cell lung carcinoma tumor growth without morphological evidence of neo-angiogenesis. *The American journal of pathology* 1997;151:1417-1423.

103.   Tang ER, Schreiner AM, Pua BB. Advances in lung adenocarcinoma classification: A summary of the new international multidisciplinary classification system (iaslc/ats/ers). *Journal of thoracic disease* 2014;6:S489-501.

104.   Auerbach R, Auerbach W, Polakowski I. Assays for angiogenesis: A review. *Pharmacology & therapeutics* 1991;51:1-11.

105.   Shi P, Hong J, Huang Y, Zhang Z, Zhang M, Zhang L. Automated computational framework of blood vessel quantification in chick chorioallantoic membrane angiogenesis. *Journal of biomedical optics* 2014;19:106005.

106.   Xiao X, Zhou X, Ming H, Zhang J, Huang G, Zhang Z, Li P. Chick chorioallantoic membrane assay: A 3d animal model for study of human nasopharyngeal carcinoma. *PloS one* 2015;10:e0130935.

107.   Deryugina EI, Quigley JP. Chapter 2. Chick embryo chorioallantoic membrane models to quantify angiogenesis induced by inflammatory and tumor cells or purified effector molecules. *Methods in enzymology* 2008;444:21-41.

108.   Andrade SP, Fan TP, Lewis GP. Quantitative in-vivo studies on angiogenesis in a rat sponge model. *British journal of experimental pathology* 1987;68:755-766.

109.   Passaniti A, Taylor RM, Pili R, Guo Y, Long PV, Haney JA, Pauly RR, Grant DS, Martin GR. A simple, quantitative method for assessing angiogenesis and antiangiogenic agents using reconstituted basement membrane, heparin, and fibroblast growth factor. *Laboratory investigation; a journal of technical methods and pathology* 1992;67:519-528.

110.   Nicoli S, Ribatti D, Cotelli F, Presta M. Mammalian tumor xenografts induce neovascularization in zebrafish embryos. *Cancer research* 2007;67:2927-2931.

111.   Ackermann M, Konerding MA. Vascular casting for the study of vascular morphogenesis. *Methods Mol Biol* 2015;1214:49-66.

112.   Shelton SE, Lee YZ, Lee M, Cherin E, Foster FS, Aylward SR, Dayton PA. Quantification of microvascular tortuosity during tumor evolution using acoustic angiography. *Ultrasound in medicine & biology* 2015;41:1896-1904.

113.   Chand R, Chandra H, Chandra S, Verma SK. Role of microvessel density and vascular endothelial growth factor in angiogenesis of hematological malignancies. *Bone marrow research* 2016;2016:5043483.

114. Freitas-Andrade M, Slinn J, Charlebois C, Moreno MJ. Histological assessment of angiogenesis in the hypoxic central nervous system. *Methods Mol Biol* 2014;1135:157-175.

115. Xia H, Zhao YN, Yu CH, Zhao YL, Liu Y. Inhibition of metabotropic glutamate receptor 1 suppresses tumor growth and angiogenesis in experimental non-small cell lung cancer. *European journal of pharmacology* 2016;783:103-111.

116. Kumar VV, Krishanappa SJ, Prakash SG, Channabasaviah GH, Murgod S, Pujari R, Kamat MS. Quantification and correlation of angiogenesis with macrophages by histomorphometric method in central and peripheral giant cell granuloma: An immunohistochemical analysis. *Journal of clinical and diagnostic research : JCDR* 2016;10:ZC01-05.

117. Spaks A, Svirina D, Spaka I, Jaunalksne I, Breiva D, Tracums I, Krievins D. Cxc chemokine ligand 4 (cxcl4) is predictor of tumour angiogenic activity and prognostic biomarker in non-small cell lung cancer (nsclc) patients undergoing surgical treatment. *Biomarkers : biochemical indicators of exposure, response, and susceptibility to chemicals* 2016:1-4.

118. Dababneh L, Cikach F, Alkukhun L, Dweik RA, Tonelli AR. Sublingual microcirculation in pulmonary arterial hypertension. *Annals of the American Thoracic Society* 2014;11:504-512.

119. Judge EP, Fabre A, Adamali HI, Egan JJ. Acute exacerbations and pulmonary hypertension in advanced idiopathic pulmonary fibrosis. *The European respiratory journal* 2012;40:93-100.

120. Ilie M, Long E, Hofman V, Selva E, Bonnetaud C, Boyer J, Venissac N, Sanfiorenzo C, Ferrua B, Marquette CH, Mouroux J, Hofman P. Clinical value of circulating endothelial cells and of soluble cd146 levels in patients undergoing surgery for non-small cell lung cancer. *British journal of cancer* 2014;110:1236-1243.

121. Bidard FC, Mathiot C, Degeorges A, Etienne-Grimaldi MC, Delva R, Pivot X, Veyret C, Bergougnoux L, de Cremoux P, Milano G, Pierga JY. Clinical value of circulating endothelial cells and circulating tumor cells in metastatic breast cancer patients treated first line with bevacizumab and chemotherapy. *Annals of oncology : official journal of the European Society for Medical Oncology / ESMO* 2010;21:1765-1771.

122. Manzoni M, Mariucci S, Delfanti S, Rovati B, Ronzoni M, Loupakis F, Brugnatelli S, Tinelli C, Villa E, Falcone A, Danova M. Circulating endothelial cells and their apoptotic fraction are mutually independent predictive biomarkers in bevacizumab-based treatment for advanced colorectal cancer. *Journal of cancer research and clinical oncology* 2012;138:1187-1196.

123. Matsusaka S, Mishima Y, Suenaga M, Terui Y, Kuniyoshi R, Mizunuma N, Hatake K. Circulating endothelial progenitors and cxcr4-positive circulating endothelial cells are predictive markers for bevacizumab. *Cancer* 2011;117:4026-4032.

124. Malka D, Boige V, Jacques N, Vimond N, Adenis A, Boucher E, Pierga JY, Conroy T, Chauffert B, Francois E, Guichard P, Galais MP, Cvitkovic F, Ducreux M, Farace F. Clinical value of circulating endothelial cell levels in metastatic colorectal cancer patients treated with first-line chemotherapy and bevacizumab. *Annals of*

oncology : official journal of the European Society for Medical Oncology / ESMO 2012;23:919-927.

125.   Yuan A, Yu CJ, Chen WJ, Lin FY, Kuo SH, Luh KT, Yang PC. Correlation of total vegf mrna and protein expression with histologic type, tumor angiogenesis, patient survival and timing of relapse in non-small-cell lung cancer. *International journal of cancer* 2000;89:475-483.

126.   Addison CL, Ding K, Seymour L, Zhao H, Laurie SA, Shepherd FA, Goss GD, Bradbury PA. Analysis of serum protein levels of angiogenic factors and their soluble receptors as markers of response to cediranib in the ncic ctg br.24 clinical trial. *Lung Cancer* 2015;90:288-295.

127.   Blumenschein GR, Jr., Reck M, Fossella F, Stewart DJ, Lathia C, Pena C. Plasma biomarkers correlating with clinical outcome in a phase ii study of sorafenib in advanced nsclc. *Cancer biomarkers : section A of Disease markers* 2011;10:287-298.

128.   Bieche I, Vacher S, Vallerand D, Richon S, Hatem R, De Plater L, Dahmani A, Nemati F, Angevin E, Marangoni E, Roman-Roman S, Decaudin D, Dangles-Marie V. Vasculature analysis of patient derived tumor xenografts using species-specific pcr assays: Evidence of tumor endothelial cells and atypical vegfa-vegfr1/2 signalings. *BMC cancer* 2014;14:178.

129.   Rudolph AM, Heymann MA. The circulation of the fetus in utero. Methods for studying distribution of blood flow, cardiac output and organ blood flow. *Circulation research* 1967;21:163-184.

130.   Savai R, Wolf JC, Greschus S, Eul BG, Schermuly RT, Hanze J, Voswinckel R, Langheinrich AC, Grimminger F, Traupe H, Seeger W, Rose F. Analysis of tumor vessel supply in lewis lung carcinoma in mice by fluorescent microsphere distribution and imaging with micro- and flat-panel computed tomography. *The American journal of pathology* 2005;167:937-946.

131.   Jacob RE, Lamm WJ, Einstein DR, Krueger MA, Glenny RW, Corley RA. Comparison of ct-derived ventilation maps with deposition patterns of inhaled microspheres in rats. *Experimental lung research* 2015;41:135-145.

132.   Sukkar A, Jenkins J, Sanchez J, Wagner EM. Inhibition of cxcr2 attenuates bronchial angiogenesis in the ischemic rat lung. *J Appl Physiol (1985)* 2008;104:1470-1475.

133.   Nijmeh J, Moldobaeva A, Wagner EM. Role of ros in ischemia-induced lung angiogenesis. *American journal of physiology Lung cellular and molecular physiology* 2010;299:L535-541.

134.   Macklem PT. A theoretical analysis of the effect of airway smooth muscle load on airway narrowing. *American journal of respiratory and critical care medicine* 1996;153:83-89.

135.   Baile EM, Sotres-Vega A, Pare PD. Airway blood flow and bronchovascular congestion in sheep. *The European respiratory journal* 1994;7:1300-1307.

136.   Ribatti D, Puxeddu I, Crivellato E, Nico B, Vacca A, Levi-Schaffer F. Angiogenesis in asthma. *Clinical and experimental allergy : journal of the British Society for Allergy and Clinical Immunology* 2009;39:1815-1821.

137.   Antoniou KM, Tzouvelekis A, Alexandrakis MG, Sfiridaki K, Tsiligianni I, Rachiotis G, Tzanakis N, Bouros D, Milic-Emili J, Siafakas NM. Different angiogenic

activity in pulmonary sarcoidosis and idiopathic pulmonary fibrosis. *Chest* 2006;130:982-988.

138.   Milne EN. Circulation of primary and metastatic pulmonary neoplasms. A postmortem microarteriographic study. *The American journal of roentgenology, radium therapy, and nuclear medicine* 1967;100:603-619.

139.   Tacelli N, Remy-Jardin M, Copin MC, Scherpereel A, Mensier E, Jaillard S, Lafitte JJ, Klotz E, Duhamel A, Remy J. Assessment of non-small cell lung cancer perfusion: Pathologic-ct correlation in 15 patients. *Radiology* 2010;257:863-871.

140.   Kiessling F, Boese J, Corvinus C, Ederle JR, Zuna I, Schoenberg SO, Brix G, Schmahl A, Tuengerthal S, Herth F, Kauczor HU, Essig M. Perfusion ct in patients with advanced bronchial carcinomas: A novel chance for characterization and treatment monitoring? *European radiology* 2004;14:1226-1233.

141.   Milne EN, Zerhouni EA. Blood supply of pulmonary metastases. *Journal of thoracic imaging* 1987;2:15-23.

142.   Nambu Y, Tamamura H, Ohguchi M, Mouri M, Kobayashi Y, Yamanouchi K, Toga H, Ohya N. [bronchial arterial hemodynamics after thoracic irradiation therapy in lung cancer patients]. *Nihon Kyobu Shikkan Gakkai zasshi* 1994;32:644-649.

143.   Weiholt Christian MR, Haworth Steven, Roerig David, Dawson Christopher. Quantificaiton of bronchial ciruclation perfusion in rats. *Medical Imaging* 2004;5369:387-393.

144.   Fournier LS, Cuenod CA, de Bazelaire C, Siauve N, Rosty C, Tran PL, Frija G, Clement O. Early modifications of hepatic perfusion measured by functional ct in a rat model of hepatocellular carcinoma using a blood pool contrast agent. *European radiology* 2004;14:2125-2133.

145.   Kan Z, Kobayashi S, Phongkitkarun S, Charnsangavej C. Functional ct quantification of tumor perfusion after transhepatic arterial embolization in a rat model. *Radiology* 2005;237:144-150.

146.   Osimani M, Bellini D, Di Cristofano C, Palleschi G, Petrozza V, Carbone A, Laghi A. Perfusion mdct of prostate cancer: Correlation of perfusion ct parameters and immunohistochemical markers of angiogenesis. *AJR American journal of roentgenology* 2012;199:1042-1048.

147.   Ma G, Bai R, Jiang H, Hao X, Ling Z, Li K. Assessment of hemodynamics in a rat model of liver cirrhosis with precancerous lesions using multislice spiral ct perfusion imaging. *BioMed research international* 2013;2013:813174.

148.   Yeung TP, Kurdi M, Wang Y, Al-Khazraji B, Morrison L, Hoffman L, Jackson D, Crukley C, Lee TY, Bauman G, Yartsev S. Ct perfusion imaging as an early biomarker of differential response to stereotactic radiosurgery in c6 rat gliomas. *PloS one* 2014;9:e109781.

149.   Neyazaki T, Ikeda M, Seki Y, Egawa N, Suzuki C. Bronchial artery infusion therapy for lung cancer. *Cancer* 1969;24:912-922.

150.   Yoshida T, Kamada K, Miura K, Goto T, Ohshima S, Sato W, Shibuya T, Dohmen T, Kanata R, Sakai T, Chiba M, Fujiwara J, Sugimoto Y, Ishioka M, Hasegawa I, Takahashi K, Minami S, Fujita A, Hashimoto M, Ohnishi H. Successful treatment of hepatocellular carcinoma with lung metastasis using hepatic and bronchial artery infusion chemotherapy. *Intern Med* 2014;53:2493-2497.

151.   Yan D, Zhou CW, Liu DZ, Chen Y, Zeng HY, Li H. [evaluation of the efficacy of bronchial arterial infusion chemotherapy for the treatment of central non-small cell lung cancer]. *Zhonghua Zhong Liu Za Zhi* 2011;33:302-304.

152.   Razazi K, Parrot A, Khalil A, Djibre M, Gounant V, Assouad J, Carette MF, Fartoukh M, Cadranel J. Severe haemoptysis in patients with nonsmall cell lung carcinoma. *The European respiratory journal* 2015;45:756-764.

153.   Fujita T, Tanabe M, Moritani K, Matsunaga N, Matsumoto T. Immediate and late outcomes of bronchial and systemic artery embolization for palliative treatment of patients with nonsmall-cell lung cancer having hemoptysis. *Am J Hosp Palliat Care* 2014;31:602-607.

154.   Jakobsson L, Franco CA, Bentley K, Collins RT, Ponsioen B, Aspalter IM, Rosewell I, Busse M, Thurston G, Medvinsky A, Schulte-Merker S, Gerhardt H. Endothelial cells dynamically compete for the tip cell position during angiogenic sprouting. *Nature cell biology* 2010;12:943-953.

155.   Pascale F, Ghegediban SH, Bonneau M, Bedouet L, Namur J, Verret V, Schwartz-Cornil I, Wassef M, Laurent A. Modified model of vx2 tumor overexpressing vascular endothelial growth factor. *Journal of vascular and interventional radiology : JVIR* 2012;23:809-817 e802.

156.   Scappaticci FA. Mechanisms and future directions for angiogenesis-based cancer therapies. *Journal of clinical oncology : official journal of the American Society of Clinical Oncology* 2002;20:3906-3927.

157.   Herbst RS, Fidler IJ. Angiogenesis and lung cancer: Potential for therapy. *Clinical cancer research : an official journal of the American Association for Cancer Research* 2000;6:4604-4606.

158.   Li A, Dubey S, Varney ML, Dave BJ, Singh RK. Il-8 directly enhanced endothelial cell survival, proliferation, and matrix metalloproteinases production and regulated angiogenesis. *J Immunol* 2003;170:3369-3376.

159.   Aalinkeel R, Nair B, Chen CK, Mahajan SD, Reynolds JL, Zhang H, Sun H, Sykes DE, Chadha KC, Turowski SG, Bothwell KD, Seshadri M, Chen C, Schwartz SA. Nanotherapy silencing the interleukin-8 gene produces regression of prostate cancer by inhibition of angiogenesis. *Immunology* 2016.

160.   Aird WC. Endothelial cell heterogeneity. *Critical care medicine* 2003;31:S221-230.

161.   Feng D, Nagy JA, Hipp J, Dvorak HF, Dvorak AM. Vesiculo-vacuolar organelles and the regulation of venule permeability to macromolecules by vascular permeability factor, histamine, and serotonin. *The Journal of experimental medicine* 1996;183:1981-1986.

162.   Wisse E, De Zanger RB, Charels K, Van Der Smissen P, McCuskey RS. The liver sieve: Considerations concerning the structure and function of endothelial fenestrae, the sinusoidal wall and the space of disse. *Hepatology* 1985;5:683-692.

163.   Majno G, Palade GE. Studies on inflammation. 1. The effect of histamine and serotonin on vascular permeability: An electron microscopic study. *The Journal of biophysical and biochemical cytology* 1961;11:571-605.

164.   Lacorre DA, Baekkevold ES, Garrido I, Brandtzaeg P, Haraldsen G, Amalric F, Girard JP. Plasticity of endothelial cells: Rapid dedifferentiation of freshly isolated

high endothelial venule endothelial cells outside the lymphoid tissue microenvironment. *Blood* 2004;103:4164-4172.

165.   Burridge KA, Friedman MH. Environment and vascular bed origin influence differences in endothelial transcriptional profiles of coronary and iliac arteries. *American journal of physiology Heart and circulatory physiology* 2010;299:H837-846.

166.   Chi JT, Chang HY, Haraldsen G, Jahnsen FL, Troyanskaya OG, Chang DS, Wang Z, Rockson SG, van de Rijn M, Botstein D, Brown PO. Endothelial cell diversity revealed by global expression profiling. *Proceedings of the National Academy of Sciences of the United States of America* 2003;100:10623-10628.

167.   Nagy JA, Chang SH, Shih SC, Dvorak AM, Dvorak HF. Heterogeneity of the tumor vasculature. *Seminars in thrombosis and hemostasis* 2010;36:321-331.

168.   Morikawa S, Baluk P, Kaidoh T, Haskell A, Jain RK, McDonald DM. Abnormalities in pericytes on blood vessels and endothelial sprouts in tumors. *The American journal of pathology* 2002;160:985-1000.

169.   Franses JW, Baker AB, Chitalia VC, Edelman ER. Stromal endothelial cells directly influence cancer progression. *Science translational medicine* 2011;3:66ra65.

170.   Gebb S, Stevens T. On lung endothelial cell heterogeneity. *Microvascular research* 2004;68:1-12.

171.   Parker JC, Yoshikawa S. Vascular segmental permeabilities at high peak inflation pressure in isolated rat lungs. *American journal of physiology Lung cellular and molecular physiology* 2002;283:L1203-1209.

172.   Chetham PM, Babal P, Bridges JP, Moore TM, Stevens T. Segmental regulation of pulmonary vascular permeability by store-operated ca2+ entry. *The American journal of physiology* 1999;276:L41-50.

173.   Kelly JJ, Moore TM, Babal P, Diwan AH, Stevens T, Thompson WJ. Pulmonary microvascular and macrovascular endothelial cells: Differential regulation of ca2+ and permeability. *The American journal of physiology* 1998;274:L810-819.

174.   Ochoa CD, Wu S, Stevens T. New developments in lung endothelial heterogeneity: Von willebrand factor, p-selectin, and the weibel-palade body. *Seminars in thrombosis and hemostasis* 2010;36:301-308.

175.   Wu S, Zhou C, King JA, Stevens T. A unique pulmonary microvascular endothelial cell niche revealed by weibel-palade bodies and griffonia simplicifolia. *Pulmonary circulation* 2014;4:110-115.

176.   Ismail JA, Poppa V, Kemper LE, Scatena M, Giachelli CM, Coffin JD, Murry CE. Immunohistologic labeling of murine endothelium. *Cardiovascular pathology : the official journal of the Society for Cardiovascular Pathology* 2003;12:82-90.

177.   Robertson RT, Levine ST, Haynes SM, Gutierrez P, Baratta JL, Tan Z, Longmuir KJ. Use of labeled tomato lectin for imaging vasculature structures. *Histochemistry and cell biology* 2015;143:225-234.

178.   Christian S, Pilch J, Akerman ME, Porkka K, Laakkonen P, Ruoslahti E. Nucleolin expressed at the cell surface is a marker of endothelial cells in angiogenic blood vessels. *The Journal of cell biology* 2003;163:871-878.

179.   Zhang F, Tang Z, Hou X, Lennartsson J, Li Y, Koch AW, Scotney P, Lee C, Arjunan P, Dong L, Kumar A, Rissanen TT, Wang B, Nagai N, Fons P, Fariss R, Zhang Y, Wawrousek E, Tansey G, Raber J, Fong GH, Ding H, Greenberg DA, Becker KG,

Herbert JM, Nash A, Yla-Herttuala S, Cao Y, Watts RJ, Li X. Vegf-b is dispensable for blood vessel growth but critical for their survival, and vegf-b targeting inhibits pathological angiogenesis. *Proceedings of the National Academy of Sciences of the United States of America* 2009;106:6152-6157.

180. Carmeliet P, Jain RK. Molecular mechanisms and clinical applications of angiogenesis. *Nature* 2011;473:298-307.

181. Hayashi JN, Ito H, Kanayasu T, Asuwa N, Morita I, Ishii T, Murota S. Effects of glucose on migration, proliferation and tube formation by vascular endothelial cells. *Virchows Archiv B, Cell pathology including molecular pathology* 1991;60:245-252.

182. Movafagh S, Hobson JP, Spiegel S, Kleinman HK, Zukowska Z. Neuropeptide y induces migration, proliferation, and tube formation of endothelial cells bimodally via y1, y2, and y5 receptors. *FASEB journal : official publication of the Federation of American Societies for Experimental Biology* 2006;20:1924-1926.

183. Pan Y, Wu Q, Qin L, Cai J, Du B. Gold nanoparticles inhibit vegf165-induced migration and tube formation of endothelial cells via the akt pathway. *BioMed research international* 2014;2014:418624.

Lindsey Eldridge

Date of Birth: July 24, 1986 Pittsburgh, PA
4104 Chardel Rd Apt 2A• Nottingham, MD 21236
Phone: 412-607-9638 • E-Mail: leldrid3@jhu.edu

Education

Johns Hopkins Bloomberg School of Public Health   2011-2016

PhD in the Department of Environmental Health Science, Division of Toxicology Physiology and Molecular Mechanisms

Pennsylvania State University   2004-2008

BS in Kinesiology, College of Health and Human Development

Research Experience

Johns Hopkins Bloomberg School of Public Health   2011-2016

Ph.D. Successfully defended thesis: June 2016

During the course of my PhD program I independently established a novel animal model for studying lung tumor angiogenesis as well as advanced imaging techniques for quantifying lung tumor perfusion. Subsequently, I developed an innovative procedure for surgically ablating the bronchial circulation resulting in blockage of tumor growth. I wrote and submitted a first author manuscript to the journal of Cancer Research defining the role of bronchial artery angiogenesis in lung tumor perfusion. I would consider myself a subject matter expert in lung physiology, vascular biology and lung tumor angiogenesis.

- Created unique orthotopic pre-clinical model for studying lung tumor angiogenesis in immunodeficient rats
- Established imaging protocols for measuring systemic lung perfusion with high resolution CT scans
- Developed novel bronchial artery ablation surgery inhibiting lung tumor growth
- Presented thesis work highlighting endothelial cell heterogeneity at international conference (American Thoracic Society 2014)
- Won ATCC photo contest for histological images of in vivo lung tumor
- Extensively investigated the angiogenic potential of primary endothelial cell lines
- Devised explant and co-culture assays for in vitro determination of adenocarcinoma/endothelial cell interactions
- Utilized FACS analysis to study angiogenesis, cell proliferation, and cell surface markers of in vivo lung tumors
- Acquired expert surgical skills from over 8 years experience working on small animal models of lung cancer, asthma and ischemia; trained lab staff on microsurgical techniques
- Conceptualized, budgeted and submitted grant to Lung Cancer Research Foundation.
- Designed and lead review sessions and private tutoring as a teaching assistant of graduate level Physiology for over 60 students
- Contributed original imaging protocols and surgical expertise to collaborative projects and manuscripts

Johns Hopkins School of Medicine

Research Specialist   2008-2011

I was hired at Johns Hopkins University as a research technician and was promoted to research specialist. I quickly mastered micro-surgical procedures for an *in vivo* mouse model of pulmonary ischemia, and several microbiological techniques. I received independent projects, contributed to manuscript and grant writing, presented research at American Thoracic Society and published a first author manuscript in the American Journal of Physiology. A list of acquired laboratory skills is listed below.

140

Publications

Moldobaeva A, Baek A, **Eldridge L**, Wagner EM. Differential activity of pro-angiogenic CXC chemokines
Microvascular Res. 80(1):18-22, 2010. PMID 20144627 PMCID: PMC2879473

Eldridge L, Moldobaeva A, Wagner EM Increased Hyaluronan Fragmentation During Pulmonary Ischemia
Am J Physiol: Lung, Cell, Mol Physiol 301 (5):L782-8, 2011. PMID: 21821727 PMCID: PMC3213986

Wagner EM, Jenkins J, Schmieder A, **Eldridge L**, Zhang Q, Moldobaeva A, Whang H, Allen JS, Mitzner W, Keupp J, Caruthers DS, Wickline SA, Lanza GM. Angiognesis and Airway Reactivity in Asthmatic Brown Norway Rats. Angiogenesis (Aug 2014) PMID: 25149641 PMCID: PMC4281493

Eldridge L, Moldobaeva A, Zhong Q, Jenkins J, Snyder M, Brown RH, Mitzner W, Wagner EM. Bronchial artery angiogenesis drives lung tumor growth. Cancer Research (Submitted for Publication April 2016, Accepted July 2016)

Lanza GM, Jenkins J, Schmieder A, Moldobaeva A, Cui G, Zhang H, Yang X, Zhang Q, Kuepp J, Paranandi K, **Eldridge L**, Allen J, Williams T, Scott M, Wickline S, Razani B, Wagner EM. Anti-Angiogenic Nanotherapy Inhibits Airyway Remodeling and Hyper-Responsiveness of Dust Mite Triggered Asthma in Brown Norway Rat. (Submitted for Publication May 2016)

Scientific Presentations

Eldridge L, Moldobaeva A, Wagner EM. Increased Lung Hyaluronan During Pulmonary Ischemia
American Thoracic Society 2010

Moldobaeva A, **Eldridge L**, Wagner EM. Monocyte differentiation after ischemic stress.
American Thoracic Society 2010

Eldridge L, Moldobaeva A, Tankersley CG, Wagner EM. Hyaluronan fragmentation and MMP-12 expression during pulmonary ischemia.
Experimental Biology 2011

Moldobaeva A, **Eldridge L**, Kim E, Wagner EM. Monocyte differentiation in the ischemic lung.
Experimental Biology 2011.

Eldridge L, Wagner EM Inhibition of mTOR by Rapamycin in Systemic Angiogenesis
American Thoracic Society 2014

Eldridge L, Wagner EM. The Bronchial Artery in Lung Tumor Growth
Medimmune/ JHU Science Day 2015

Eldridge L, Wagner EM. Bronchial Artery Angiogenesis Drives Lung Tumor Growth
EHS Research Retreat 2016. Awarded 2nd Place in poster competition.

Acquired Laboratory Skills

Small Animal Models
- Microsurgical procedures in models of lung cancer, asthma and pulmonary ischemia in mice and rats
- Animal handling, husbandry, and breeding
- Pulmonary function test; Diffusing Capacity, Pressure Volume loop analysis, airway resistance by FlexiVent
- Microfil casting of vasculature, vascular perfusion fixation
- Blood perfusion measurements by contrast enhanced High Resolution Computed Tomography
- Lung Fixation
- Injections: tail vein, intraperitoneal, subcutaneous and gavage
- Retro-orbital bleeds, terminal cardiac puncture bleeding

Microbiological Techniques

- Immunohistochemistry, antigen retrieval (frozen and paraffin imbedded blocks)
- Western Blot Analysis
- ELISA
- Genotyping
- RNA isolation, QPCR, RT-qPCR, microarray
- Primary Cell Line Isolation
- FACS for analysis and cell sorting
- Gel Electrophoresis
- Magnetic Bead cell purification
- Explant tube formation assays
- Cell differential counting

Computer Software

- Microsoft office
- Prism graphpad
- Image J
- Image Pro
- Osirix